Dynamic Response of Geared Shaft Systems with Time-Dependent Boundary Conditions Subjected to Static Transmission Error

Joydip Sanyal

A Thesis

in

The Department

of

Mechanical and Industrial Engineering

Presented in Partial Fulfillment of the Requirements

for the Degree of Master of Applied Science

in

Mechanical Engineering

at Concordia University

Montréal, Québec,

Canada

December 2007

Your file Votre référence
ISBN: 978-0-494-40922-0
Our file Notre référence
ISBN: 978-0-494-40922-0

ABSTRACT

Joydip Sanyal

A rotating gear pair experiences high vibration and noise mainly due to tooth profile error, mounting error, tooth wear, friction backlash and periodic change of meshing stiffness. The combined effect of the manufacturing error, mounting error and elastic tooth deformation is considered as the static transmission error that introduces internal displacement excitation within the gear pair. Such internal excitation generates torsional vibration through the driving and driven shafts even in absence of external excitations. Thus the vibration problem of a geared system involves homogeneous equations of motion with time dependent boundary conditions. The present research is to investigate the torsional vibrations of a geared system by developing a continuous model that converts the homogeneous equations with non-homogeneous boundary conditions into non-homogeneous equations with homogeneous boundary conditions. The influence of friction, tooth wear, backlash and other nonlinear variables have been ignored in the formulation.

The free vibration results of the proposed model are validated by developing the classical Rayleigh-Ritz model with Bhat's boundary characteristic orthogonal polynomial functions. The results are also validated by performing experiments in the laboratory for a simple geared system. Torsional vibration responses are determined in both time and frequency domains. In addition to the proposed continuous model the discrete model is

simulated to determine torsional vibrations and dynamic torque generated due to static tooth error.

The experimental investigations are carried out by measuring free torsional vibrations with strain gauge and frequency analysis by a spectrum analyzer.

ACKNOWLEDGEMENTS

The author is sincerely thankful and deeply grateful to his supervisors Dr. Rama B. Bhat for his scholastic guidance and continuous support during the course of this work.

I would like to thank the technical support staff in Mechanical and Industrial Engineering Department, Danny Juras, Brian Cooper, and Gilles Huard, and Brad Luckhart.

The help and useful discussions during the course of this work are gratefully acknowledged from my colleagues and friends.

Finally, thanks go to my parents, my wife and our only son for their continuous moral support throughout the research period.

TABLE OF CONTENTS

LIST OF FIGURES

LIST OF TABLES

LIST OF SYMBOLS

Notation	Description	Unit
A	Area of cross section	m^2
f_n	Natural Frequency	Hz
G	Modulus of rigidity	N/m^2
$I_{p1}, I_{p2}, I_{p3}, I_{p4}$	Mass moment of inertia of rigid masses	Kgm^2
$J_{p1}, J_{p2}, J_{p3}, J_{p4}$	Polar moment of inertia	m^4
$[J]$	Mass moment of inertia matrix of discrete model	Kgm^2
$[K]$	Stiffness Matrix of discrete model	Nm/rad
K_1, K_2, K_3	Torsional stiffness of shafts of discrete model	Nm/rad
L_i	Length of the continuous shaft from the free end Inertia of the driving shaft	m
$\overline{L}_i$	Dimensionless Length of the continuous shaft from the free end Inertia of the driving shaft	-
m	Combined rotational mass	kg
N	Gear ratio	-
$Q(t)$	Dynamic torque due to internal excitation	Nm
q_i	Angular displacement of rigid masses	rad
$\dot{q}_i$	Time derivative of Angular displacement of rigid masses	rad/s
T	Kinetic energy of the vibrating system	$Joule$
$T_{\max}$	Maximum Kinetic energy of the vibrating system	$Joule$

$T^*_{\max}$	$T_{\max} / \omega^2$.	$Joule/(rad/s)^2$
U	Potential energy	$Joule$
$U_{\max}$	Maximum Potential energy of the vibrating system	$Joule$
θ_i	Angular deflection of the continuous system	rad
$\dot{\theta}_i$	Time derivative of angular deflection	rad/s
$\ddot{\theta}_i$	Second degree time derivative of angular deflection	rad/s^2
θ'_i	Space derivative of angular deflection	rad/m
θ''_i	Second degree space derivative of angular deflection	rad/m^2
ξ_i	Non-dimensional variable $= x/L$	-
λ	Eigen Values $= \omega_n^2$	$(rad/s)^2$
μ	Poisson's ratio	-
ρ	Density of shaft	Kg/m^3
ω	Forcing frequency	rad/s
ω_n	Natural frequency of the system	rad/s
$\gamma(t)$	Periodic Total Transmission Error	rad
$\dot{\gamma}(t)$	Time derivative of Total Transmission Error	rad/s

DYNAMIC RESPONSE OF GEARED SHAFT SYSTEMS WITH TIME –DEPENDENT BOUNDARY CONDITIONS SUBJECTED TO STATIC TRANSMISSION ERROR

1 Introduction

1.1 General

Gears are most often regarded as the icon of Mechanical Engineering. Gear is a toothed wheel that transmits torque to another toothed component when they are meshed together. It transmits rotary motion from one shaft to another and normally turns the driven shaft at a different speed from the driving shaft. It also sometimes adjusts direction of rotation of the driven shaft to a desired angle with respect to the driving shaft.

One of the primary objectives of gear design is to ensure uniform rotary motion transmission from the driving shaft to the driven shaft. The closer the rotary motion transmission is to the constant angular velocity transmission, the lower is the vibration and noise level within the gear drive. High-speed and high power gear transmission systems experience significant dynamic loads due to variation of relative velocities of the mating members. Manufacturing errors, eccentric mounting of gears and bearings, periodic tooth stiffness variations, variation of meshing position, backlash, sliding friction and tooth wear are the major factors of dynamic loading on gears in meshing. At slow speeds, load on gear teeth is mainly due to the transmitted torque. However with increase in speed, dynamic load exceeds the tooth load caused by the transmitted torque.

Geared shafts experience torsional vibration even when prime movers or driven machines do not transmit external excitation. The periodic internal excitation generated within the gear pair introduces dynamic loading that becomes significant with increase in total transmission error. Total transmission error is the deviation of angular rotation of the driven gear with respect to the driving gear generated by tooth profile error, periodic changes of tooth elasticity and variation of meshing position. Mounting error of gears and bearings and misalignment of the geared shafts, as well as the askew input/ output shafts further contribute to the transmission error. As a result gears within the robust gearboxes generate vibration and noise which can reach catastrophic levels if not monitored and addressed in time.

1.2 History of Gear

Gear is one of the oldest mechanical components in power transmission system. Over 3000 years ago primitive gears first meshed with each other and transmitted rotary motion. The earliest gears were made of hard wood. Water wheels were used to convert energy of moving water into mechanical (rotational) energy. Wooden gears were mostly used to connect the water wheels to the machines that would grind wheat and hammer metals. In the middle age stone gears were used in Sweden. Greeks introduced metallic gears with wedge shaped teeth for the first time. The Romans made considerable use of gears in their mills. Later on invention of steam engines and electric motors created a substantial demand for heavy duty gears.

The industrial revolution in Britain in the eighteenth century experienced an extensive explosion in the use of metal gearing. Use of high speed steam turbines and gas turbines in power plants and high speed compressors and pumps in chemical process industries motivated analysis of gear dynamics that gradually improved gear design all through the nineteenth century.

1.3 Basic Geometry of Spur Gears:

The fundamentals of gearing are illustrated in figure 1.3.1 through the spur-gear tooth since it is the simplest and the most widely used gear.

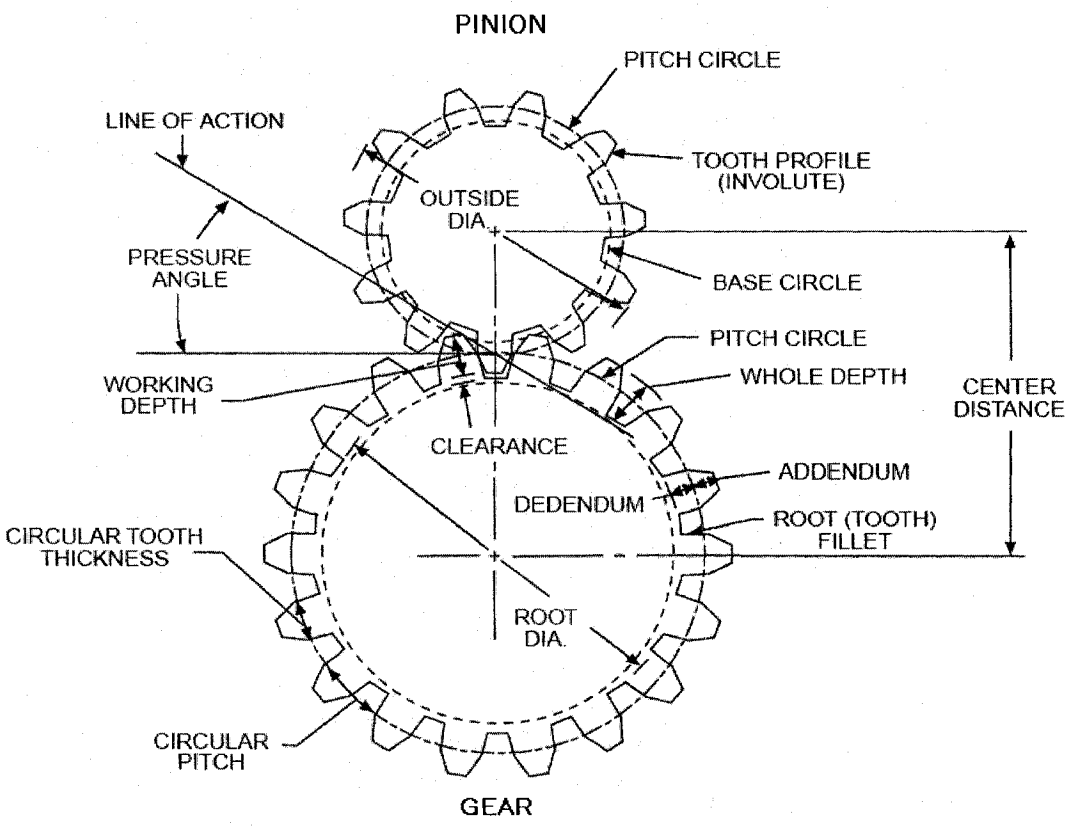

Figure: 1.3.1 Geometry and nomenclature of a spur-gear pair

Following is the brief description of basic geometry and nomenclature of a spur-gear mesh as shown in figure 1.3.1.

1.3.1 Pinion - When two gears mesh together, the one with the smaller number of teeth is called the pinion.

1.3.2 Gear - When two gears mesh together, the one with the larger number of teeth is called the gear.

1.3.3 Pitch point - The point at which the pitch circle diameters of two gears in mesh collinear.

1.3.4 Pitch Circle - The circle derived from a number of teeth and a specified diametral or circular pitch. Circle on which spacing or tooth profiles is established and from which the tooth proportions are constructed.

1.3.5 Diametral pitch (P_d) - The number of teeth per inch of pitch circle diameter. The diametral pitch determines the size of gear tooth. A higher P_d indicates finer tooth spacing.

1.3.6 Module (m) - Used for metric gears and is the ratio of pitch circle diameter (in mm) to the number of teeth; a higher module indicates coarser tooth spacing.

1.3.7 Addendum (a) - is the height of the tooth above the pitch circle diameter, i. e. is the height by which a tooth projects beyond the pitch circle or pitch line.

1.3.8 Dedendum (b) - is the depth of a tooth space below the pitch line. It is normally greater than the addendum of the mating gear to provide clearance.

1.3.9 Clearance (c) - is the amount by which the dedendum in a given gear exceeds the addendum of its mating gear.

1.3.10 Whole depth (h_t) - is the total depth of a tooth space, equal to the sum of the addendum and the dedendum. It is also equal to the working depth plus clearance.

1.3.11 Working depth (h_k) – is the total depth of the space between adjacent teeth, i.e. the depth of engagement of two gears; that is, the sum of their addendums.

1.3.12 Outside diameter (D_o) – is the outside diameter of the gear.

1.3.13 Base Circle diameter (D_b) - is the diameter of the base cylinder from which the involute portion of a tooth profile is generated.

1.3.14 Pitch circle diameter (D) – is the diameter of the pitch circle. In parallel shaft gears, the pitch diameters can be determined directly from the center distance and the number of teeth.

1.3.15 Root Diameter (D_r) - is the diameter at the base of the tooth space.

1.3.16 Circular tooth thickness (t) - is the length of arc between the two sides of a gear tooth on the pitch circle, unless otherwise specified, i.e. the width of a tooth measured along the arc at the pitch circle diameter.

1.3.17 Involute Teeth - of spur gears, helical gears and worms are those in which the active portion of the profile in the transverse plane is the involute of a circle.

1.3.18 Pressure angle (ϕ) – is the angle at a pitch point between the line of pressure which is normal to the tooth surface, and the plane tangent to the pitch surface. In involute teeth, pressure angle is often described also as the angle between the line of action and the line tangent to the pitch circle. Standard pressure angles are established in connection with standard gear-tooth proportions.

1.3.19 Backlash (B) - is the amount by which the width of a tooth space exceeds the thickness of the engaging tooth on the pitch circles. As actually indicated by measuring devices, backlash may be determined variously in the transverse, normal, or axial-planes, and either in the direction of the pitch circles or on the

line of action. Such measurements should be corrected to corresponding values on transverse pitch circles for general comparisons.

1.3.20 Contact Ratio (m_c) -in general, the number of angular pitches through which a tooth surface rotates from the beginning to the end of contact.

1.3.21 Centre distance (C) - The distance between the axes of two gears in mesh.

1.4 Dynamic Load on Gear

Gear teeth experience dynamic loads when a pair of teeth mesh together to transmit torque and the resulting motion is not smooth. Each successive tooth pair of mating gears would pick up some dynamic load even when they are accurately manufactured and properly mounted. Due to elasticity, or springiness of gear tooth material a single pair of teeth under significant amount of load deflect from their unloaded ("perfect") positions. Deflection of teeth allows the rest of the driving gear to move slightly ahead of its theoretical undeflected position and the rest of the driven gear to lag slightly behind its theoretical undeflected position. Eccentric mounting of gear, backlash, sliding friction, shaft misalignment etc. further deviate the tooth from its perfect position.

These phenomena shift all unloaded teeth of gear and pinion slightly out of their correct positions with respect to the tooth-pair carrying the load. Because of it, when the next tooth-pair comes into mesh, they touch each other earlier than they would if there

were no deviation. Thus they pick up a disproportionate amount of the load very quickly. This sudden load application produces an impact force, which can cause the teeth to bounce apart and re-contact later in the mesh causing another impact. With increase in speed the forces exerted by the teeth become significantly greater than the load applied by the transmitted torque.

It is not always possible to manufacture absolutely perfect gear teeth. The AGMA Quality Number is a measure of the accuracy of the tooth locations and the tooth profiles. A gear with a lower Quality Number has greater errors in tooth location and tooth profile. As the errors in tooth location and profile increase, the magnitude of the dynamic load increases. Misalignment and mounting errors further increase the dynamic load with increased vibration and noise and reduce gear life.

1.5 Factors Influencing Gear Dynamics

1.5.1 PRIMARY FACTORS:

Primary factors that influence the meshing action directly and are present in all types of gears are given below.

a. Gear Transmission Error: Also known as Total transmission error, it comprises manufacturing errors, mounting errors and teeth deflection and / or deformation under applied load. This combined error is dynamic in nature. For any instantaneous position of a gear it is defined as the departure of the mating gear from the position it would occupy if the system were ideal with constant velocity ratio and constant contact ratio.

b. Variable Mesh Stiffness: Stiffness of teeth pair is a function of contact or load position. It varies with change in load position. Load sharing between the teeth when more than one pair of teeth are in contact, is influenced by the variable mesh stiffness.

c. Non-Linear Backlash Element: With lightly loaded gears at higher speed, tooth separation and subsequent reverse or forward impact can occur resulting in higher dynamic loads.

1.5.2 SECONDARY FACTORS:

a. Shaft Elasticity: Variation of shaft elasticity shifts the system natural frequencies, indicating the influence of other factors in the system on the gear dynamics.

b. System Inertia: Like shaft elasticity it also determines the influence of other components in drive on gear dynamics.

c. Damping in the System: While the primary factors and system inertia determine the critical regions, the severity of the response at the critical regions is determined by the damping in the system.

d. Input Torque Fluctuation: It has significant influence on system stability.

e. Variation in Contact Ratio: It is the ratio of contact patch to the base pitch, and indicates how many teeth share the load for how long during one mesh period.

f. Effect of Friction: Induces non-linearity and requires elasto-hydrodynamic lubrication study.

g. Coupling Between Torsional and Lateral Modes: At higher speeds it is necessary to include the effect of coupling between torsional and lateral modes.

A complete and accurate study, covering all the above factors has not yet been carried out to evaluate the actual pattern of gear dynamics. Among the above variables the gear transmission error plays the most dominating role.

1.6 Literature Survey

Primitive gear design mainly emphasized on the strength of gear material. Real studies on gear dynamics in fact commenced in the eighteenth century with developing empirical formulas of dynamic factor. It was a great initiative to focus gear design from the static load bearing capacity of gears to its dynamic behavior. Spring-mass vibratory models were introduced in gear dynamics in 1950s that inaugurated comprehensive studies of a number of dynamic properties of gear drives.

Earlier studies considered tooth stiffness as the potential energy storing element in the system and devised single degree of freedom spring mass systems neglecting stiffness of shafts and bearings. Later objectives of dynamic modeling of gears emphasize studies of bending stress, transmission efficiency, natural frequencies of the system, lateral, axial and torsional vibratory motion, stability analysis and loads on driver and driven machine

components. Dynamic behavior of gears in mesh appeared with vibratory models that incorporated many of the variables with linear and non linear properties. Models between 1970s and 1980s include effect of three-dimensional stiffness of gear teeth, non-linearity of the system elements, damping and frictional effects. Later on discrete model analysis of torsional, lateral and axial mode vibrations of gears came forward. In recent years finite element analysis and other numerical approaches are used to study the coupled lateral, torsional and axial vibrations. Increasing demand of high-speed machinery induced extensive research on dynamic analysis of gearing since 1920s. Most representative ones of different study-focuses are referenced here.

Buckingham [1] developed a dynamic load equation referring change in tooth profiles due to elastic deformation and/or manufacturing error behind the cause of gear load variation. It was shown that load variation mainly depends on effective masses, effective errors and speed of gears.

Tuplin [2-3] introduced the first spring-mass model with equivalent constant mesh stiffness. Dynamic loads due to transient excitation were modeled by the insertion and withdrawal of wedges of various shapes at the base of the spring. This model ignored periodicity of the excitation and can be used to estimate dynamic factors of lightly loaded gears at conditions well below resonance.

Harris [4] first emphasized the effect of transmission errors in the dynamic load of gear teeth. A SDOF photo-elastic gear model was used to identify the manufacturing errors, variation in tooth stiffness and nonlinearity in tooth stiffness as the sources of gear

vibration. The excitation was treated as periodic and specified "static transmission error" as the magnitude of the excitation function. Dynamic instability due to parametric excitation of the gear mesh was also studied.

Johnson [5] investigated the influence of elastic deformation of teeth on gear dynamics. It was found that elastic deformation of teeth dominates over the tooth profile error at higher speed and heavy load condition. The departure of constant velocity ratio due to elastic deformation was indicated as the main forcing function behind the dynamic loading. However, the study assumed constant stiffness and the characteristics of the forcing function was shown in the frequency domain.

Gregory *et al.* [6] assumed the stiffness variation as sinusoidal function and devised a torsional vibratory model for dynamic analysis of geared system. With extensive experimental observations it was shown that non linear effects diminish with increase in system damping. For heavily damped systems, they have referred simple linear damping model to be a perfect choice. Aida *et al.* [7] first considered time varying mesh stiffness along with periodic tooth profile errors for analyzing dynamic load. The stability regions and steady state vibration were also determined by the study.

Ozguvent and Houser [8] conducted a comprehensive survey on mathematical models used in the dynamic gear analysis with a brief discussion on the assumptions and approximations made in most of the models. 188 papers from 1910 to mid eighties were

classified into five groups: (i) Simple Dynamic Factor Models, (ii) Models with Tooth Compliance, (iii) Models for Gear Dynamics, (iv) Models for Geared Rotor Dynamics and (v) Models for Torsional Vibrations. Simple Dynamic Factor Models included empirical and semi-empirical approaches to determine the dynamic factor used in gear root stress formulae. The second group models studied the influence of tooth stiffness as the only potential energy storing system, neglecting the flexibility of shafts and bearings. While the third group included the uncoupled lateral and coupled lateral-torsional models considering the flexibility of shafts and bearings besides the tooth properties. The fourth group, however, extended the study including whirling motion of shafts. Models of Torsional Vibrations within the detailed survey neglected flexibility of gear teeth and included the constant torsional stiffness of shafts connected with rigid gears.

Among the recent works Velex and Maatar [9] analyzed the influence of shape deviations and mounting errors on three-dimensional gear dynamics by a lumped parameter non-linear model. A unified approach was followed including time-dependent non-linear mesh stiffness, mounting errors, flank modifications, profile, and lead errors in that analysis. It was found that amplitude of vibration due to eccentricity is weaker than the pitch errors. Mesh resonance frequency lowers with increase in misalignment for spur gears. The transmission error considered for the study combines rigid body and static deflection and varies from point to point along the face width.

Huang and Liu [10] developed a lateral continuous model considering the teeth of a spur gear as a variable cross-section Timoshenko beam with involute cross section to

investigate dynamic response of a single tooth and a gear pair. Dynamics of two gears were also modeled by two beams connected by non linear contact stiffness. In the single tooth model the time varying stiffness method was incorporated in order to investigate the response of a gear tooth subject to meshing force. It was found that initial meshing causes displacement at the tooth tip, followed by a sinusoidal displacement with an exponential decay. Blank portion of the gear generates lower frequency vibration with less amplitude whereas higher modes generated by the toothed portion play dominant role. Damping ratio does not significantly influence the peak amplitudes at higher modes.

Nodolski and Pielorz [11] used a discrete-continuous model with two torsionally deformable shafts and four rigid bodies with constant inertia in order to investigate the effect of variable tooth stiffness on dynamic load of a single pair gear transmission system. They also studied the influence of the number of gear teeth, damping and mass moments of inertia on amplitude of response at various rotating speeds. It was shown that with the decrease of number of teeth the resonant region widens. However in all cases significant changes of the amplitude of the dynamic loads occur in third resonant region and above this speed amplitudes remain almost constant. With increase in damping the amplitude decreases in the first and third resonant regions, while in the second resonant region amplitude increases with damping.

Theodossiades and Natasivas [12] analyzed periodic steady state motions and their stability properties by a two DOF torsional model under the excitations generated by torsional moments and gear geometry errors. The interaction of backlash and non-

linearities (damping) was focused with variable mesh stiffness to investigate the response and stability of some practical gear-pair models. The nonlinear periodic motion was assumed for the single side tooth impact and the double side tooth impact on mating gears. It was shown that an increase in stiffness gradually decreases the effect of double side tooth impact and the resulting non linearity and decreases the resonant response amplitude. For relatively large values of external forcing parameter, effect of backlash and damping on response is negligible and for small values of the forcing parameter, linear effect of meshing stiffness becomes weak.

Parker *et al.*[13] used contact mechanics besides finite element analysis to investigate the influence of nonlinear dynamic mesh forces due to change in teeth number in mesh and contact loss across a wide range of operating speeds and torques. In order to isolate the tooth meshing effects from other complications, the shaft and supports were considered rigid and the response was assumed to be purely due to gear rotation. It was shown that amplitude of resonance significantly increases with increasing torque. Torque independent time-varying stiffness showed non-linear behavior whereas in case of torque dependent stiffness, non-linearity decreased. It was also shown that the maximum tooth load is considerably larger when contact loss occurs. Such contact loss of meshing teeth was identified as the main source of non linear behavior.

Vaishya and Singh [14] modeled a two DOF discrete torsional system for a spur gear and incorporated nonlinearity induced by sliding friction. The harmonic balance method was employed to study the influence of frictional coefficient, static damping ratio

and contact ratio subject to sliding friction on the dynamic transmission error. With increase in friction, amplitude of second harmonic region significantly decreases. Increase in damping ratio results in unstable responses with strong sub-harmonics at higher frequency zone. However, with increase in contact ratio resonant frequency region widens. It was shown that at certain resonant conditions, the non-linear sliding friction acts like system damper reducing oscillation, however, at non-resonant speeds it has no significant role.

Velex and Sainsot [15] analyzed the tooth friction excitations in errorless spur and helical gears using Coulomb model. The pinion and the gear of a pair were modeled as two rigid cylinders linked by a time-varying set of stiffnesses due to contact deformation and structural deflection of gear teeth. The influence of gear geometry on torsional and translational tooth friction excitation was found almost identical. It was shown that contact length variation has minimum influence on frictional excitation. However, depending on the position of the actual pitch point, high contact ratio gears can generate substantial friction excitation. It was also observed that torsional vibration is much less sensitive to tooth friction than bending vibration.

Wojnarowski and Onishchenko [16] investigated the effect of deformation and tooth wear on spur gear dynamics with the help of geometric and kinematic models and an elastic two DOF model. The geometric model identified tooth wear as the dominating factor behind the change of the gear ratio over mounting and manufacturing errors. The same phenomena were observed in a rigid model with a single-DOF system and in an

elastic model with a two-DOF system. It was also shown that the variation of dynamic load is harmonic and amplitude varies with the degree of teeth wear.

Vedmar and Anderson [17] calculated the dynamic gear tooth force and bearing forces for different speeds of the gears using a model that mounts gears on linear elastic bearings and external inertias on stiff bearings. Time-variant gear stiffness, non linear friction between gear teeth in contact and viscous damping in the gear mesh were also incorporated in the dynamic load analysis. It was observed that the number of natural frequencies with flexible bearings is higher than those with stiff bearings. Two additional frequencies appear in both frictional and normal direction of gear contact. The frequencies in normal direction are dynamically coupled through gear contact, while those in frictional direction are uncoupled to each other. The influence of gear deformation on gear forces is dominating over other factors. It was also shown that friction can produce significant bearing forces depending on the natural frequencies in frictional direction.

Li and Yu [18] investigated the effect of parallel and angular misalignment of gear shaft developing a non-linear coupled lateral torsional vibration model of rotor-bearing-gear coupling system using Lagrange's equations of motion. Involute tooth profile and the engagement relations between the hub and the sleeve of gear coupling were represented in the moving co-ordinate system, fixed with the sleeve. It was shown that even-integer multiples of the rotating speed of lateral vibration and odd-integer multiples of the torsional vibrations occur in the misaligned system and the integer

multiples of vibrations are apparent around the gear coupling. The vibrations of rotors far away from the couplings are not visible.

Li *et al.* [19] analyzed the coupled vibration of lateral, torsional and axial displacements of a rotor-bearing system of bevel gears. Critical speeds, threshold speed of stability and unbalance responses of the rotor bearing system were examined using Lagrange's equations of motion. It was shown that coupling between lateral and torsional vibrations is more significant in most of the modes while axial displacement is momentous in a few higher modes. However, critical speeds are roughly independent of pitch cone angle of bevel gears. The threshold speed of stability of coupled system is less than that of the uncoupled system. Significant unbalance responses were also noticed along axial and torsional directions besides the lateral direction.

Luo *et al.* [20] introduced substructural modal synthesis method to analyze the effect of coupling of torsional-lateral-axial vibration on multistage and multi-mesh complex geared systems. Finite element method was used for the dynamic analysis of individual substructures disengaging each pair of gears. The modal synthesis method incorporated matrix operations to extract useful data from a set of information about the modes of all of the substructures. The modal analysis involving the first two natural frequencies identified cross coupled interaction of lateral, torsional and axial vibrations.

Ananda Rao *et al.* [21] analyzed torsional-lateral vibrations of a three-pinion complex geared shaft system. Substructural modal synthesis method was used to

investigate the effects of backlash on torsional frequencies and effect of gear-meshing stiffness on the torsional-lateral coupled frequencies. A two-node six DOF beam element was employed for modeling each shaft. Lateral and torsional motions were coupled with the introduction of meshing spring at each of the gear pair. It was also observed that the influence of backlash in lower modes depends on the meshing stiffness, while backlash effect in higher modes is insignificant. Coupled natural frequencies increase with increase in gear-mesh stiffness.

Lee *et al.* [22] studied coupled lateral and torsional vibration responses of a speed increasing geared rotor-bearing system. A detailed examination was carried out to analyze the coupled and uncoupled free vibrations at variable gear mesh stiffness with rotating speeds under consideration. The result showed that some modes may yield coupled lateral and torsional mode characteristics with the increase of gear mesh stiffness over a certain range. However, a given dominant mode may change from an initial lateral one to torsional one or vice versa.

Vinayak et al [23] examined the multi-mesh transmissions of external, involute, fixed center, helical and spur gears. Each spur or helical gear is modeled as a rigid body with six degrees of freedom. The stiffness matrix coupled all six degrees of freedom between gear teeth to describe position varying teeth contacts. Meanwhile the rolling element bearings of the geared shafts were modeled as simple radial stiffness elements to device a combined bearing-shaft-gear model. The steady state response of linearized equations with time or position-varying coefficient (LTV) model was calculated by using

two solution techniques: numerical integration and Galerkin's multi-harmonic balance method as a semi-analytical approach. The eigen values of the linear time-invariant (LTI) model for single and multi-mesh gears well matched with the results of finite element method using ANSYS software.

Rook and Singh [24] developed a lumped parameter torsional model for studying the impact effects on a reverse-idler geared system. The concept of effective stiffness was introduced to determine the natural frequencies of non-linear system with the existence of backlash and rattle phenomena in each gear in addition to the viscous damping. External pulsating torque was considered as the only source of excitation without considering the static transmission error. The periodic response of a system with multiple clearances was calculated by using Galerkin method (multi harmonic balance method). The Floquet theory is used to study the stability of such solutions. The result of the multi-harmonic method well matched with the predictions of the numerical integration techniques.

Yuksel and Kahraman [25] developed a computational model of a planetary gear set to study the influence of surface wear on the dynamic behavior of planetary gear set formed by spur gears. The wear model employed a quasi-static gear contact mechanics model to compute contact pressures and Archard's wear model to determine the wear depth distributions. Different amounts of wear depths were introduced in the dynamic model to quantify the differences in dynamic behavior from the baseline behavior representing a gear set having no wear. It was observed that the tooth surface wear

influences the fundamental harmonic of the gear mesh forces the most. It was also shown that wear has negligible influence on the nonlinear behavior.

Lee and Ha [26] developed a finite element model to study the unbalance response orbit of a gear-coupled two-shaft rotor-bearing system. The method was applied to the unbalance response analysis of a turbo-chiller rotor-bearing system, having a bull-pinion speed increasing gear. The driver rotor-bearing system consists of the motor and bull gear and the driven rotor-bearing system consists of the compressor impeller and pinion gear. The coupled and uncoupled unbalance responses of the driver and driven rotor-bearings were found almost identical except a bump at the first torsional natural frequency. The torsional resonance has influenced the lateral unbalance responses because of the coupling effect of the lateral and torsional dynamics due to gear meshing. It was also predicted that the lateral coupling between the driver and driven rotor systems is very limited.

Litak and Friswell [27] examined the effect of broken tooth and meshing stiffness fluctuations on the vibration response of nonlinear geared systems. Periodic change of meshing stiffness was considered in the analysis. Various types of tooth errors were analyzed with a random distance between their increasing teeth contact. It was identified that regular and chaotic dynamic jump phenomenon are present in the vibration response. It was shown that the system is more sensitive to errors in the teeth pitch than fluctuations in the stiffness magnitude, although the qualitative effect is almost similar. One broken tooth has little influence on the dynamics of the gears, although two broken teeth can

have a significant effect. If two adjacent teeth are broken, a complex response is observed with the jump phenomenon changing from the regular to the chaotic attractor. The time history also detected the reverse jump from chaotic to regular attractor. It was predicted that for a sufficiently large noise level, the vibration response returns to the intermittent behavior with jumps between the regular and chaotic phenomena.

Velex and Ajmi [28] investigated the role of transmission errors as excitations in gear dynamics using some existing models and devising three-dimensional models of single-stage geared transmissions. It was observed that the time derivatives of no-load transmission errors (NLTE) appear as additional excitations whose contributions increase with speed and also depend on the nature of tooth deviations/errors. The spectrum analysis depicted that amplitude of low-frequency vibration generated from eccentricities and cumulative pitch errors are moderate in terms of time derivatives of NLTE. However, higher frequencies associated with individual tooth deviations yield amplitudes lower than those associated with low frequencies. It was deduced that minimizing the fluctuations of quasi-static transmission error under load, reduces displacements and reduces dynamic tooth loads.

Bonori and Pellicano [29] used the classical one-degree-freedom model to analyze non linear vibrations of spur gears in the presence of manufacturing errors. One-degree-of-freedom system included backlash, profile errors and time varying stiffness that was obtained on static basis by means of a finite element analysis. Statistical approach was used to involve transmission error combining profile error distribution given for each

tooth as a random basis. It was shown that manufacturing errors induce a considerable vibration amplitude increase at all frequencies. This behavior is more evident at low speeds, where contact loss can also occur. The presence of manufacturing errors magnifies the amplitude of vibration and leads to chaotic vibrations in a wide range of rotation speeds when the external torque is negligible. On the other hand, an extremely narrow region of chaos is observed in the absence of manufacturing errors. The use of measured errors gives more realistic information; however, a large set of gear pairs have to be measured in order to obtain a full statistical error distribution.

Mahalingam and Bishop [30] used modal analysis technique to resolve a multi-DOF discrete torsional system coupled by a pair of gears. An internal displacement excitation was applied within two mating gears as a harmonic function of total transmission error. Total transmission error is considered as the combination of mounting error of the geared system, manufacturing error of teeth, and elastic deformation of teeth. With a numerical example of a simplified four DOF system, natural frequencies and principal modes are derived. The modal inertia and stiffness coefficients are calculated to investigate the transient and periodic response and dynamic torque due to the internal displacement excitation. The resonant response and dynamic torque of the most influencing mode are calculated assuming a reasonable dynamic magnification factor.

1.7 Motivation for the Thesis Work

Above vibratory models investigated gear dynamics from different perspectives and identified several factors contributing to dynamic loads in geared systems. Manufacturing error, mounting error of bearings and gears, periodic variation of tooth elasticity, variation of meshing position, tooth wear, backlash, friction etc. are identified as the major sources of dynamic loading on gears generated by the system itself. The effect of the individual factors varies with rotation of gears and causes internal excitation, investigation of which does not capture the overall picture as a consequence of the combined effect. Finite Element Method is extensively used in recent works to analyze dynamic loads incorporating most of the above contributing factors and also to investigate coupling of lateral, torsional and axial responses. Such a discretization method, however, involves a large number of degrees of freedom that is in fact computationally less efficient and sometimes yields incorrect results.

Total transmission error approach [30] was found to be more realistic to investigate dynamic loads caused by internal excitation within the meshing gears as a periodic function of combined effect of manufacturing error, mounting error and elastic deformation. The interest grew more when modern optical encoder and highly sensitive accelerometers make it possible to precisely measure the total transmission error resulting from the tooth wear, manufacturing error, improper mounting of shafts, bearings and gears as well as the periodic changes of meshing stiffness. However, the discrete model holds a constant value for the torsional stiffness of the shafts and ignores the distributed mass and elasticity of the shafts. Moreover, the equivalent mass approach for lumping the gear pair is not able to investigate the responses of the gear and the pinion individually.

Mode shape of the discrete analysis on the other hand lacks consideration of rotational direction of the driving and driven gears. A continuous model is considered to be better for the investigation of the self-excited vibration that incorporates mass and physical properties of the shafts as well as the direction of rotation of the meshing gears.

1.8 Objectives and Scope of Work

The main objective of the thesis is to develop a continuous model to study the influence of self-excitation on torsional vibration of a geared shaft system. In the absence of external excitation, the equation of motion of the torsional vibration becomes homogeneous. However, the internal displacement excitation between the gear and the pinion introduces time-variable boundary conditions to the homogeneous partial differential equation of torsional vibration. Proposed model resolves the problem by converting the homogeneous equation of motion with non-homogeneous boundary conditions into a non-homogeneous equation with a set of homogeneous boundary conditions. It is a new continuous approach for analyzing the self-excited torsional vibration of geared system.

It is proposed to first study the lumped mass model [30] and then to develop a SIMULINK model for analyzing dynamic load of gear due to transient and steady state transmission error. The results of free torsional vibration of the proposed continuous model will be compared with the results of the numerical example in [30] based on the discrete model. Then the higher mode natural frequencies will be verified by devising the classical Rayleigh-Ritz model for the geared system. Boundary characteristic orthogonal

polynomial functions [39] will be used as deflection shape functions in the Rayleigh-Ritz model. A simplified gear model will be designed and tested to validate the proposed mathematical model and for rendering future extension of this study.

1.9 Organization of Thesis

In Chapter 1, an introduction to gear geometry, dynamic loading of gear, factors influencing the gear loadings are briefly explained. A complete literature review is provided, which gives an insight into the research done for analyzing the influence of different factors on dynamic loading of gears. It also includes the motivation, objectives and scope of the thesis work.

In Chapter 2, the 4DOF example [30] has been analyzed by developing a SIMULINK model to determine the response and dynamic torque due to the transient and steady state transmission error. Simulation results are analyzed and discussed. Magnification factor of resonant dynamic torque at the most influential mode is compared with the assumptions made in the numerical illustration [30], while determining the responses of individual lumped masses.

Chapter 3 develops a new continuous model for torsional vibration analysis of the geared system due to internal displacement excitation as a harmonic function approximating the total transmission error. The torsional vibration of the geared system is analyzed considering continuously distributed mass and torsional rigidity of the shafts. The proposed mathematical model resolves the problem of homogeneous partial differential equation of motion with non-homogeneous boundary conditions caused by

the harmonic transmission error in the gear pair. The natural frequencies and mode shape of the first four modes have been compared with the results of the discrete analysis. The responses of the driving and driven gears are displayed in time and frequency domains.

In chapter 4, the Rayleigh-Ritz torsional model for geared system is developed to compare the free vibration results of the continuous model. Boundary Characteristic Orthogonal Polynomial Functions are used as deflection shape functions. Deviations of natural frequencies from the Rayleigh –Ritz model are also analyzed.

Chapter 5 presents the experimental investigations on a simplified geared shaft. Results of the experimental model of the geared system are also displayed and discussed.

Chapter 6 discusses conclusions based on the results obtained and recommendations for the extension of the work in future.

CHAPTER 2

DISCRETE MODEL FOR GEARED SHAFT

2.1 Introduction to Discrete Model

The numerical example discussed in [30] is shown in figure 2.2.1 and is used as a base for the comparison of the results of the proposed mathematical model with the non-homogeneous time dependent boundary conditions. The angular deflection of the rotating masses are considered as the generalized co-ordinates of the torsional vibration model. The time variable ordinary differential equation of motion of the system is obtained using Lagrange's equations.

In this chapter natural frequencies and principal vibration modes of the 4DOF torsional model are analyzed. Periodic responses due to harmonic transmission error and torsional excitation have been analyzed employing SIMULINK models. The magnification factor of the resonant dynamic torque, approximated for the solution of the 4DOF torsional model [30] is also investigated.

2.2 Equations of Motion:

The geared system A has a driving sub-system B and driven sub-system C coupled by a pair of rigid gears $3'$ and $3''$. The sub-system B consists of two shafts having torsional stiffness K1 and K_2 and three rigid bodies having mass moments of inertia I_{P1}, I_{P2} and $I_{P3'}$ where as the sub-system C consists of one shaft with torsional stiffness K_3 and two rigid bodies with mass moments of inertia $I_{P3''}$ and I_{P4}.

A schematic diagram of the 4 DOF geared shaft system is shown in figure 2.2.1

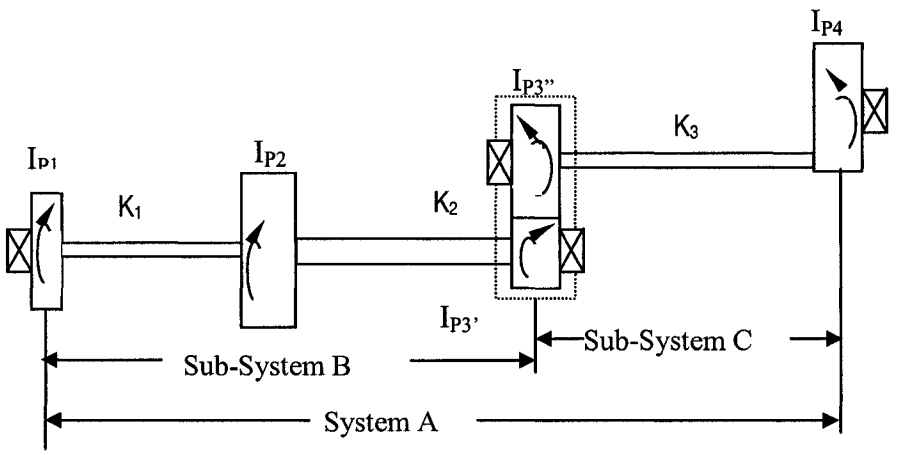

Figure 2.2.1 Schematic diagram of a 4-DOF lumped mass torsional model

For simplicity, disks and gears have been considered to be rigid and the shafts to be massless having constant elasticity all along the length. Non-linear effects such as backlash, friction, or gap between meshing teeth pair have been neglected.

With a constant gear ratio N, ideally the sub-system C rotates at N times the rotation of the sub-system B. Even accurately mounted gears with perfect tooth profile introduce an additional angular displacement due to variation of tooth deflection, which is termed as angular transmission error. With inclusion of mounting error and/ or teeth profile error the total transmission error further increases and the driven gear gets an additional angle of twist with respect to the driving gear.

If $q_{3'}$ and $q_{3''}$ are the angular displacements of the driving and driven gears and $\gamma(t)$ is the time variant angular transmission error, then $q_{3''}(t) = Nq_{3'}(t) + \gamma(t)$.

Similarly $\dot{q}_{3''}(t) = N\dot{q}_{3'}(t) + \dot{\gamma}(t)$

Since the sub-system B is capable of rotating the sub-system C, the total kinetic energy of the system is given by

$$T = \frac{1}{2}[I_{P1}\dot{q}_1^2 + I_{P2}\dot{q}_2^2 + I_{P3'}\dot{q}_{3'}^2 + I_{P3''}(N\dot{q}_{3'} + \dot{\gamma})^2 + I_{P4}\dot{q}_4^2]$$

$$= \frac{1}{2}[I_{P1}\dot{q}_1^2 + I_{P2}\dot{q}_2^2 + (I_{P3'} + N^2 I_{P3''})\dot{q}_{3'}^2 + 2NI_{P3''}\dot{q}_{3'}\dot{\gamma} + I_{P3''}\dot{\gamma}^2 + I_{P4}\dot{q}_4^2]$$

$$T = \frac{1}{2}[I_{P1}\dot{q}_1^2 + I_{P2}\dot{q}_2^2 + I_{P3}\dot{q}_3^2 + 2NI_{P3''}\dot{\gamma}\dot{q}_{3'} + I_{P3''}\dot{\gamma}^2 + I_{P4}\dot{q}_4^2] \qquad (2.1)$$

The mass moments of inertia of the mating gears are referred to the driving side and hence $I_{P3} = I_{P3'} + N^2 I_{P3''}$ and the corresponding angular displacement is that of the driving gear ($q_3 = q_{3'}$).

Strain energy of the system is given by

$$U = \frac{1}{2}\left[K_1(q_1 - q_2)^2 + K_2(q_2 - q_{3'})^2 + K_3(q_{3''} - q_4)^2\right]$$

$$= \frac{1}{2}\left[K_1(q_1 - q_2)^2 + K_2(q_2 - q_3)^2 + K_3(Nq_3 + \gamma - q_4)^2\right]$$

$$U = \frac{1}{2}K_1 q_1^2 + \frac{1}{2}K_1 q_2^2 - K_1 q_1 q_2 + \frac{1}{2}K_2 q_2^2 + \frac{1}{2}K_2 q_3^2 - K_2 q_2 q_3 + \frac{1}{2}K_3 N^2 q_3^2$$

$$+ \frac{1}{2}K_3\gamma^2 + \frac{1}{2}K_3 q_4^2 + NK_3 q_3\gamma - K_3\gamma q_4 - NK_3 q_3 q_4 \qquad (2.2)$$

Applying Lagrange's equation with generalized co-ordinates q_i, $\frac{d}{dt}(\frac{\partial T}{\partial \dot{q}_i}) + \frac{\partial U}{\partial q_i} = Q_i$,

One can get four equations of motion for *i = 1, 2, 3, 4*, which can be written in the matrix form as:

$$\begin{bmatrix} I_{P1} & 0 & 0 & 0 \\ 0 & I_{P2} & 0 & 0 \\ 0 & 0 & I_{P3} & 0 \\ 0 & 0 & 0 & I_{P4} \end{bmatrix} \begin{Bmatrix} \ddot{q}_1 \\ \ddot{q}_2 \\ \ddot{q}_3 \\ \ddot{q}4 \end{Bmatrix} + \begin{bmatrix} K_1 & -K_1 & 0 & 0 \\ -K_1 & (K_1 + K_2) & -K_2 & 0 \\ 0 & -K_2 & K_2 + N^2 K_3 & -NK_3 \\ 0 & 0 & -NK_3 & K_3 \end{bmatrix} \begin{Bmatrix} q_1 \\ q_2 \\ q_3 \\ q_4 \end{Bmatrix} =$$

$$\begin{Bmatrix} Q_1 \\ Q_2 \\ Q_3 - NK_3\gamma - NI_{P3}\ddot{\gamma} \\ Q_4 + K_3\gamma \end{Bmatrix} \qquad (2.3)$$

where Q_1, Q_2, Q_3, Q_4 *are* the periodic torsional load applied to the system and $\gamma(t)$ is the internal displacement excitation due to the periodic transmission error within the meshed teeth. Even in the absence of the external torsional loading, the equation (2.3) remains non-homogeneous.

$$\begin{bmatrix} I_{P1} & 0 & 0 & 0 \\ 0 & I_{P2} & 0 & 0 \\ 0 & 0 & I_{P3} & 0 \\ 0 & 0 & 0 & I_{P4} \end{bmatrix} \begin{Bmatrix} \ddot{q}_1 \\ \ddot{q}_2 \\ \ddot{q}_3 \\ \ddot{q}4 \end{Bmatrix} + \begin{bmatrix} K_1 & -K_1 & 0 & 0 \\ -K_1 & (K_1+K_2) & -K_2 & 0 \\ 0 & -K_2 & K_2+N^2K_3 & -NK_3 \\ 0 & 0 & -NK_3 & K_3 \end{bmatrix} \begin{Bmatrix} q_1 \\ q_2 \\ q_3 \\ q_4 \end{Bmatrix} = \begin{Bmatrix} 0 \\ 0 \\ -NK_3\gamma - NI_{P3}\ddot{\gamma} \\ K_3\gamma \end{Bmatrix}$$

(2. 4)

The right hand side of the equation (2.4) thus provides the forcing function due to the internal displacement excitation generated within the meshed teeth of coupled gears.

The homogeneous form of equation (2.4) is used to study the free vibration behaviour of the system. Accordingly, the homogeneous form is given by:

$$\begin{bmatrix} I_{P1} & 0 & 0 & 0 \\ 0 & I_{P2} & 0 & 0 \\ 0 & 0 & I_{P3} & 0 \\ 0 & 0 & 0 & I_{P4} \end{bmatrix} \begin{Bmatrix} \ddot{q}_1 \\ \ddot{q}_2 \\ \ddot{q}_3 \\ \ddot{q}4 \end{Bmatrix} + \begin{bmatrix} K_1 & -K_1 & 0 & 0 \\ -K_1 & (K_1+K_2) & -K_2 & 0 \\ 0 & -K_2 & K_2+N^2K_3 & -NK_3 \\ 0 & 0 & -NK_3 & K_3 \end{bmatrix} \begin{Bmatrix} q_1 \\ q_2 \\ q_3 \\ q_4 \end{Bmatrix} = \begin{Bmatrix} 0 \\ 0 \\ 0 \\ 0 \end{Bmatrix}$$

(2.5)

The equation (2.5) can be symbolically represented as:

$$[J]\{\ddot{q}\} + [K]\{q\} = \{0\} \qquad (2.6)$$

Under free vibration conditions the system will vibrate with its natural frequencies ω_i, [i = *1, 2, 3 and 4* for a 4DOF discrete model], with

$q(t) = A\sin\omega_i t$, where A is the amplitude of the vibration, and

$\ddot{q}(t) = -A\omega_i^2 \sin\omega_i t = -\omega_i^2 q(t)$

The eigen values and eigen vectors can be obtained by solving the eigen value problem

$$[K]\{q\} - \omega_i^2[J]\{q\} = \{0\}$$

$$([K] - \lambda_i[J])\{q\} = \{0\} \text{ where, } \lambda_i = \omega_i^2 \tag{2.7}$$

Since $q(t)$ has a finite value, the nontrivial solution of the equation (2.7) is possible only if the determinant of $([K] - \lambda_i[J])$ vanishes. Hence

$$|[K] - \lambda_i[J]| = 0 \tag{2.8}$$

The roots of the characteristic equation (2.8) are the eigen values, the positive square roots of which are the natural frequencies ω_i. For each value of λ_i the equation (2.7) has a nontrivial vector solution $\{q^{(i)}\}$ termed as eigen vector which represents the natural mode of vibration.

2.3 Results of Free Vibration:

Solution of the eigen value problem in equation (2.8) will provide four natural frequencies $\omega_1, \omega_2, \omega_3$ and ω_4 and a set of modal matrix $\left[\{q_i^{(1)}\}, \{q_i^{(2)}\}, \{q_i^{(3)}\}, \{q_i^{(4)}\}\right]$. After normalization one can get the normal modes of the system as $\left[\{\psi_i^{(1)}\}, \{\psi_i^{(2)}\}, \{\psi_i^{(3)}\}, \{\psi_i^{(4)}\}\right]$.

The parameters of the numerical example in [30] used in this study are as follows:

$I_{P1} = 0.6$ kg-m^2 $\quad$ $I_{P4} = 2$ Kg-m^2 $\quad$ Gear ratio, $N = \frac{1}{3}$

$I_{P2} = 10$ Kg-m^2 $\quad$ $K_1 = 800{,}000$ N-m/rad

$I_{P3'} = 0.1$ Kg-m^2 $\quad$ $K_2 = 1{,}200{,}000$ N-m/rad

$I_{P3''} = 0.6$ Kg-m^2 $\quad$ $K_3 = 800{,}000$ N-m/rad

Table 2.3.1 provides the natural frequencies of the system. The corresponding mode shapes are given in Table 2.3.2. These mode shapes specify the actual angle of rotation at the four degrees of freedom. Each column of the table represents a mode. It must be noted that at the gear location at station 3, the angular deflection corresponds to driving side and at the station 4, the angular deflection corresponds to the driven side.

TABLE 2.3.1 NATURAL FREQUENCIES OF 4DOF LUMPED MASS MODEL

Modes	1st	2nd	3rd	4^{th}
Natural Frequencies	0	5,881	11,350	26,797

TABLE 2.3.2 NORMAL MODES:

1st	2nd	3rd	4th
1	1	1	1
1	0.7155	-0.059483	-4.906
1	-1.7359	-0.065572	313.1
0.33333	-11.199	0.0086338	-5.5851

The mode shapes are shown in figures 2.3.1 to 2.3.4.

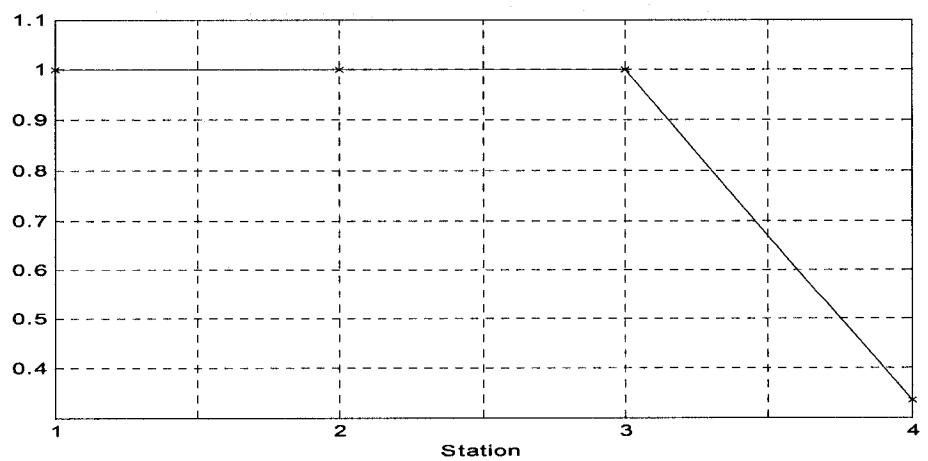

Figure 2.3.1 Mode shape at rigid body mode of the discrete model

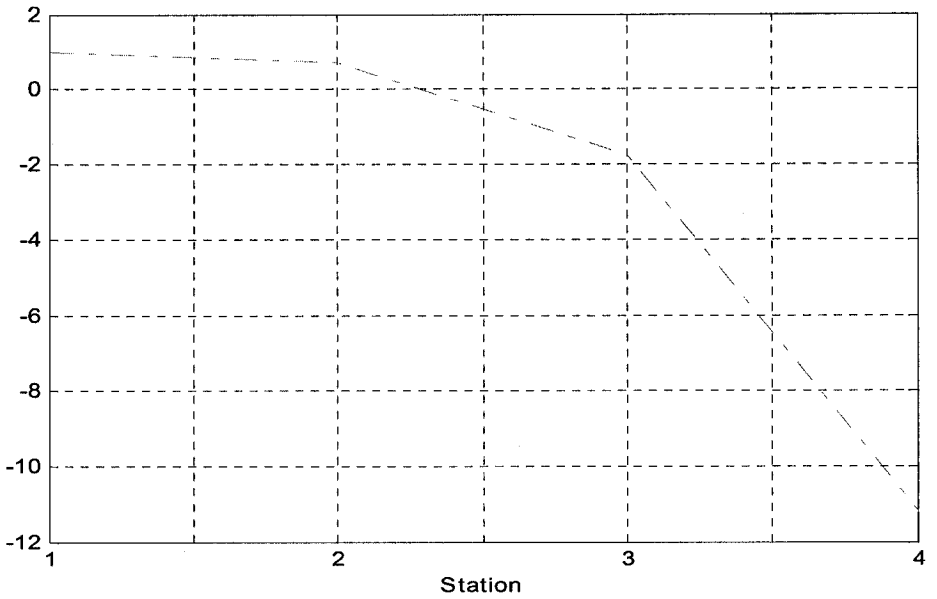

Figure 2.3.2 Mode shape at 2nd natural frequency of the discrete model

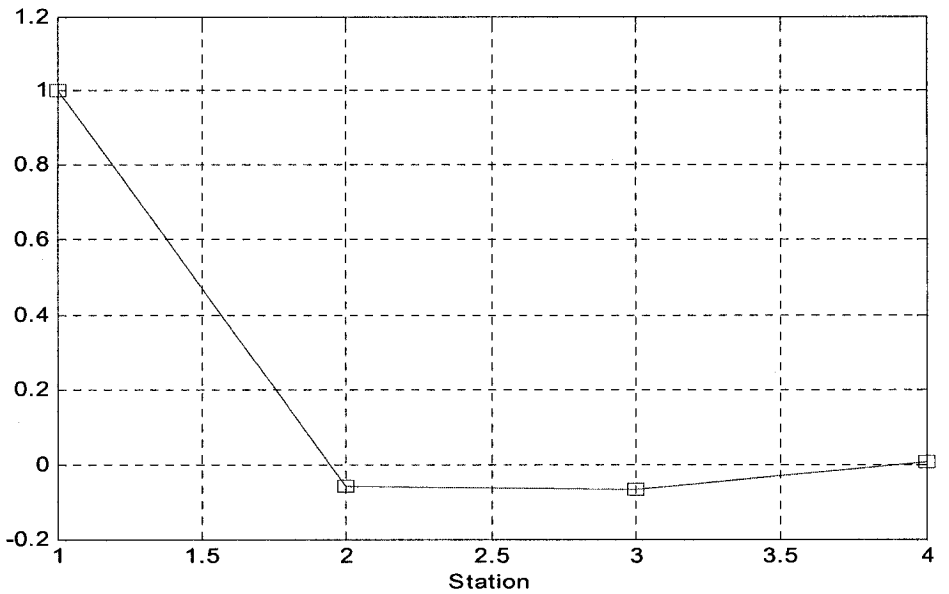

Figure 2.3.3 Mode shape at 3rd natural frequency of discrete model

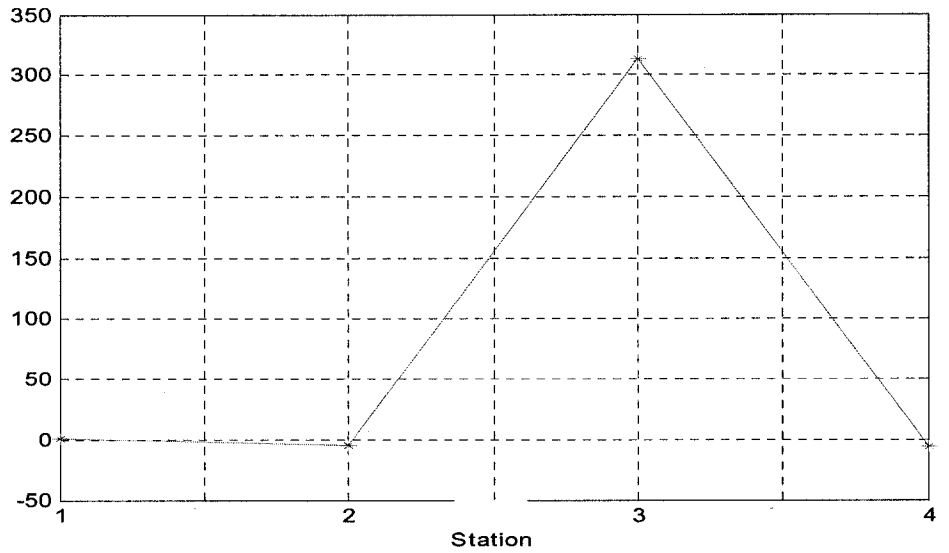

Figure 2.3.4 Mode shape at 4th natural frequency of discrete model

In a parallel geared system, direction of rotation of the driven shaft is opposite to that of the driving shaft. This phenomenon is observed in the 3rd and 4th mode shapes. Accordingly, in the rigid body mode (mode-1) and 2nd mode, angular deviations of the driving and driven gears corresponding to the stations 3 and 4 should have been in different direction. However, they are in the same direction. Thus it has been observed that the discrete analysis does not consider the direction of rotation.

2.4 Modal Analysis

With the derived normal modal matrix, the orthogonality of the normal modes can be verified. Since the mass moment of inertia matrix is a symmetric matrix, we have

$\{\psi^{(i)}\}^T [J]\{\psi^{(j)}\} = [\chi]$ for i = j

and $\{\psi^{(i)}\}^T [J]\{\psi^{(j)}\} = 0$ for i $\neq$ j

2.5 Simulation of Forced Vibration:

Equation (2.3) represents the governing equation of motion for the torsional vibration of the system illustrated here. A simulation model is formulated using MATLAB SIMULINK for equation (2.3) in order to analyze the angular deflection-responses of the four discrete masses.

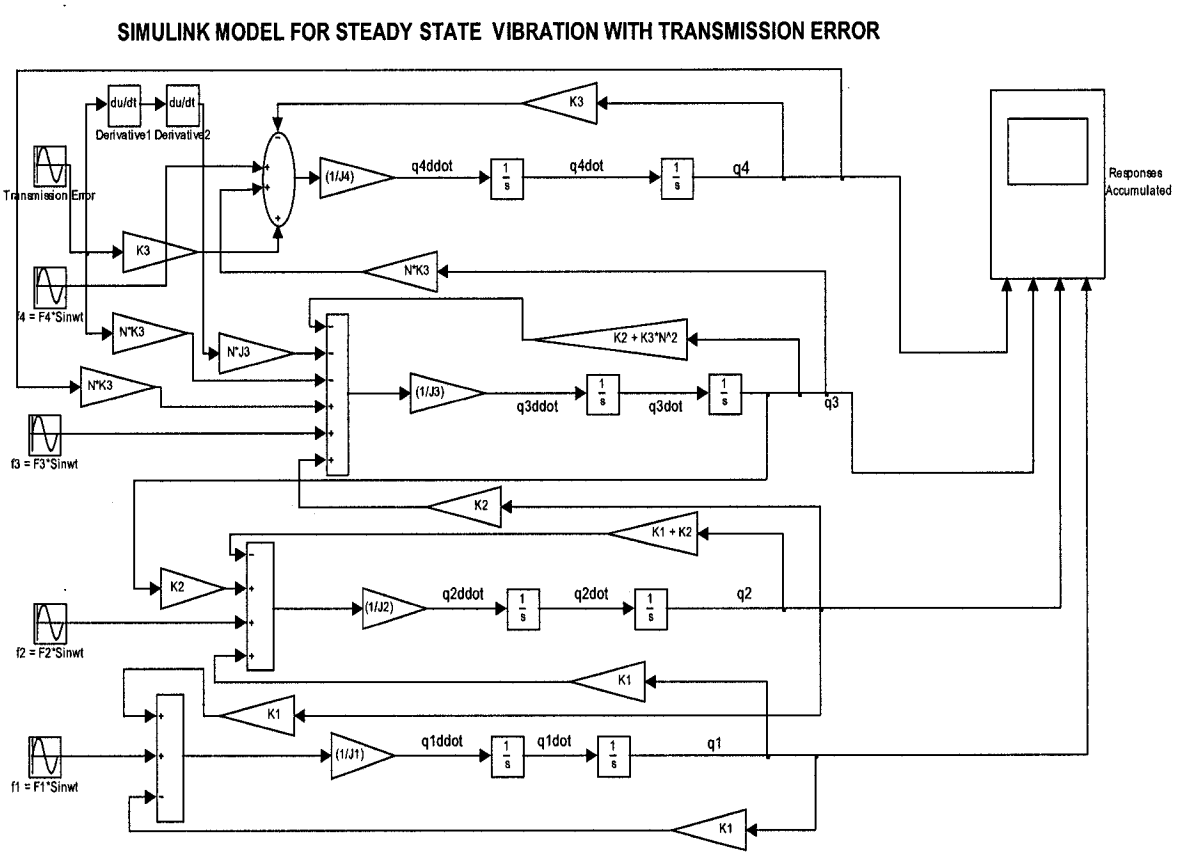

Figure 2.5.1 SIMULINK model for steady-state vibration due to internal excitation of total transmission error and external excitation

Responses of each mass element with different values of transmission errors in the absence as well as in the presence of external torsional loads are shown in the following figures 2.5.2 to 2.5.9. In each case the responses of disk-1, disk-2, and the equivalent mass 3 and disk-4 are arranged from top to bottom chronologically.

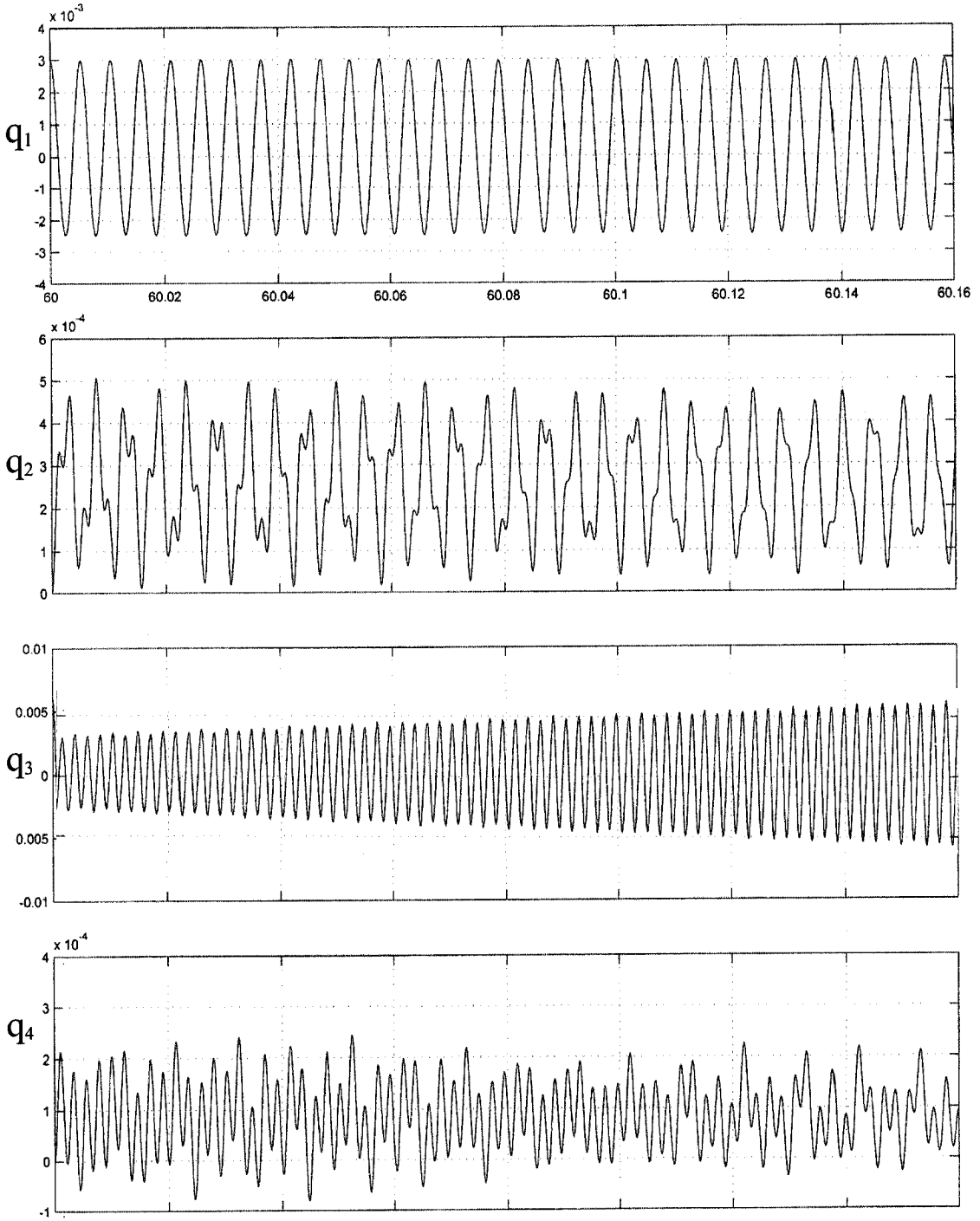

Figure 2.5.2 Responses of mass elements with transmission error in radian, $\gamma(t) = .0001 \sin \omega t$ and external excitation in N-m, $F(t) = 0$; $\omega = 1256.6$ rad/s

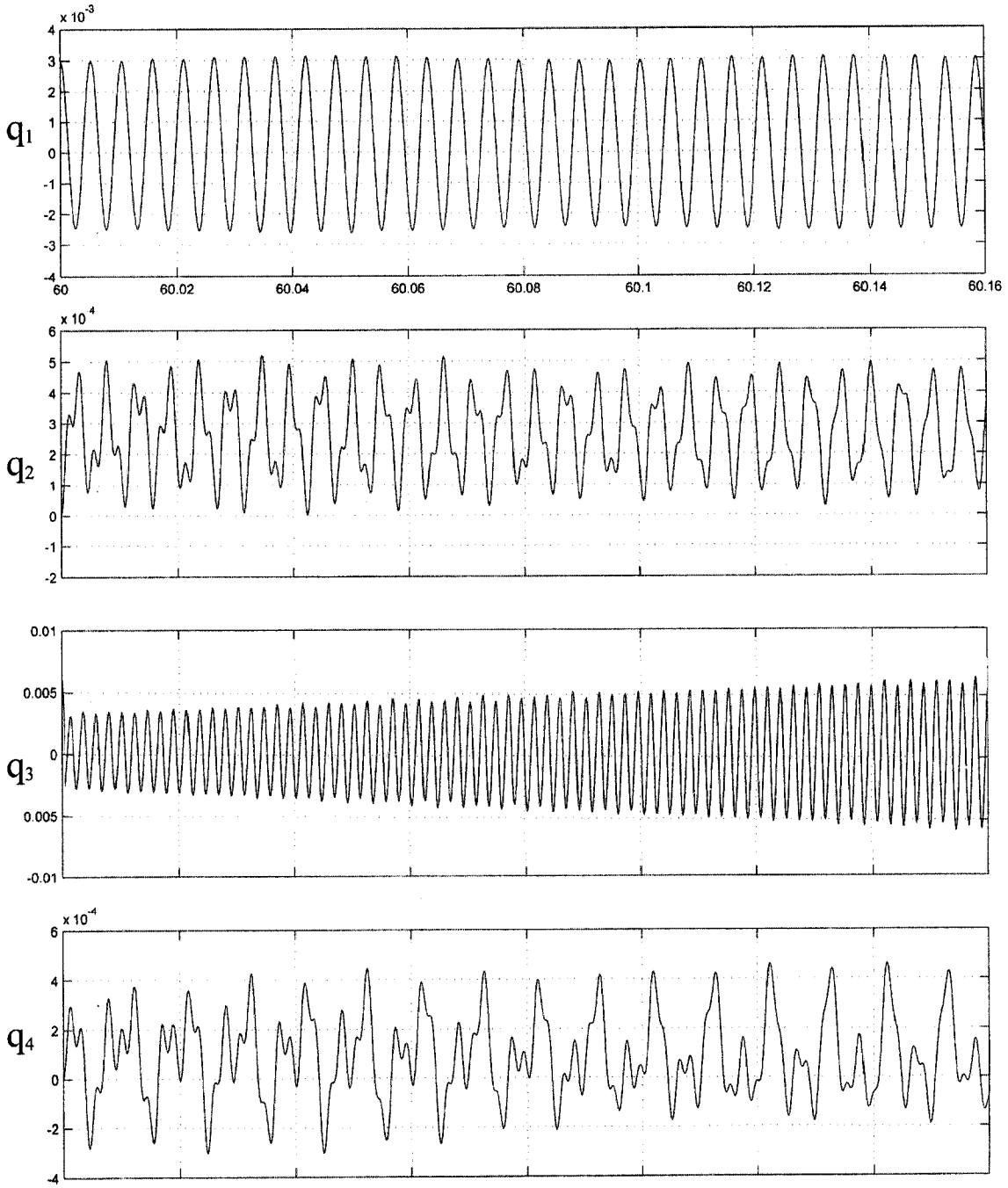

Figure 2.5.3 Responses of mass elements with transmission error in radian, $\gamma(t) = .0005 \sin \omega t$ and external excitation in N-m, $F(t) = 0$; $\omega = 1256.6$ rad/s

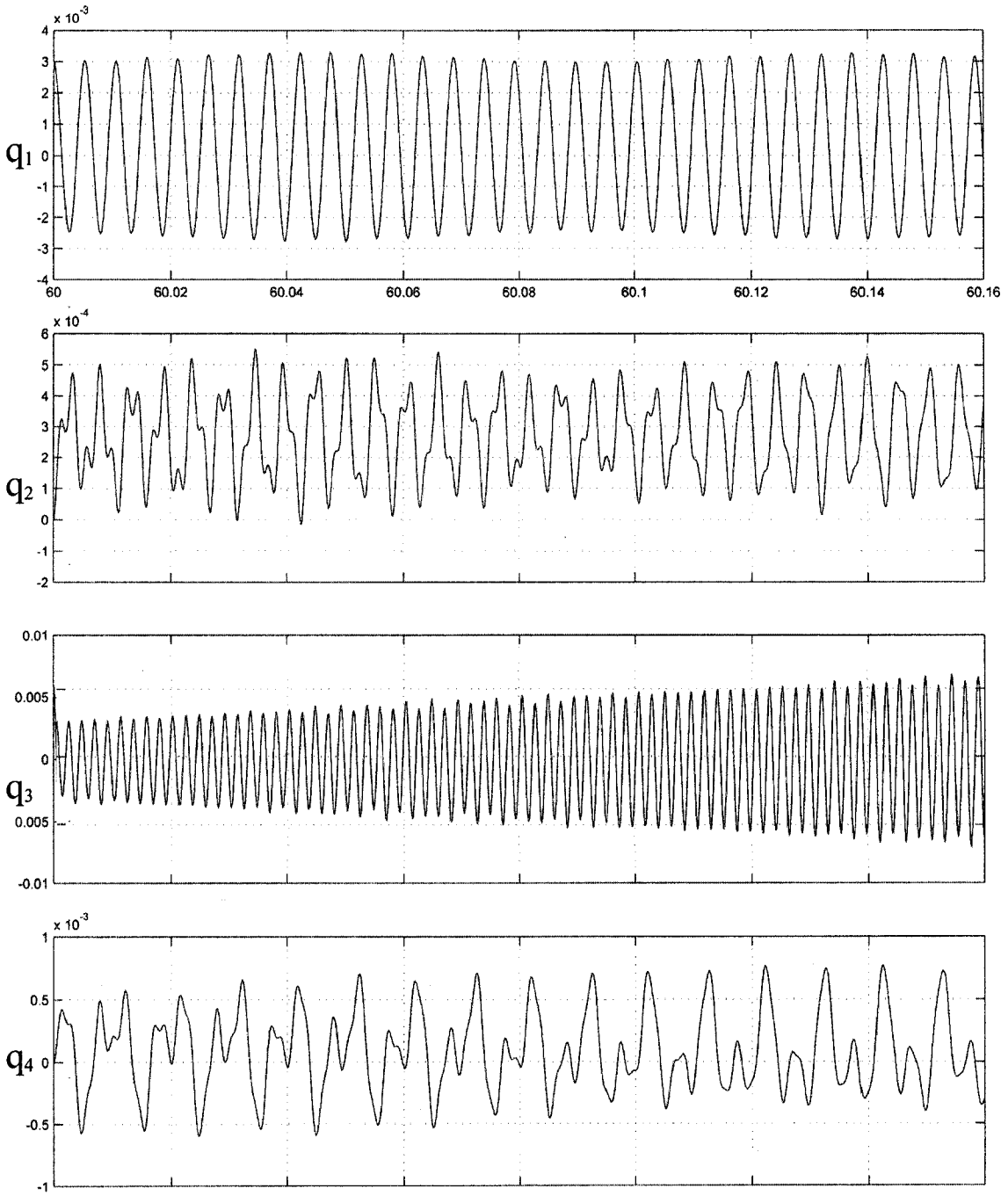

Figure 2.5.4 Responses of mass elements with transmission error in radian, $\gamma(t) = .001 \sin \omega t$ and external excitation in N-m, $F(t) = 0$; $\omega = 1256.6$ rad/s

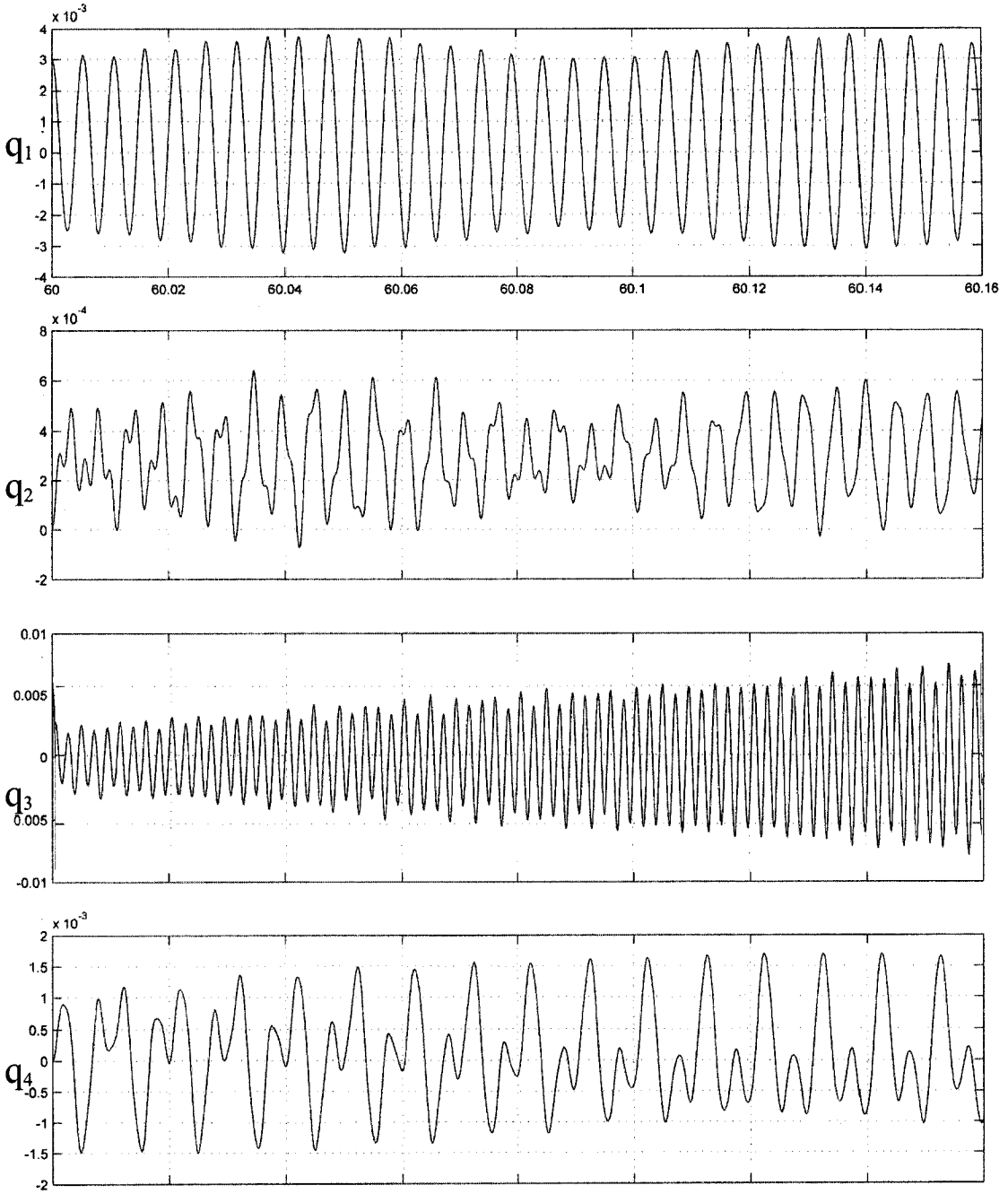

Figure 2.5.5 Responses of mass elements with transmission error in radian, $\gamma(t) = .0025 \sin \omega t$ and external excitation in N-m, $F(t) = 0$; $\omega = 1256.6$ rad/s

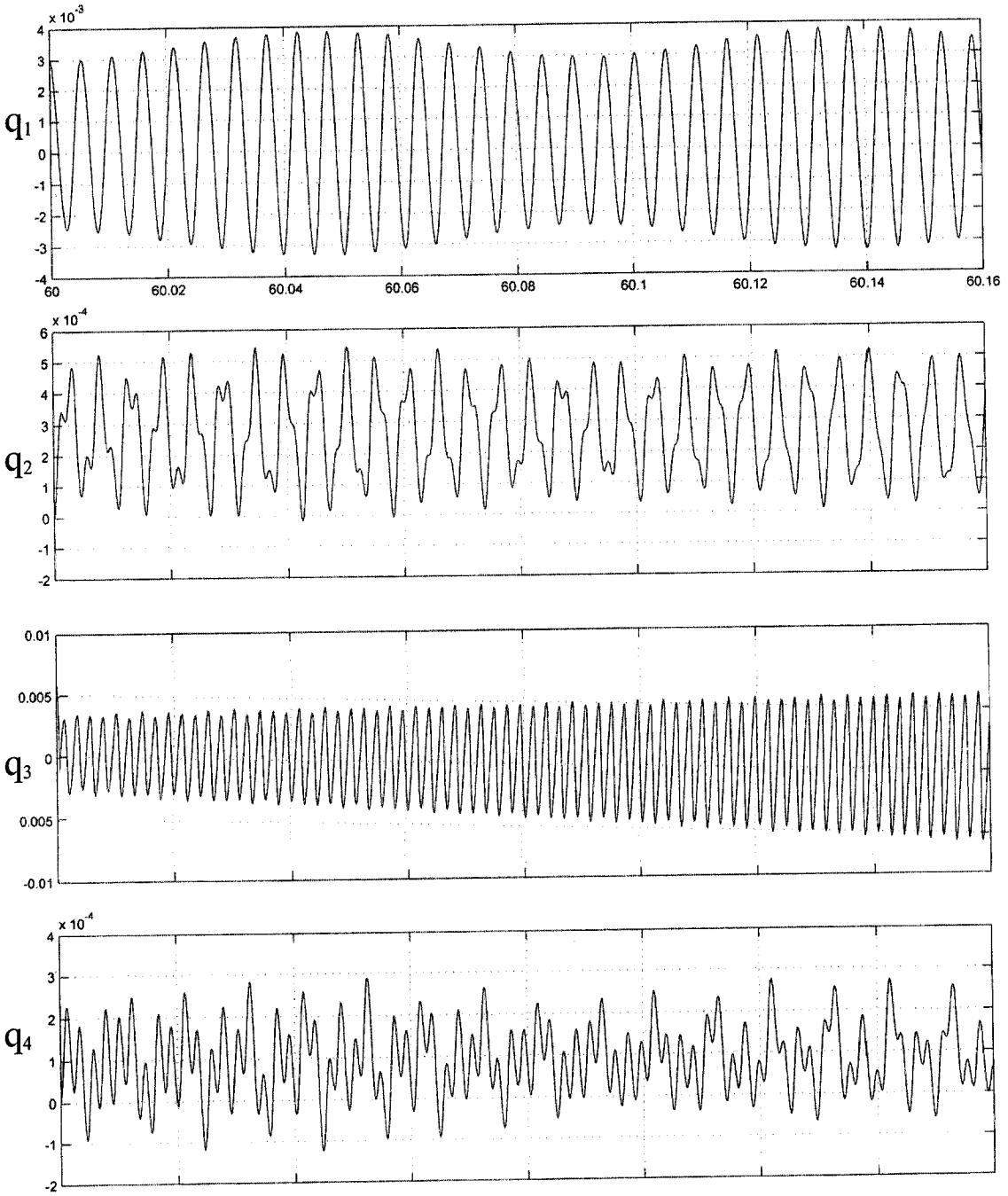

Figure 2.5.6 Responses of mass elements with transmission error in radian, $\gamma(t) = .0001 \sin \omega t$ and external excitation in N-m, $F(t) = 50 \sin \omega t$; $\omega = 1256.6$ rad/s

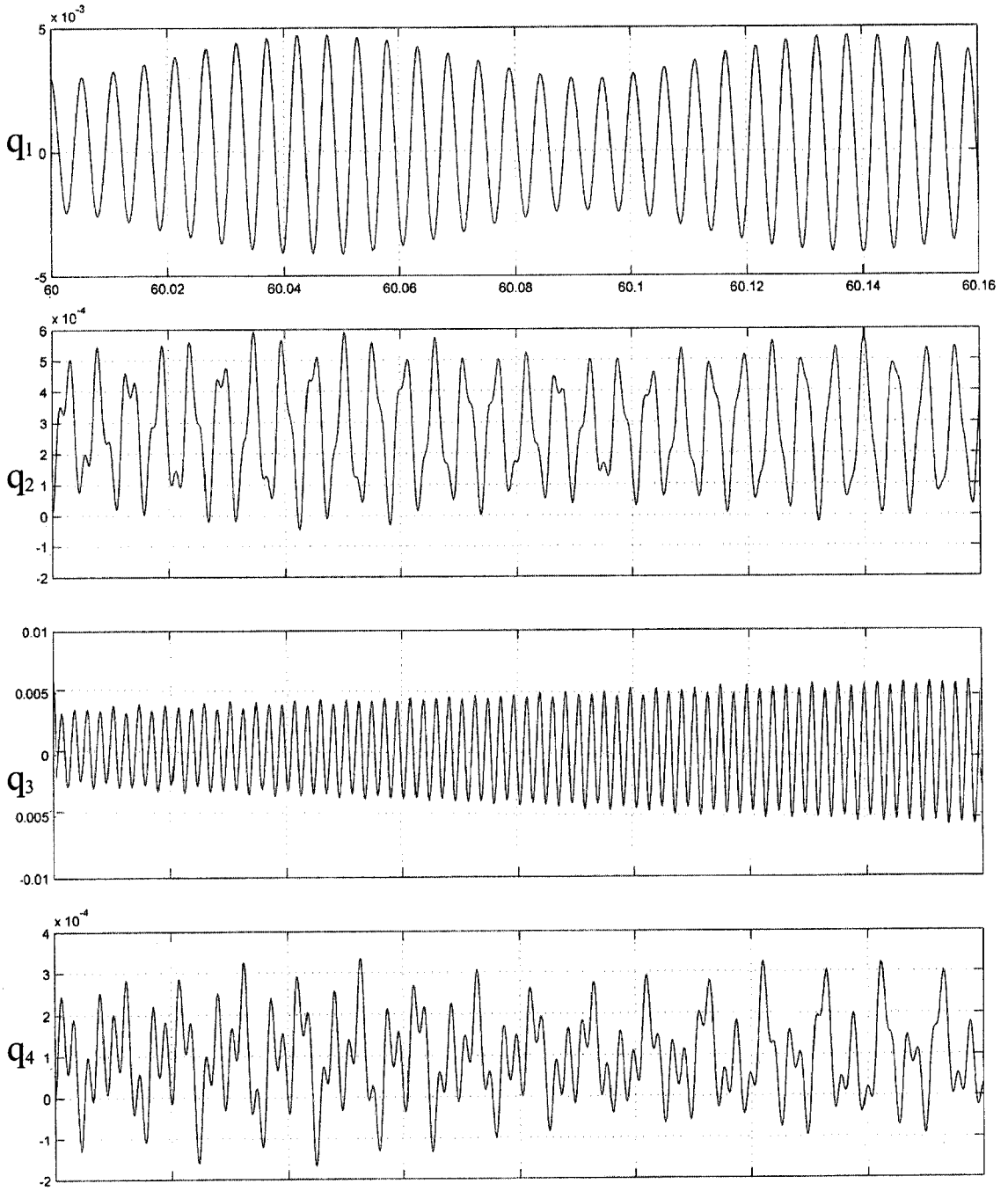

Figure 2.5.7 Responses of mass elements with transmission error in radian, $\gamma(t) = .0001 \sin \omega t$ and external excitation in N-m, $F(t) = 100 \sin \omega t$; $\omega = 1256.6$ rad/s

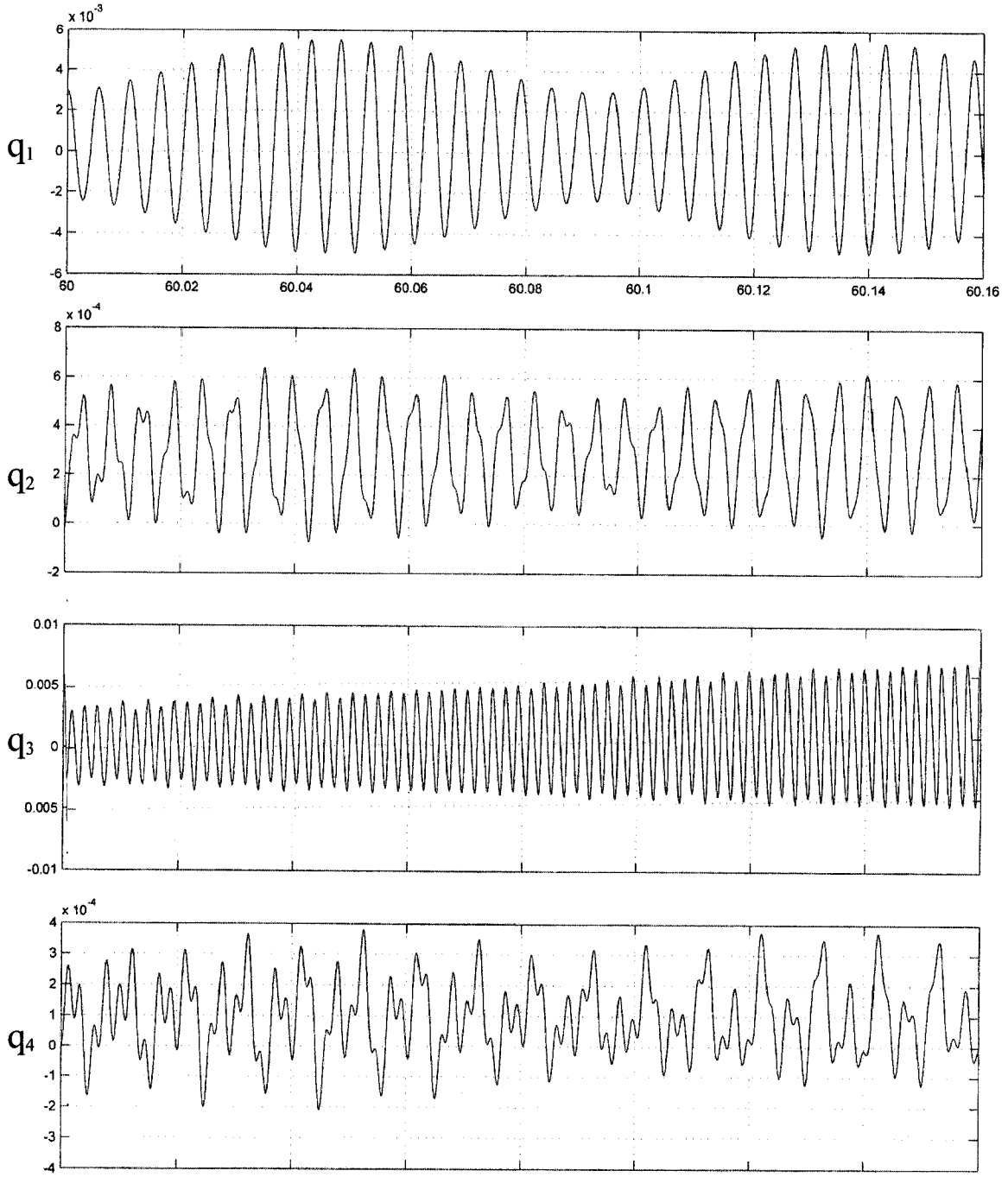

Figure 2.5.8 Responses of mass elements with transmission error in radian, $\gamma(t) = .0001 \sin \omega t$ and external excitation in N-m, $F(t) = 150 \sin \omega t$; $\omega = 1256.6$ rad/s

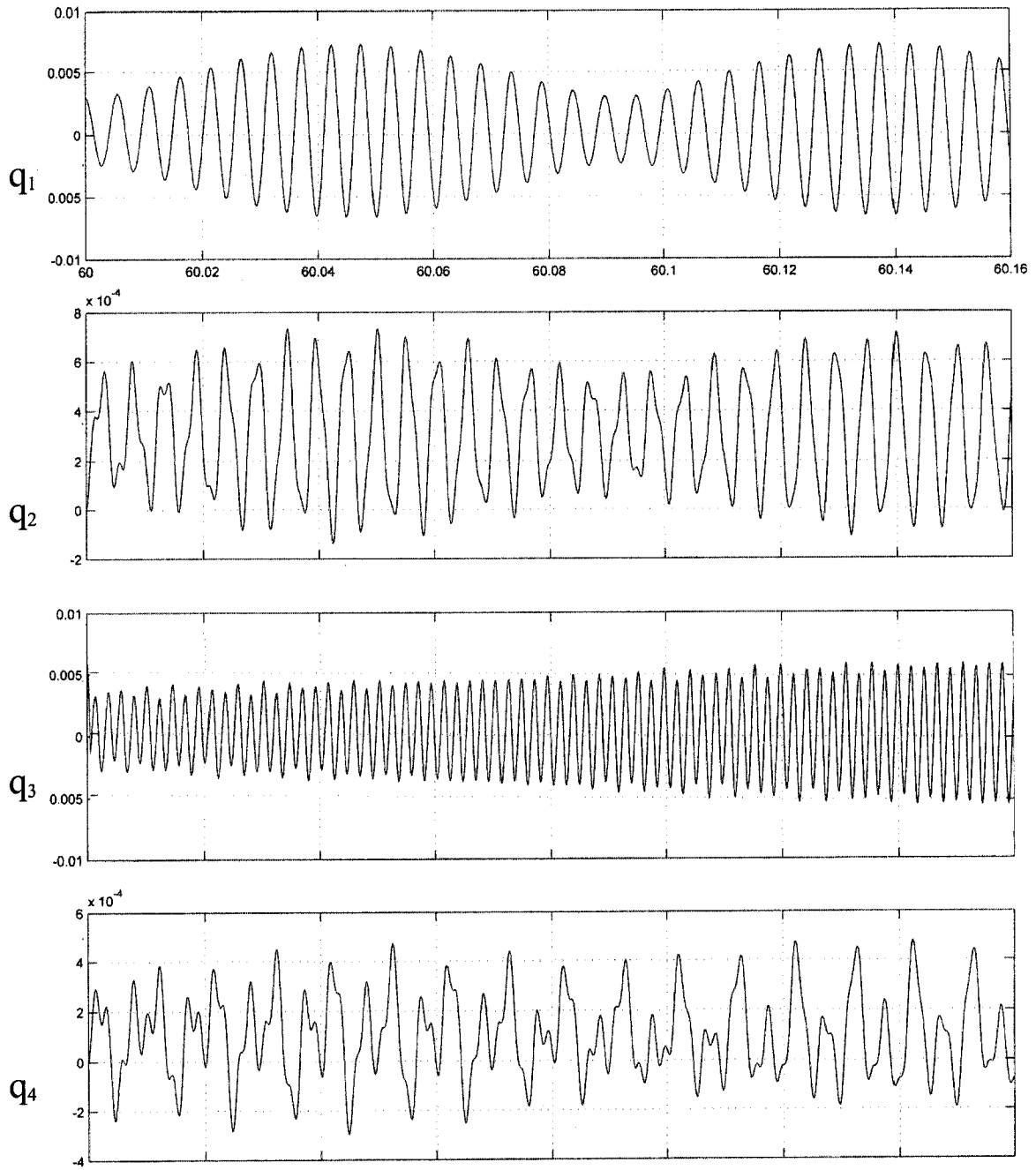

Figure 2.5.9 Responses of mass elements with transmission error in radian, $\gamma(t) = .0001 \sin \omega t$ and external excitation in N-m, $F(t) = 250 \sin \omega t$; $\omega = 1256.6$ rad/s

Figures 2.5.2 to 2.5.5 represent the steady state responses of the discrete masses due to harmonic transmission error in the absence of the external excitation. On the other hand figures 2.5.6 to 2.5.9 show the influence of the external excitation on the geared system with negligible transmission error. It has been observed that the torsional vibration of the equivalent mass (mass 3) is mainly caused by the transmission error. The 3rd mass responds more significantly at the higher transmission error. However, with increase in external excitation, torsional vibration of the equivalent mass remains the same. It has also been observed that the torsional vibration of the 4th mass gradually increase with increase in transmission error, although the response is far less than the equivalent mass. Conversely, the internal excitation has negligible influence on the 1st mass, and the 2nd mass. Torsional vibrations of these two masses are mainly occurred due to the external excitation.

External excitations at forcing frequency introduce beat vibration, which is distinctly shown in figure 2.5.8 and 2.5.9. The beat vibration occurs as the forcing frequency approaches the 3rd natural frequency. Frequency of the beat vibration is the difference of the forcing frequency, 1256.6 rad/s (12,000 cpm) and the 3rd natural frequency of the geared system, 11,350 cpm.

Frequency of the torsional vibration of the equivalent mass is observed to be 2.25 times the driving shaft frequency although the gear speed ratio is 1/3. The reason behind the phenomenon is not identified.

2.6 Dynamic Torque

The Lagrange's equation with the generalized co-ordinate $\gamma(t)$ yields the dynamic torque

$$\tau_i = \frac{d}{dt}\left(\frac{\partial T}{\partial \dot{\gamma}}\right) + \frac{\partial U}{\partial \gamma} \tag{2.7}$$

Differentiating the system kinetic energy in equation (2.1) w.r.t. $\dot{\gamma}(t)$ yields

$$\frac{\partial T}{\partial \dot{\gamma}} = NI_{P3'} + I_{P3'}\dot{\gamma}$$

Again differentiating equation (2.2) w.r.t $\gamma(t)$ reveals that $\frac{\partial U}{\partial \gamma} = K_3\gamma + NK_3q_3 - K_3q_4$

Noting that $q_3 = q_{3'}$ equation (2.7) becomes:

$$\tau(t) = NI_{P3'}\ddot{q}_3 + I_{P3'}\ddot{\gamma} + K_3\gamma + NK_3q_3 - K_3q_4 \tag{2.8}$$

The numerical example [30] analyzed the dynamic torque of an engine driven geared system with a pinion of 20 teeth. At the engine speed of 1310 rpm, the gear mesh frequency (26,200 cpm) is close to the most dominating, 4th natural frequency (26,797 cpm). Magnification factor of the resonant torque at the 4th mode was assumed to be 30 times the steady-state dynamic torque. Such magnification was used to derive torsional responses by modal analysis. A SIMULINK model of the equation (2.8) can be devised to investigate the steady-state and resonant dynamic torque.

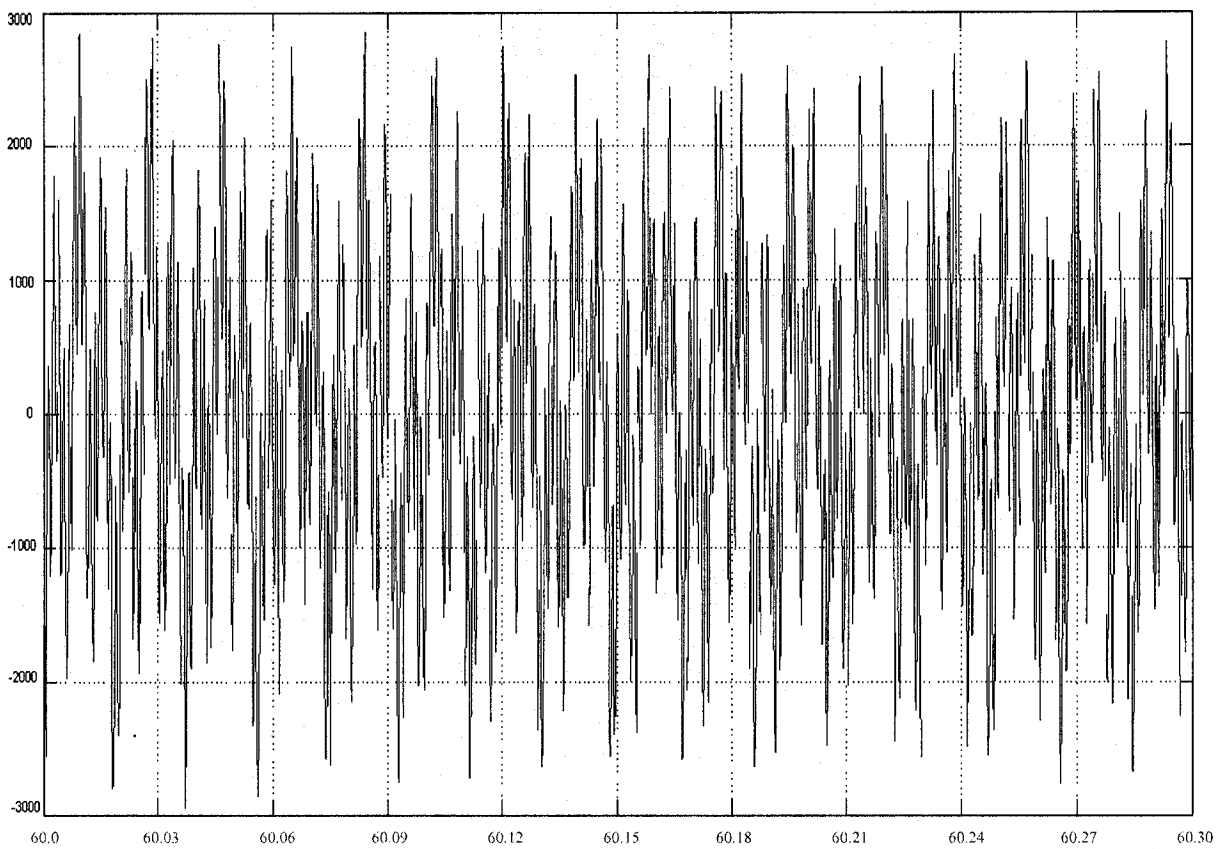

Figure 2.6.1 Dynamic torque of a geared system with transmission error in radian: $0.0001 \sin \omega t$; ω = 137.2 rad/s (f=1310 cpm)

Figure 2.6.1 shows the synchronous dynamic torque of about 2800 N-m at the shaft speed of 1310 rpm (137.2 rad/s). The amplitude of transmission error of the driven gear with respect to the driving gear has been considered as 0.0001 radian.

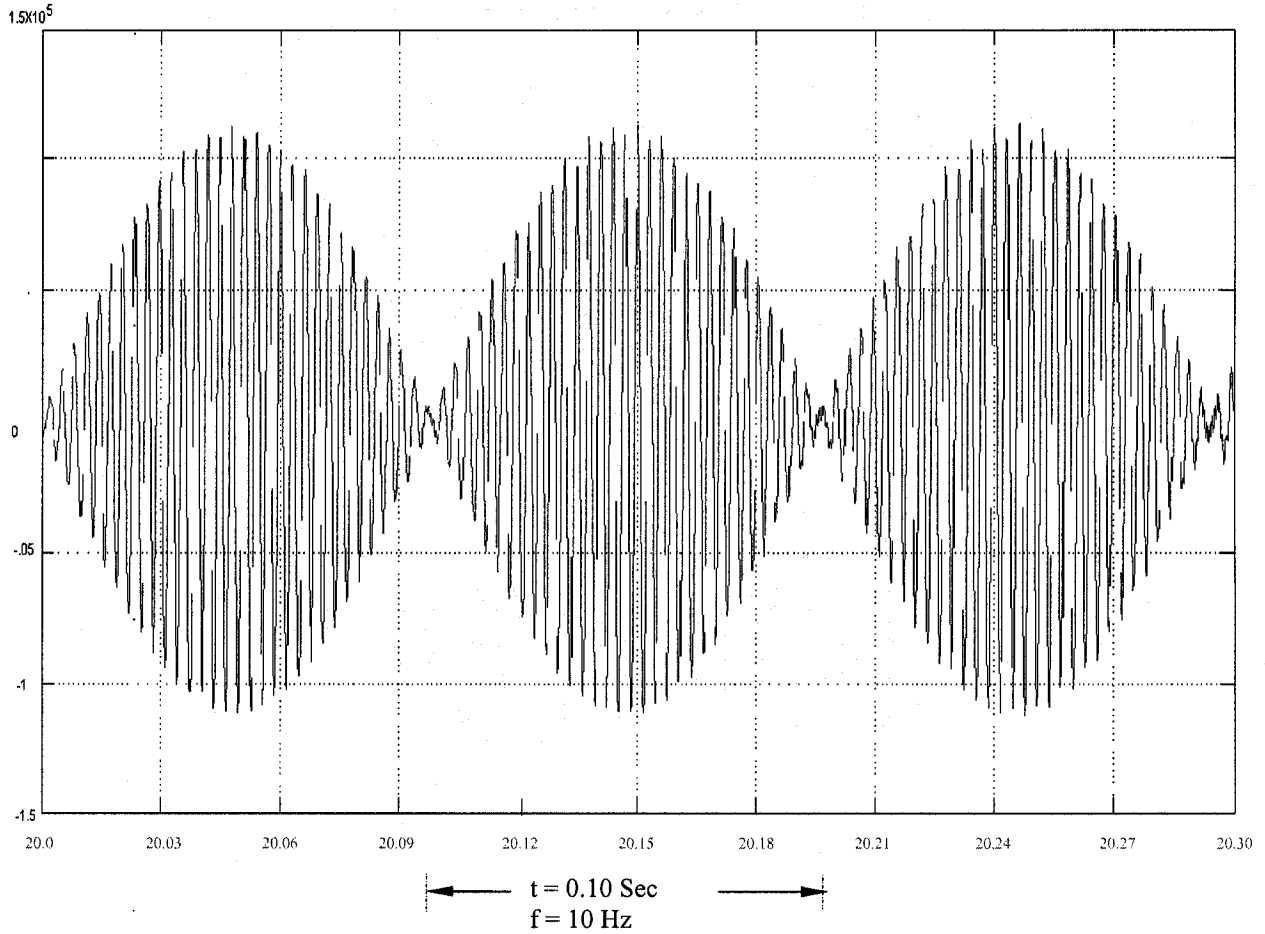

Figure 2.6.2 Dynamic torque of a geared system with transmission error in radian: $0.0001\sin\omega t$ $\omega = 2{,}743.65$ rad/s (f = 26,200 cpm)

With a driving gear of 20 teeth, the gear mesh frequency of the gear drive is 1310 X 20 cpm = 26,200 cpm which is close to the fourth natural frequency, 26,797 cpm. The resonant dynamic torque is about 117,600 N-m as shown in figure 2.6.2. Thus the amplification factor of the resonant dynamic torque is about 42 times the steady state dynamic torque at shaft frequency 1310 rpm. It can be compared to the assumed magnification factor: 30 in the numerical example [30] while deriving the 4^{th}-mode resonant responses of discrete masses by modal analysis. A beat vibration is thereby

observed at the frequency of (26,797 – 26,200) = 597 cpm = 10 Hz, due to the responses at the forcing frequency of and the fourth natural frequency.

2.7 Summary

The free vibration analysis of the 4DOF discrete model yields natural frequencies and corresponding mode shapes. It is observed from the normalized mode shapes that the discrete analysis neglects the direction of rotation of the driven gear with respect to the driving gear. Meanwhile, the forced vibration analysis indicates that the geared systems experiences torsional vibration due to internal displacement excitation in the absence of torsional excitation. The simulation results provide more realistic value of magnification factor of dynamic torque at the 4^{th} natural frequency.

In this model, Mass-3 is regarded as the equivalent mass of driving and driven gears. Thus mode shapes and responses do not clearly identify the angular deflections of driving and driven gears. Moreover, the geared shafts of discrete model are considered massless with constant elasticity. But in reality, shafts possess mass. Mass and elasticity of the shafts may also vary from point to point along the length of the shaft. For accurate investigation of the influence of internal excitation, the following chapter will study the system with shafts having continuously distributed mass and elasticity. The direction of rotation of driven gear with respect to the driving gear will also be taken under consideration.

CHAPTER 3

CONTINUOUS MODEL WITH TIME DEPENDENT BOUNDARY CONDITIONS

3.1 Introduction to Continuous Model

In the previous chapter it is observed that geared systems experience significant torsional vibrations due to the periodic transmission error even in the absence of external excitation. However, discrete analysis does not consider mass and elasticity of geared shafts. For more realistic analysis of the torsional vibration of the geared system, a continuous model is proposed in this chapter. In addition to the distributed mass and elasticity of the geared shafts, the direction of rotation of the driven sub-system with respect to the driving sub-system is maintained in the analysis.

For approaching a continuous model for the geared system illustrated in the previous chapter, position of each point in the elastic system needs to be specified using a coordinate system. The equation of motion then takes the form of a partial differential equation with respect to time and space in each of the three regions of the geared system. Each region has specific boundary conditions, which also have to be satisfied by the solution.

3.2 Mathematical Model

In the proposed continuous torsional model of the geared system it is assumed that the shape of the cross sectional area of each of the shafts is such that the motion can be regarded as a torsional twist of the cross-sectional plane as a whole and without warping. The shaft material is also considered isotropic and homogeneous.

As in the previous chapter the driving and driven sides of the geared system here also are termed as sub-systems B and C, respectively. The shafts of both the sub-systems are supported on rigid bearings. The torsional stiffness of each shaft is represented by the elastic properties.

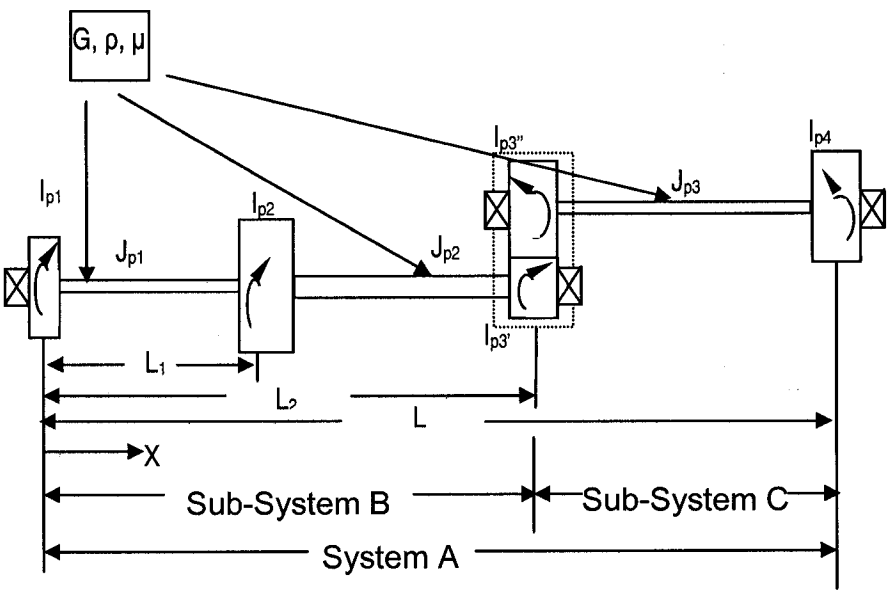

Figure 3.2.1 Schematic diagram of the proposed continuous model

The material properties are given in Table 3.2.1.

TABLE 3.2.1 MATERIAL PROPERTIES

Material Properties	Symbol	Unit	
Poisson's Ratio	μ	-	0.3
Modulus of Rigidity	G	N/m^2	$8.0769X10^{10}$
Density	ρ	Kg/m^3	7800

3.2.1 EQUATIONS OF MOTION

The three shafts are made of the same material. Consequently, the governing partial differential equation for the torsional vibration of the geared system with periodic torsional excitation $\tau(t)$ can be represented by:

$$GJ_p(x)\frac{\partial^2\theta(x,t)}{\partial x^2}+\tau(t)=\rho(x)J_p(x)\frac{\partial^2\theta(x,t)}{\partial t^2}$$

$$\text{or } \rho(x)J_p(x)\ddot{\theta}(x,t)-GJ_p(x)\theta''(x,t)=\tau(t) \qquad (3.0)$$

where the corresponding quantities in the three regions are given by

J_{p1},θ_1 in $0<x<L_1$

J_{p2},θ_2 in $L_1<x<L_2$

J_{p3},θ_3 in $L_2<x<L$

For the convenience of presentation $\rho(x)$ and $J_{Pi}(x)$ have been represented by ρ and J_{Pi}, respectively.

The scope of this thesis is to investigate the influence of internal displacement excitation on the torsional vibration of the geared system, while external excitation $\tau(t)$ is assumed to be zero. Thus the equation (3.0) becomes:

$$\rho\ddot{\theta}(x,t) - G\theta''(x,t) = 0 \tag{3.1}$$

3.2.2 BOUNDARY CONDITIONS:

The torque balance equation [31] for the constant inertia of the disk 1 at x = 0 is

$$GJ_{P1}\theta_1'(0,t) = I_{P1}\ddot{\theta}_1(0,t)$$

$$\Rightarrow GJ_{P1}\theta_1'(0,t) - I_{P1}\ddot{\theta}_1(0,t) = 0 \tag{3.2.1}$$

For the continuity of angular deflection from shaft 1 to shaft 2 at $x = L_1$

$$\theta_1(L_1,t) = \theta_2(L_1,t)$$

$$\Rightarrow \theta_1(L_1,t) - \theta_2(L_1,t) = 0 \tag{3.2.2}$$

The torque balance equation for the constant inertia of the disk 2 at $x = L_1$:

$$GJ_{P2}\theta_2'(L_1,t) - GJ_{P1}\theta_1'(L_1,t) = I_{P2}\ddot{\theta}_2(L_1,t)$$

$$\Rightarrow GJ_{P2}\theta_2'(L_1,t) - GJ_{P1}\theta_1'(L_1,t) - I_{P2}\ddot{\theta}_2(L_1,t) = 0 \tag{3.2.3}$$

For the continuity of angular deflection from shaft 2 to shaft 3 at $x = L_2$

$$-\theta_3(L_2,t) = N\theta_2(L_2,t) + \gamma(t)$$

$$\Rightarrow -\theta_3(L_2,t) - N\theta_2(L_2,t) = \gamma(t) \tag{3.2.4}$$

It should be noted that the continuity condition at the gear location considers the change in direction of rotation for the driven gear.

The force balance equation with the constant inertia of the driving gear and the driven gear at x = L_2 yields that

$$GJ_{P3}\theta_3'(L_2,t) - I_{P3''}\ddot{\theta}_3(L_2,t) = -\frac{1}{N}[GJ_{P2}\theta_2'(L_2,t) + I_{P3'}\ddot{\theta}_2(L_2,t)]$$

Substituting for $\theta_3(L_2,t)$ from equation (3.2.4) we get

$$\Rightarrow GJ_{P3}\theta_3'(L_2,t) + \frac{1}{N}GJ_{P2}\theta_2'(L_2,t) + (NI_{P3''} + \frac{I_{P3'}}{N})\ddot{\theta}_2(L_2,t) = I_{P3''}\ddot{\gamma}(t) \qquad (3.2.5)$$

The torque balance equation for the constant inertia of the disk 3 at x = L_3 reveals that

$$GJ_{P3}\theta_3'(L,t) = -I_{P4}\ddot{\theta}_3(L,t)$$

$$GJ_{P3}\theta_3'(L,t) + I_{P4}\ddot{\theta}_3(L,t) = 0 \qquad (3.2.6)$$

Equations (3.2.4) and (3.2.5) are identified as time-dependent non-homogeneous boundary conditions among the six boundary conditions [(3.2.1) to (3.2.6)].

Thus in the absence of the external torsional excitation within the geared shaft the equation of motion remains homogeneous with non-homogeneous time dependent boundary conditions due to the presence of periodic transmission error within the meshed gears.

The torsional vibration problem with time-dependent boundary conditions can be solved by using Laplace transformations. However, difficulties arise in the computation of inverse transforms which requires integration in the complex plane. Meirovitch's technique [32] solves the problem by transforming the homogeneous equation with non-homogeneous boundary conditions into the non-homogeneous equation with homogeneous boundary conditions. And finally the non-homogeneous equation can be solved by convolution integration. Such an approach was followed while analyzing lateral vibration of Bernoulli-Euler beams [33] and investigating the influence of internal cutting forces in whirling motion in deep hole-boring process [34]. The proposed continuous model is a modified approach to torsional vibration analysis of geared shafts subjected to internal displacement excitation.

At first, solution of the boundary-value problem described by equation (3.1) and boundary conditions (3.2.1) through (3.2.6) are assumed in the form

$$\begin{aligned} \vartheta_1(x,t) &= \varphi_1(x,t) && 0 < x < L_1 \\ \vartheta_2(x,t) &= \varphi_2(x,t) + f_2(x)\gamma(t) && L_1 < x < L_2 \\ \vartheta_3(x,t) &= \varphi_3(x,t) + f_3(x)\gamma(t) && L_2 < x < L_3 \end{aligned} \qquad (3.3)$$

Functions $f_2(x)$ and $f_3(x)$ are chosen so as to render the boundary conditions for the variables $\varphi_1(x,t)$, $\varphi_2(x,t)$ and $\varphi_3(x,t)$ homogeneous [32].

To introduce the boundary conditions of the current problem for $\varphi_1(x,t)$, $\varphi_2(x,t)$ and $\varphi_3(x,t)$, equations (3.3) are substituted into equations (3.2.1) through (3.2.6).

Consequently we get,

$$GJ_{P1}\varphi_1'(0,t) - I_{P1}\ddot{\varphi}_1(0,t) = 0 \tag{3.4.1}$$

$$\varphi_1(L_1,t) = \varphi_2(L_1,t) + f_2(L_1)\gamma(t)$$

$$\Rightarrow \varphi_1(L_1,t) - \varphi_2(L_1,t) = f_2(L_1)\gamma(t) \tag{3.4.2}$$

$$GJ_{P2}[\varphi_2'(L_1,t) + f_2'(L_1)\gamma(t)] - GJ_{P1}\varphi'_1(L_1,t) = I_{P2}[\ddot{\varphi}_2(L_1,t) + f_2(L_1)\ddot{\gamma}(t)]$$

$$\Rightarrow GJ_{P2}\varphi_2'(L_1,t) - GJ_{P1}\varphi_1'(L_1,t) - I_{P2}\ddot{\varphi}_2(L_1,t) = -GJ_{P2}f_2'(L_1)\gamma(t) + I_{P2}f_2(L_1)\ddot{\gamma}(t) \tag{3.4.3}$$

$$-\varphi_3(L_2,t) - f_3(L_2)\gamma(t) = N[\varphi_2(L_2,t) + f_2(L_2)\gamma(t)] + \gamma(t)$$

$$\Rightarrow -\varphi_3(L_2,t) - N\varphi_2(L_2,t) = [Nf_2(L_2) + f_3(L_2) + 1]\gamma(t) \tag{3.4.4}$$

$$GJ_{P3}[\varphi_3'(L_2,t) + f_3'(L_2)\gamma(t)] + \frac{1}{N}GJ_{P2}[\varphi_2'(L_2,t) + f_2'(L_2)\gamma(t)] +$$

$$(NI_{P3''} + \frac{I_{P3'}}{N})[\ddot{\varphi}_2(L_2,t) + f_2(L_2)\ddot{\gamma}(t)] = -I_{P3''}\ddot{\gamma}(t)$$

$$\Rightarrow GJ_{P3}\varphi_3'(L_2,t) + \frac{G}{N}J_{P2}\varphi_2'(L_2,t) + (NI_{P3''} + \frac{I_{P3'}}{N})\ddot{\varphi}_2(L_2,t) =$$

$$-\frac{1}{N}GJ_{P2}f_2'(L_2) - GJ_{P3}f_3'(L_2)]\gamma(t) - [(NI_{P3''} + \frac{I_{P3'}}{N})f_2(L_2) + I_{P3''}]\ddot{\gamma}(t) \tag{3.4.5}$$

$$GJ_{P3}[\varphi_3'(L,t) + f_3'(L)\gamma(t)] = -I_{P4}[\ddot{\varphi}_3(L,t) + f_3(L)\ddot{\gamma}(t)]$$

$$\Rightarrow GJ_{P3}\varphi_{33}'(L,t) + I_{P4}\ddot{\varphi}_3(L,t) = -I_{P4}f_3(L)\ddot{\gamma}(t) - GJ_{P3}f_3'(L)\gamma(t) \tag{3.4.6}$$

In order to get the homogeneous boundary conditions for variables $\varphi_1(x,t)$, $\varphi_2(x,t)$ and $\varphi_3(x,t)$, the terms on the right hand side of the equations (3.4.1) through (3.4.6) must be equal to zero. Accordingly,

$$f_2(L_1)\gamma(t) = 0 \tag{3.5.1}$$

$$-GJ_{P2}f_2'(L_1)\gamma(t)+I_{P2}f_2(L_1)\ddot{\gamma}(t)=0 \tag{3.5.2}$$

$$[Nf_2(L_2)+f_3(L_2)+1]\gamma(t)=0 \tag{3.5.3}$$

$$-[\frac{1}{N}GJ_{P2}f_2'(L_2)+GJ_{P3}f_3'(L_2)]\gamma(t)-[(NI_{P3''}+\frac{I_{P3'}}{N})f_2(L_2)+I_{P3''}]\ddot{\gamma}(t)=0 \tag{3.5.4}$$

$$-I_{P4}f_3(L)\ddot{\gamma}(t)-GJ_{P3}f_3'(L)\gamma(t)\ =0 \tag{3.5.5}$$

The fundamental harmonic of the periodic transmission error, $\gamma(t)$ is assumed as the dominant component given by $\gamma(t)=\gamma_0 Sin\omega t$.

Since $\gamma(t)\neq 0$, equation (3.5.3) indicates the relation between $f_3(x)$ and $f_2(x)$ as

$$f_3(x)=-[1+Nf_2(x)] \tag{3.6}$$

Similarly equations (3.5.1), (3.5.2), (3.5.4) and (3.5.5) yield

$$f_2(L_1)\ =0 \tag{3.7.1}$$

$$-GJ_{P2}f_2'(L_1)-\omega^2 I_{P2}f_2(L_1)=0 \tag{3.7.2}$$

$$-[\frac{1}{N}GJ_{P2}f_2'(L_2)+GJ_{P3}f_3'(L_2)]+\omega^2[(NI_{P3''}+\frac{I_{P3'}}{N})f_2(L_2)+I_{P3''}]=0 \tag{3.7.3}$$

$$\omega^2 I_{P4}f_3(L)-GJ_{P3}f_3'(L)=0 \tag{3.7.4}$$

Since there are four conditions to be satisfied by $f_2(x)$, let us assume

$$f_2'(x)=D_1x^2+D_2x+D_3$$

$$f_2(x)\ =\ D_1\frac{x^3}{3}+D_2\frac{x^2}{2}+D_3x+D_4 \tag{3.8.1}$$

$$f_3(x) = -[1 + N\{D_1 \frac{x^3}{3} + D_2 \frac{x^2}{2} + D_3 x + D_4\}] \quad (3.8.2)$$

The constants are evaluated using equations (3.7.1) through (3.7.4), and they are given in Table 3.2.2.

TABLE 3.2.2 CONSTANTS OF THE FUNCTIONS TO RENDER THE BOUNDARY CONDITIONS HOMOGENEOUS

Natural Freq cpm	0	5,882	11,348	26,803
D1	0	1.0192	1.002	-8.3596
D2	0	-0.4893	0.0647	19.3619
D3	0	0.0498	0.164	-5.5251
D4	0	-0.002	-0.0706	0.8692

Equation of motion in the zone $0 < x < L_1$:

$$\rho J_{p1} \ddot{\theta}_1(x,t) - G J_{p1} \theta_1''(x,t) = 0 \quad (3.9)$$

$$\rho J_{p1} \ddot{\varphi}_1(x,t) - G J_{p1} \varphi_1''(x,t) = 0 \quad \text{since } \vartheta_1(x,t) = \varphi_1(x,t)$$

Here the forcing function $F_1(x,t) = 0$ (3.10.1)

Equation of motion in the zone $L_1 < x < L_2$:

$$\rho J_{p2} \ddot{\theta}_2(x,t) - G J_{p2} \theta_2''(x,t) = 0$$

Since $\vartheta_2(x,t) = \varphi_2(x,t) + f_2(x)\gamma(t)$

$\ddot{\vartheta}_2(x,t) = \ddot{\varphi}_2(x,t) + f_2(x)\ddot{\gamma}(t)$ and $\vartheta_2''(x,t) = \varphi_2''(x,t) + f_2''(x)\gamma(t)$

Equation of motion becomes

$$\rho J_{p2}\ddot{\varphi}_2(x,t) - GJ_{p2}\varphi_2''(x,t) = GJ_{p2}f_2''(x)\gamma(t) - \rho J_{p2}f_2(x)\ddot{\gamma}(t)$$

The forcing function here is $F_2(x,t) = GJ_{p2}f_2''(x)\gamma(t) - \rho J_{p2}f_2(x)\ddot{\gamma}(t)$ (3.10.2)

Equation of motion in the zone $L_2 < x < L$:

$$N^2\rho J_{p3}\ddot{\theta}_3(x,t) - GJ_{p3}\theta_3''(x,t) = 0$$

Since $\vartheta_3(x,t) = \varphi_3(x,t) + f_3(x)\gamma(t)$

$\ddot{\vartheta}_3(x,t) = \ddot{\varphi}_3(x,t) + f_3(x)\ddot{\gamma}(t)$ and $\vartheta_3''(x,t) = \varphi_3''(x,t) + f_3''(x)\gamma(t)$

$$\rho J_{p3}\ddot{\phi}_3(x,t) - GJ_{p3}\phi_2''(x,t) = GJ_{p3}f_3''(x)\gamma(t) - \rho J_{p3}f_3(x)\ddot{\gamma}(t)$$

In this region, $F_3(x,t) = GJ_{p3}f_3''(x)\gamma(t) - \rho J_{p3}f_3(x)\ddot{\gamma}(t)$ (3.10.3)

Thus the Homogeneous equation (3.1) with time dependent non-homogeneous boundary conditions takes the following general form of non-homogeneous differential equation with homogeneous boundary conditions:

$$\rho J_p\ddot{\varphi}(x,t) - GJ_p\varphi''(x,t) = F(t) \tag{3.11}$$

After substituting equations (3.7.1) to (3.7.6) into equations (3.4.1) to (3.4.6) those take the form of six homogeneous boundary conditions:

$$GJ_{P1}\varphi_1'(0,t) - I_{P1}\ddot{\varphi}_1(0,t) = 0$$

$$\Rightarrow GJ_{P1}\varphi_1'(0,t) + I_{P1}\omega^2\varphi_1(0,t) = 0 \tag{3.12.1}$$

$$\varphi_1(\bar{L}_1,t) - \varphi_2(\bar{L}_1,t) = 0 \tag{3.12.2}$$

$$GJ_{P2}\varphi_2'(\overline{L}_1,t) - GJ_{P1}\varphi_1'(\overline{L}_1,t) - I_{P2}\ddot{\varphi}_2(\overline{L}_1,t) = 0$$

$$\Rightarrow GJ_{P2}\varphi_2'(\overline{L}_1,t) - GJ_{P1}\varphi_1'(\overline{L}_1,t) + I_{P2}\omega^2\varphi_2(\overline{L}_1,t) = 0 \qquad (3.12.3)$$

$$-\varphi_3(\overline{L}_2,t) - N\varphi_2(\overline{L}_2,t) = 0 \qquad (3.12.4)$$

$$GJ_{P3}\varphi_3'(L_2,t) + \frac{1}{N}GJ_{P2}\varphi_2'(L_2,t) + (NI_{P3''} + \frac{I_{P3'}}{N})\ddot{\varphi}_2(L_2,t) = 0$$

$$\Rightarrow GJ_{P3}\varphi_3'(L_2,t) + \frac{1}{N}GJ_{P2}\varphi_2'(L_2,t) - \omega^2(NI_{P3''} + \frac{I_{P3'}}{N})\ddot{\varphi}_2(L_2,t) = 0 \qquad (3.12.5)$$

$$GJ_{P3}\varphi_3'(\overline{L},t) - I_{P4}\ddot{\varphi}_3(\overline{L},t) = 0$$

$$\Rightarrow GJ_{P3}\varphi_3'(\overline{L},t) + I_{P4}\omega^2\varphi_3(\overline{L},t) = 0 \qquad (3.12.6)$$

A set of partial differential equations [(3.10.1) to (3.10.3)] with homogeneous boundary conditions [(3.12.1) to (3.12.6)] define a boundary value problem.

If there remains no internal displacement excitation, $\gamma(t) = 0$, and the system experiences free vibration. Then $F(t) = 0$ and the equation (3.11) becomes

$$\rho\ddot{\varphi}(x,t) - G\varphi_2''(x,t) = 0 \qquad (3.13)$$

Assuming a free vibration solution, we have $\varphi(x,t) = \phi(x)Sin\omega t$

$$\ddot{\varphi}(x,t) = -\omega^2\phi(x)Sin\omega t$$

$$[\rho\omega^2\phi(x) + G\phi''(x)]Sin\omega t = 0 \quad \text{since } Sin\omega t \neq 0$$

$$\rho\omega^2\phi(x) + G\frac{d^2}{dx^2}\phi(x) = 0 \qquad (3.14)$$

Since the equation (3.14) and six boundary conditions (3.12.1 to 3.12.6) are homogeneous and depend on the values of ω^2 the problem becomes an Eigen value problem. The non-trivial solution is possible only for certain values of ω^2.

Let the non-dimensional distance along the axial direction, $\bar{x} = \frac{x}{L}$

Then $\frac{d\bar{x}}{dx} = \frac{1}{L}$

and $\frac{d}{dx} = \frac{1}{L}\frac{d}{d\bar{x}}$

Similarly $\frac{d^2}{dx^2} = \frac{1}{L^2}\frac{d^2}{d\bar{x}^2}$:

Then equation (3.14) becomes $\rho\omega^2\phi(\bar{x}) + \frac{G}{L^2}\frac{d^2}{d\bar{x}^2}\phi(\bar{x}) = 0$

$$\frac{\rho\omega^2 L^2}{G}\phi(\bar{x}) + \frac{d^2}{d\bar{x}^2}\phi(\bar{x}) = 0$$

$$\phi''(\bar{x}) + \beta_i^2\phi(\bar{x}) = 0 \qquad (3.15)$$

where $\beta_i^2 = \frac{\rho\omega_i^2\bar{L}_i^2}{G}$

$\beta_{1i}^2 = \frac{\rho\omega_i^2\bar{L}_1^2}{G}$ and $\bar{L}_1 = \frac{L_1}{L}$

$\beta_{2i}^2 = \frac{\rho\omega_i^2\bar{L}_2^2}{G}$ and $\bar{L}_2 = \frac{L_2}{L}$

$\beta_{3i}^2 = \frac{\rho\omega_i^2\bar{L}^2}{G}$ and $\bar{L} = \frac{L}{L} = 1$

The complementary solutions for the three zones are:

$$\phi_1(\bar{x}) = A_1 Sin(\beta_1 \bar{x}) + A_2 Cos(\beta_1 \bar{x}) \qquad 0 < \bar{x} < \bar{L}_1$$

$$\phi_2(\bar{x}) = A_3 Sin(\beta_2 \bar{x}) + A_4 Cos(\beta_2 \bar{x}) \qquad \bar{L}_1 < \bar{x} < \bar{L}_2 \qquad (3.16)$$

$$\phi_3(\bar{x}) = A_5 Sin(\beta_3 \bar{x}) + A_6 Cos(\beta_3 \bar{x}) \qquad \bar{L}_2 < \bar{x} < 1$$

Again for the i-th mode, $\beta_{1i}^{\ 2} = \omega_i^{\ 2} \frac{\rho}{G} C_1^{\ 2} \bar{L}^2$ where $C_1 = \frac{\bar{L}_1}{\bar{L}}$

$\beta_{2i}^{\ 2} = \omega_i^{\ 2} \frac{\rho}{G} C_2^{\ 2} \bar{L}^2$ where $C_2 = \frac{\bar{L}_2}{\bar{L}}$

$\beta_{3i}^{\ 2} = \omega_i^{\ 2} \frac{\rho}{G} \bar{L}^2$

Let $a_i = \omega_i^{\ 2}$

$\bar{C}_1^{\ 2} = \frac{\rho}{G} C_2^{\ 2} \bar{L}^2$

$\bar{C}_2^{\ 2} = \frac{\rho}{G} C_2^{\ 2} \bar{L}^2$

$\bar{C}_3^{\ 2} = \frac{\rho}{G} \bar{L}^2$

With the above relations, equation (3.16) takes form of

$$\phi_{1i}(\bar{x}) = A_1 Sin(\bar{C}_1 \sqrt{a_i}\, \bar{x}) + A_2 Cos(\bar{C}_1 \sqrt{a_i}\, \bar{x}) \qquad 0 < \bar{x} < \bar{L}_1$$

$$\phi_{2i}(\bar{x}) = A_3 Sin(\bar{C}_2 \sqrt{a_i}\, \bar{x}) + A_4 Cos(\bar{C}_2 \sqrt{a_i}\, \bar{x}) \qquad \bar{L}_1 < \bar{x} < \bar{L}_2 \qquad (3.17)$$

$$\phi_{3i}(\bar{x}) = A_5 Sin(\bar{C}_3 \sqrt{a_i}\, \bar{x}) + A_6 Cos(\bar{C}_3 \sqrt{a_i}\, \bar{x}) \qquad \bar{L}_2 < \bar{x} < 1$$

Constants A_1, A_2..... A_6 can be evaluated by the six homogeneous boundary conditions stated in equation (3.12.1) to (3.12.6).

Substituting the variables of equation (3.16) and their respective derivatives into the equations (3.12.1) through (3.12.6) six equations are obtained which can be arranged in the following matrix form: $[H]_{6X6}\{A\}_{6X1} = \{0\}_{6X1}$

For a nontrivial solution, $|H| = 0$, which ultimately yields the characteristic equation. Here $|H|$ is the determinant of the coefficient matrix $[H]$

$$|H| = \begin{vmatrix} H_{11} & H_{12} & 0 & 0 & 0 & 0 \\ H_{21} & H_{22} & H_{23} & H_{24} & 0 & 0 \\ H_{31} & H_{32} & H_{33} & H_{34} & 0 & 0 \\ 0 & 0 & H_{43} & H_{44} & H_{45} & H_{46} \\ 0 & 0 & H_{53} & H_{54} & H_{55} & H_{56} \\ 0 & 0 & 0 & 0 & H_{65} & H_{66} \end{vmatrix} \tag{3.18}$$

$$H_{11} = GJ_{p1}\overline{C}_1\sqrt{a_i}$$

$$H_{12} = a_i I_{p1}$$

$$H_{21} = Sin(\overline{C}_1\overline{L}_1\sqrt{a_i})$$

$$H_{22} = Cos(\overline{C}_1\overline{L}_1\sqrt{a_i})$$

$$H_{23} = -Sin(\overline{C}_2\overline{L}_1\sqrt{a_i})$$

$$H_{24} = -Cos(\overline{C}_2\overline{L}_1\sqrt{a_i})$$

$$H_{31} = -GJ_{p1}\overline{C}_1\sqrt{a_i}Cos(\overline{C}_1\overline{L}_1\sqrt{a_i})$$

$$H_{32} = GJ_{p1}\overline{C}_1\sqrt{a_i}Sin(\overline{C}_1\overline{L}_1\sqrt{a_i})$$

$$H_{33} = a_i I_{P2}Sin(\overline{C}_2\overline{L}_1\sqrt{a_i}) + GJ_{p2}\overline{C}_2\sqrt{a_i}Cos(\overline{C}_2\overline{L}_1\sqrt{a_i})$$

$$H_{34} = a_i I_{P2}Cos(\overline{C}_2\overline{L}_1\sqrt{a_i}) - GJ_{p2}\overline{C}_2\sqrt{a_i}Sin(\overline{C}_2\overline{L}_1\sqrt{a_i})$$

$$H_{43} = -NSin(\overline{C}_2\overline{L}_2\sqrt{a_i})$$

$$H_{44} = -NCos(\overline{C}_2\overline{L}_2\sqrt{a_i})$$

$$H_{45} = -Sin(\overline{C}_3\overline{L}_2\sqrt{a_i}) \qquad (3.19)$$

$$H_{46} = -Cos(\overline{C}_3\overline{L}_2\sqrt{a_i})$$

$$H_{53} = \frac{1}{N}GJ_{p2}Cos(\overline{C}_2\overline{L}_2\sqrt{a_i})\overline{C}_2\sqrt{a_i} - a(NI_{p3'} + \frac{I_{p3'}}{N})Sin(\overline{C}_2\overline{L}_2\sqrt{a_i})$$

$$H_{54} = -\frac{1}{N}GJ_{p2}\overline{C}_2\sqrt{a_i}Sin(\overline{C}_2\overline{L}_2\sqrt{a_i}) - a_i(NI_{p3'} + \frac{I_{p3'}}{N})Cos(\overline{C}_2\overline{L}_2\sqrt{a_i})$$

$$H_{55} = GJ_{p3}\overline{C}_3\sqrt{a_i}Cos(\overline{C}_3\overline{L}_2\sqrt{a_i}) + I_{P3'}a_i\sin(\overline{C}_2\overline{L}_2\sqrt{a_i})$$

$$H_{56} = -GJ_{p3}\overline{C}_3\sqrt{a_i}Sin(\overline{C}_3\overline{L}_2\sqrt{a_i}) + I_{P3'}a_i\cos(\overline{C}_2\overline{L}_2\sqrt{a_i})$$

$$H_{65} = GJ_{p3}\overline{C}_3\sqrt{a_i}Cos(\overline{C}_3\overline{L}\sqrt{a_i}) - a_iI_{p4}Sin(\overline{C}_3\overline{L}\sqrt{a_i})$$

$$H_{66} = -GJ_{p3}\overline{C}_3\sqrt{a_i}Sin(\overline{C}_3\overline{L}\sqrt{a_i}) - a_iI_{p4}Cos(\overline{C}_3\overline{L}\sqrt{a_i})$$

Solution of equation (3.18) will provide the natural frequencies and the equation $[H]\{A\} = \{0\}$ will provide the corresponding mode shapes. Further the non-homogeneous problem is solved as follows.

Dividing both sides by GJ_p equation (3.11) becomes

$$\frac{\rho}{G}\ddot{\varphi}(\overline{x},t) - \varphi''(\overline{x},t) = Q(t) \qquad (3.20)$$

where $Q(t) = \dfrac{F(t)}{GJ_P}$

$= 0 \qquad 0 < \overline{x} < \overline{L}_1$

$$= f_2''(\bar{x})\gamma(t) - \frac{\rho}{G} f_2(\bar{x})\ddot{\gamma}(t) \qquad \bar{L}_1 < \bar{x} < \bar{L}_2$$

$$= f_3''(\bar{x})\gamma(t) - \frac{\rho}{G} f_3(\bar{x})\ddot{\gamma}(t) \qquad \bar{L}_2 < \bar{x} < 1$$

To solve the non-homogeneous equation (3.20) one can assume the solution in terms of normal modes:

$$\varphi(\bar{x},t) = \sum_{i=1}^{\infty} \varphi_i(\bar{x}) q_i(t) \tag{3.21}$$

where $q_i(t)$ is the modal coordinate.

Then equation (3.20) takes the form of $\sum_{i=1}^{\infty}\left(\frac{\rho}{G}\varphi_i(\bar{x})\ddot{q}_i(t) - \varphi_i''(\bar{x})q_i(t)\right) = Q(t)$ (3.22)

Since $\varphi_{1i}(\bar{x}), \varphi_{2i}(\bar{x}), \varphi_{3i}(\bar{x})$ and ω_i satisfy equation (3.15)

$$\frac{d^2}{d\bar{x}^2}\phi_i(\bar{x}) = -\frac{\rho\omega_i^{\,2}L^2}{G}\phi_i(\bar{x})$$

Thus equation (3.22) takes the form of

$$\sum_{i=1}^{\infty}\left((\ddot{q}_i(t) + \omega_i^2 q_i(t))\frac{\rho}{G}\varphi_i(\bar{x})\right) = Q(t) \tag{3.23}$$

where $Q(t) = 0 \qquad 0 < \bar{x} < \bar{L}_1$

$$= f_2''(\bar{x})\gamma(t) - \frac{\rho}{G} f_2(\bar{x})\ddot{\gamma}(t) \qquad \bar{L}_1 < \bar{x} < \bar{L}_2$$

$$= f_3''(\bar{x})\gamma(t) - \frac{\rho}{G} f_3(\bar{x})\ddot{\gamma}(t) \qquad \bar{L}_2 < \bar{x} < 1$$

To obtain the solution in the three regions equation (3.15) can be multiplied by $\varphi_j(\bar{x})$ throughout and integrated in each region with respect to $\bar{x}$. The equations will then be uncoupled in view of the following orthogonal property:

$$\int_0^{\bar{L}_1} \phi_{1i}(\bar{x})\phi_{1j}(\bar{x})d\bar{x} + \int_{\bar{L}_1}^{\bar{L}_2} \phi_{2i}(\bar{x})\phi_{2j}(\bar{x})d\bar{x} + \int_{\bar{L}_2}^{1} \phi_{3i}(\bar{x})\phi_{3j}(\bar{x})d\bar{x} = \alpha_i \qquad For\ i = j$$

$$\int_0^{\bar{L}_1} \phi_{1i}(\bar{x})\phi_{1j}(\bar{x})d\bar{x} + \int_{\bar{L}_1}^{\bar{L}_2} \phi_{2i}(\bar{x})\phi_{2j}(\bar{x})d\bar{x} + \int_{\bar{L}_2}^{1} \phi_{3i}(\bar{x})\phi_{3j}(\bar{x})d\bar{x} = 0 \qquad \text{For } i \neq j \qquad (3.24)$$

Thus one will get an infinite set of uncoupled ordinary differential equations for the three regions of the shaft:

$$\ddot{q}_i(t) + \omega_i^2 q_i(t) = \frac{1}{\alpha_i} R_i(t) \quad \text{For } i = j$$

$$= 0 \qquad \text{For } i \neq j \qquad (3.25)$$

$$R_i(t) = \int_0^{\bar{L}_1} \phi_{1i}(\bar{x})Q(t)d\bar{x} + \int_{\bar{L}_1}^{\bar{L}_2} \phi_{2i}(\bar{x})Q(t)d\bar{x} + \int_{\bar{L}_2}^{1} \phi_{3i}(\bar{x})Q(t)d\bar{x}$$

where $Q(t) = 0 \qquad 0 < \bar{x} < \bar{L}_1$

$$= I_{2i}^{*}\gamma(t) - \frac{\rho}{G} I_{2i}\ddot{\gamma}(t) \qquad \bar{L}_1 < \bar{x} < \bar{L}_2$$

$$= I_{3i}^{*}\gamma(t) - \frac{\rho}{G} I_{3i}\ddot{\gamma}(t) \qquad \bar{L}_2 < \bar{x} < 1$$

$$I_{2i}^{*} = \int_{\bar{L}_1}^{\bar{L}_2} \phi_{2i}(\bar{x}) f_2''(\bar{x}) d\bar{x}$$

$$I_{2i} = \int_{\bar{L}_1}^{\bar{L}_2} \frac{\rho}{G} \phi_{2i}(\bar{x}) f_2(\bar{x}) d\bar{x} \qquad (3.26)$$

$$I_{3i}^{*} = \int_{\bar{L}_2}^{1} \phi_{3i}(\bar{x}) f_3''(\bar{x}) d\bar{x}$$

$$I_{3i} = \int_{\bar{L}_2}^{1} \frac{\rho}{G} \phi_{3i}(\bar{x}) f_3(\bar{x}) d\bar{x}$$

The uncoupled non-homogeneous equations can be solved by convolution integration. It is done by taking a dummy variable of the integration λ between the limits of integration 0 and time t and elemental impulse is $h(\lambda)d\lambda$. Here original time variable t is a parameter, which represents a particular value of λ.

Then the complete solution for these equations with zero initial conditions is:

$$q_i(t) = \left(\frac{1}{\alpha_i \omega_i} \int_o^t R_i(\lambda) \sin \omega_i (t - \lambda) d\lambda \right)$$

The complete solution for the current problem for the three regions is as follows:

$$\theta_1(\bar{x},t) = \sum_{i=1}^{\infty} \frac{1}{\alpha_i \omega_i} \varphi_{1i}(\bar{x}) \left(\int_o^t R_i(\lambda) \sin \omega_i (t - \lambda) d\lambda \right) \qquad 0 < \bar{x} < \bar{L}_1$$

$$\theta_2(\bar{x},t) = \sum_{i=1}^{\infty} \frac{1}{\alpha_i \omega_i} \varphi_{2i}(\bar{x}) \left(\int_o^t R_i(\lambda) \sin \omega_i (t - \lambda) d\lambda \right) + f_2(\bar{x}) \gamma(t) \qquad \bar{L}_1 < \bar{x} < \bar{L}_2 \qquad (3.27)$$

$$\theta_3(\bar{x},t)=\sum_{i=1}^{\infty}\frac{1}{\alpha_i\omega_i}\varphi_{3i}(\bar{x})\left(\int_o^t R_i(\lambda)\sin\omega_i(t-\lambda)d\lambda\right)+f_3(\bar{x})\gamma(t)\qquad \bar{L}_2<\bar{x}<1$$

Substituting the values of $R_i(\lambda)$ in the equation (3.27) we get

$$\theta_1(\bar{x},t)=\sum_{i=1}^{\infty}\frac{1}{\omega_i}\varphi_{1i}(\bar{x})\left(\int_o^t\left(I_{2i}^*\gamma(\lambda)-\frac{\rho}{G}I_{2i}\ddot{\gamma}(\lambda)+I_{3i}^*\gamma(\lambda)-\frac{\rho}{G}I_{3i}\ddot{\gamma}(\lambda)\right)\sin\omega_i(t-\lambda)d\lambda\right)$$

$$\theta_2(\bar{x},t)=\sum_{i=1}^{\infty}\frac{1}{\omega_i}\varphi_{2i}(\bar{x})\left(\int_o^t\left(I_{2i}^*\gamma(\lambda)-\frac{\rho}{G}I_{2i}\ddot{\gamma}(\lambda)+I_{3i}^*\gamma(\lambda)-\frac{\rho}{G}I_{3i}\ddot{\gamma}(\lambda)\right)\sin\omega_i(t-\lambda)d\lambda\right)+f_2(\bar{x})\gamma(t)$$

$$\theta_3(\bar{x},t)=\sum_{i=1}^{\infty}\frac{1}{\omega_i}\varphi_{3i}(\bar{x})\left(\int_o^t\left(I_{2i}^*\gamma(\lambda)-\frac{\rho}{G}I_{2i}\ddot{\gamma}(\lambda)+I_{3i}^*\gamma(\lambda)-\frac{\rho}{G}I_{3i}\ddot{\gamma}(\lambda)\right)\sin\omega_i(t-\lambda)d\lambda\right)+f_3(\bar{x})\gamma(t)$$

(3.28)

Substituting $\gamma(\lambda)=\gamma_0 Sin(\omega_i\lambda)$ and $\ddot{\gamma}(\lambda)=-\omega_i{}^2\gamma_0 Sin(\omega_i\lambda)$ into equation (3.28)

$$\theta_1(\bar{x},t)=\sum_{i=1}^{\infty}\frac{1}{\omega_i}\varphi_{1i}(\bar{x})\gamma_0\left(I_{2i}^*+\frac{\rho}{G}I_{2i}+I_{3i}^*\gamma(\lambda)+\frac{\rho}{G}I_{3i}\right)\int_o^t Sin(\omega_i\lambda)Sin\omega_i(t-\lambda)d\lambda;\qquad 0<\bar{x}<\bar{L}_1$$

$$\theta_2(\bar{x},t)=\sum_{i=1}^{\infty}\frac{1}{\omega_i}\varphi_{2i}(\bar{x})\left(I_{2i}^*+\frac{\rho}{G}I_{2i}+I_{3i}^*\gamma(\lambda)+\frac{\rho}{G}I_{3i}\right)\int_o^t Sin(\omega_i\lambda)Sin\omega_i(t-\lambda)d\lambda+f_2(\bar{x})\gamma_0\sin(\omega_i t);$$

$$\bar{L}_1<\bar{x}<\bar{L}_2$$

$$\theta_3(\bar{x},t)=\sum_{i=1}^{\infty}\frac{1}{\omega_i}\varphi_{3i}(\bar{x})\left(I_{2i}^*+\frac{\rho}{G}I_{2i}+I_{3i}^*\gamma(\lambda)+\frac{\rho}{G}I_{3i}\right)\int_o^t Sin(\omega_i\lambda)Sin\omega_i(t-\lambda)d\lambda+f_3(\bar{x})\gamma_0 Sin(\omega_i t)$$

$$\bar{L}_2<\bar{x}<1$$

(3.29)

For each of the three regions the definite integral term is given by

$$\int_o^t Sin(\omega_i\lambda)Sin\omega_i(t-\lambda)d\lambda=\frac{Sin(\omega_i t)}{2\omega_i}-t\frac{Cos(\omega_i t)}{2}\qquad (3.30)$$

3.3 Analytical Results

The proposed analytical model for a geared system with homogeneous equations of motion and time dependent non-homogeneous boundary conditions validated by comparing the natural frequencies and the mode shapes with those obtained by the discrete model illustrated in the previous chapter.

Since the three shafts of the lumped-mass model have non-variable stiffness K_1, K_2 and K_3 the corresponding polar moment of inertia of the 1st, 2nd and 3rd shafts with constant cross-section are:

$$J_{P1} = \frac{K_1 l_1}{G}$$

$$J_{P2} = \frac{K_2 l_2}{G}$$

$$J_{P3} = \frac{K_3 l_3}{G}$$

where l_1, l_2 and l_3 are the length of the shafts.

3.3.1 NATURAL FREQUENCIES OF THE CONTINUOUS MODEL

With the numerical data of the geared system and the material properties such as density, $\rho = 7800\,\text{Kg/m}^3$, modulus of elasticity, $E = 2.1X10^{11}\ \text{N/m}^2$ and Poisson's ratio, $\mu = 0.3$ the components of the equation (3.19) are derived. Plotting the above characteristic equation against $a_i (= \omega_i^2)$ as shown in figures 3.3.1 to 3.3.5, the fist six roots are found as:

$a_1 = \omega_1^2 = 0$ (Radian/s)^2

$a_2 = \omega_2^2 = 0.3807X10^6$ (Radian/s)^2

$a_3 = \omega_3^2 = 1.4082X10^6$ (Radian/s)^2

$a_4 = \omega_4^2 = 7.8952X10^6$ (Radian/s)^2

$a_5 = \omega_5^2 = 4.0249X10^8$ (Radian/s)^2

$a_6 = \omega_6^2 = 1.38076X10^9$ (Radian/s)^2 and so on.

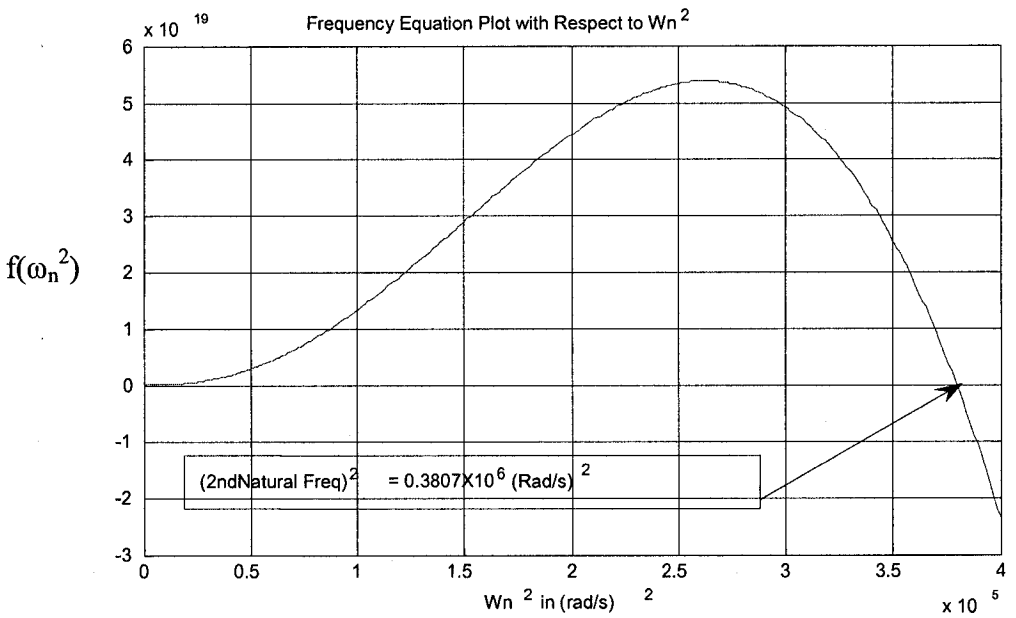

Figure 3.3.1 Plot for the 2nd root of the characteristic equation

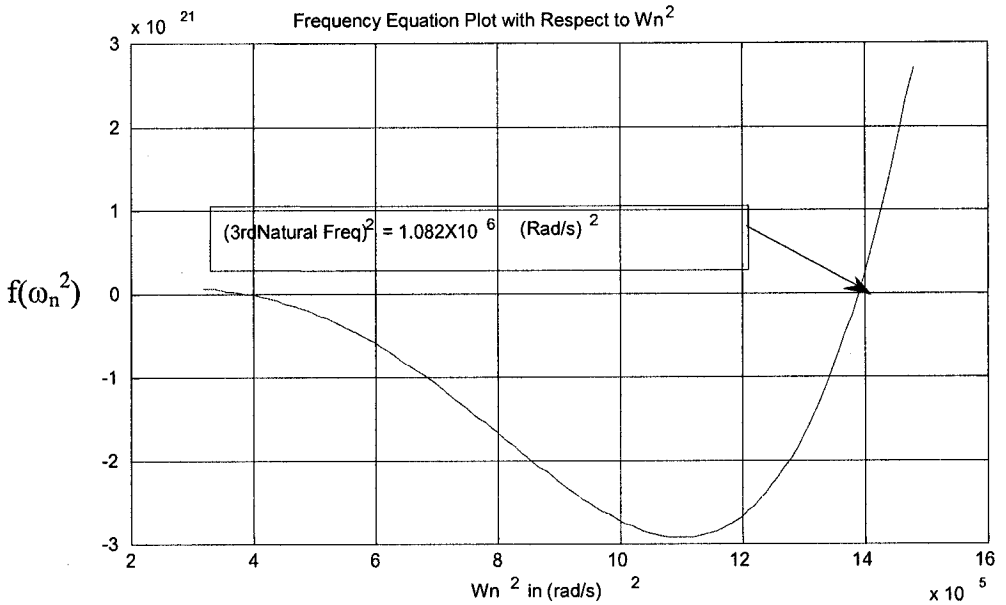

Figure 3.3.2 Plot for the 3rd root of the Characteristic Equation

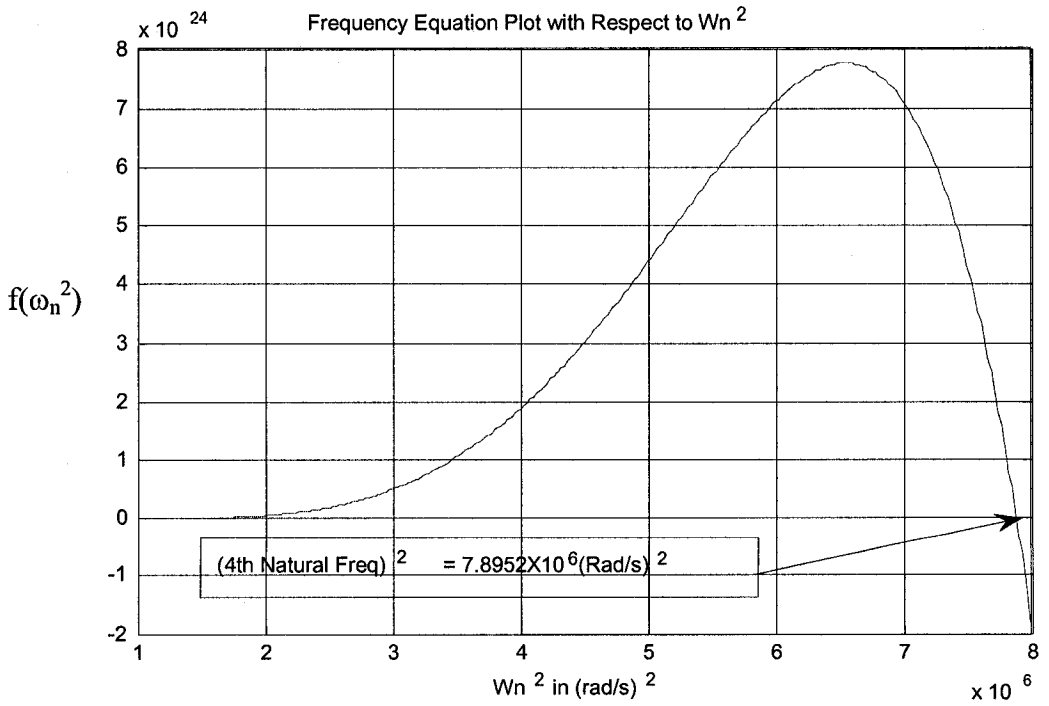

Figure 3.3.3 Plot for the 4th root of the Characteristic Equation

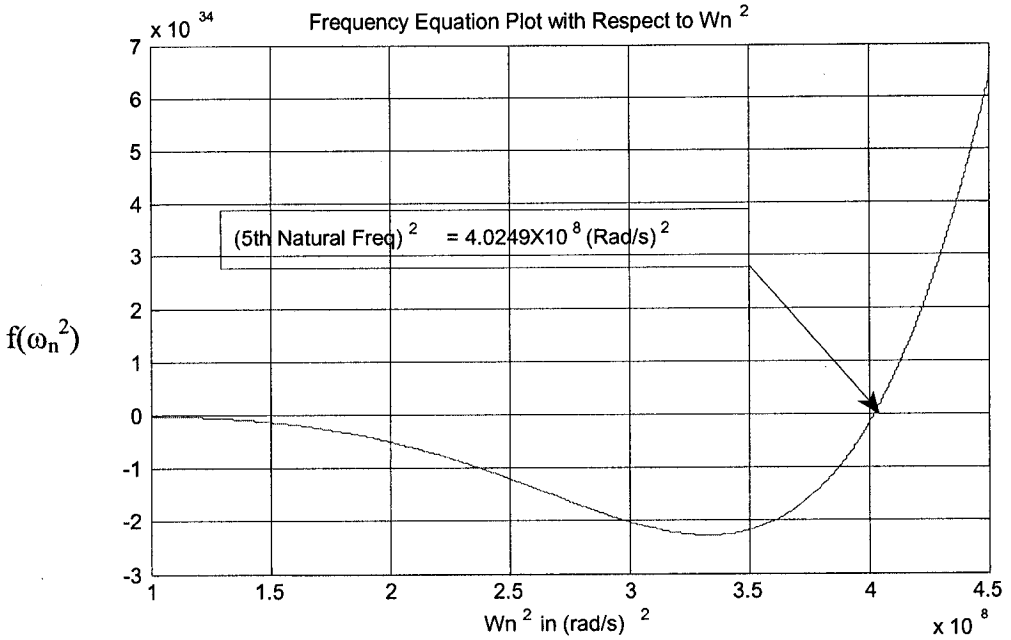

Figure 3.3.4 Plot for the 5th root of the Characteristic Equation

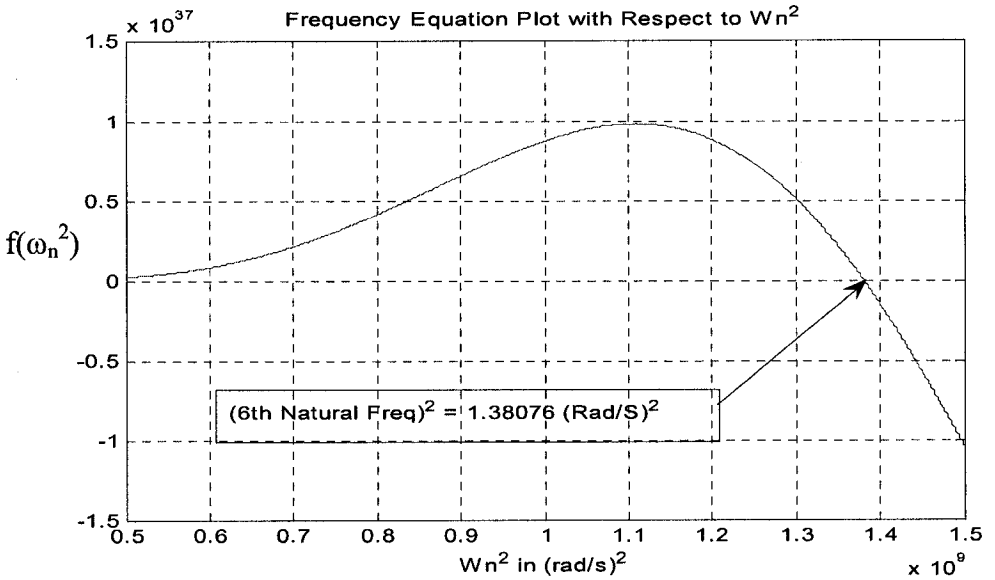

Figure 3.3.5 Plot for the 6th root of the Characteristic Equation

Natural frequencies of the continuous model are compared with those of the discrete model in Table 3.3.1.

TABLE 3.3.1 NATURAL FREQUENCIES OF CONTINUOUS MODEL IN COMPARISON TO DISCRETE MODEL

Mode	Discrete Model	Proposed Continuous Model	
	f_n (cpm)	f_n (cpm)	Difference %
1st	0	0	0
2nd	5,881	5,892	0.19
3rd	11,350	11,332	-0.16
4th	26,797	26,833	0.13
5th	-	191,580	-
6th	-	354,838	-

Mode shapes of the continuous system are shown in figures 3.3.6 to 3.3.10. It must be noted that the directions of rotation change at the gear locations following the gear ratio.

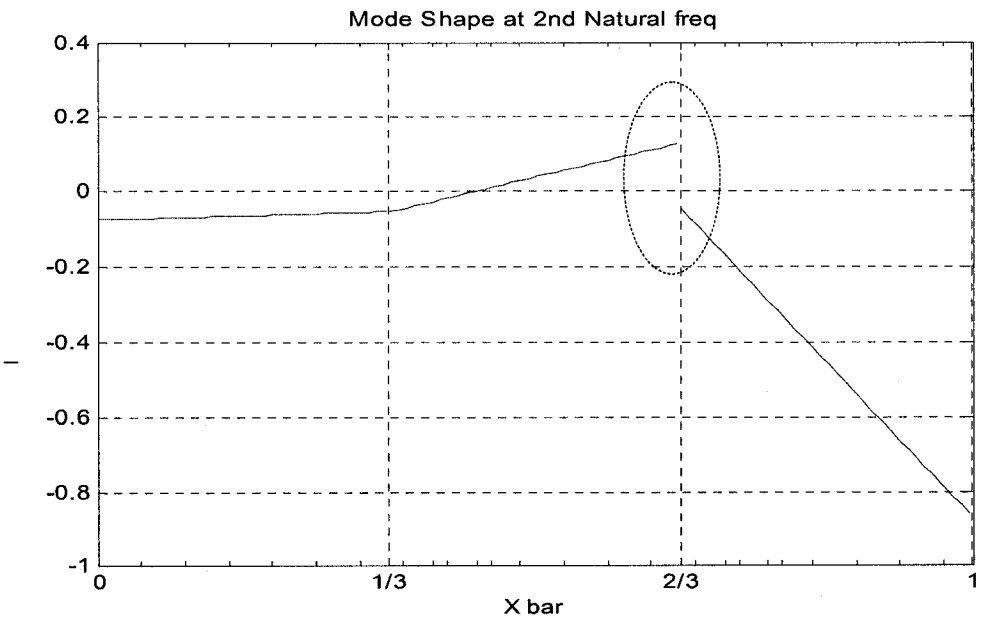

Figure 3.3.6 Mode shape at the 2nd natural frequency

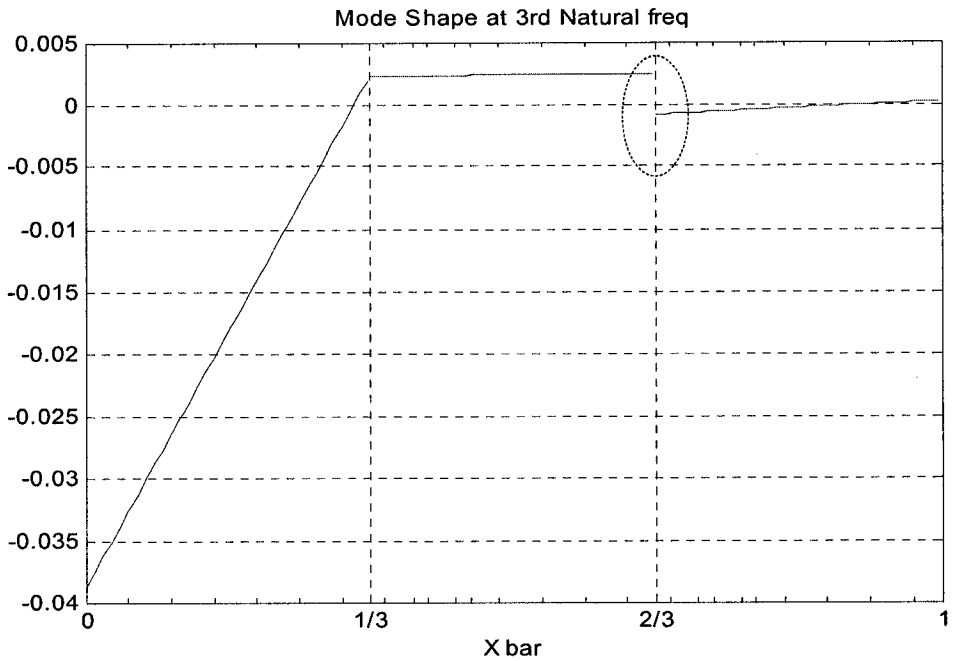

Figure 3.3.7 Mode shape at 3rd Natural Frequency

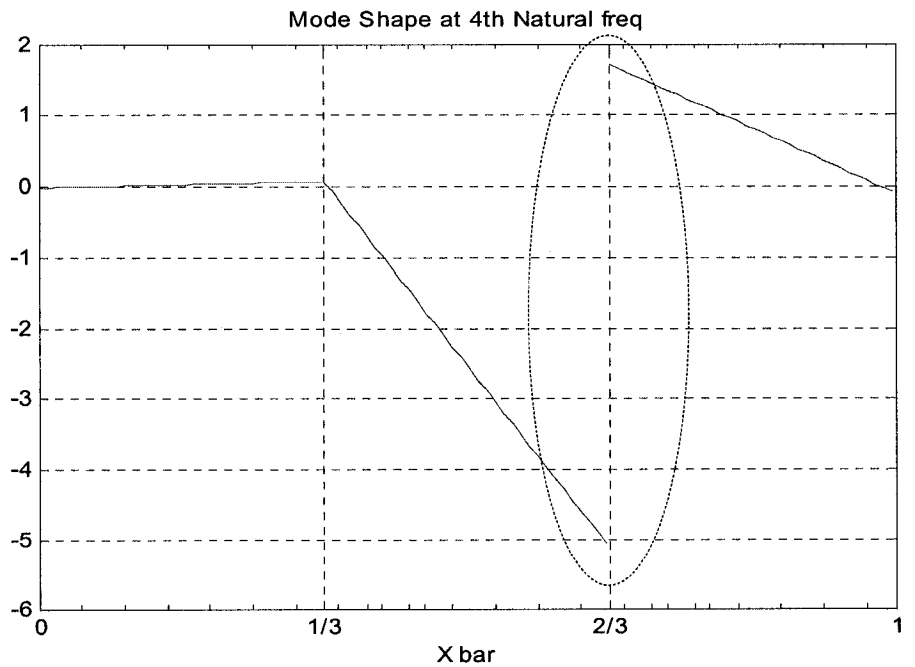

Figure 3.3.8 Mode shape at the 4th natural frequency

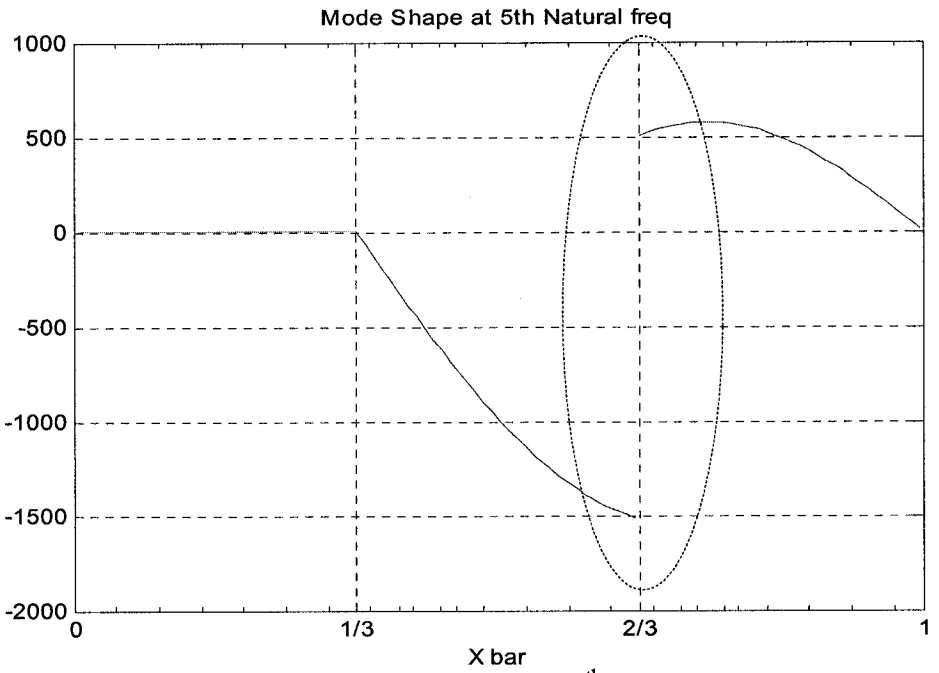

Figure 3.3.9 Mode shape at the 5th natural frequency

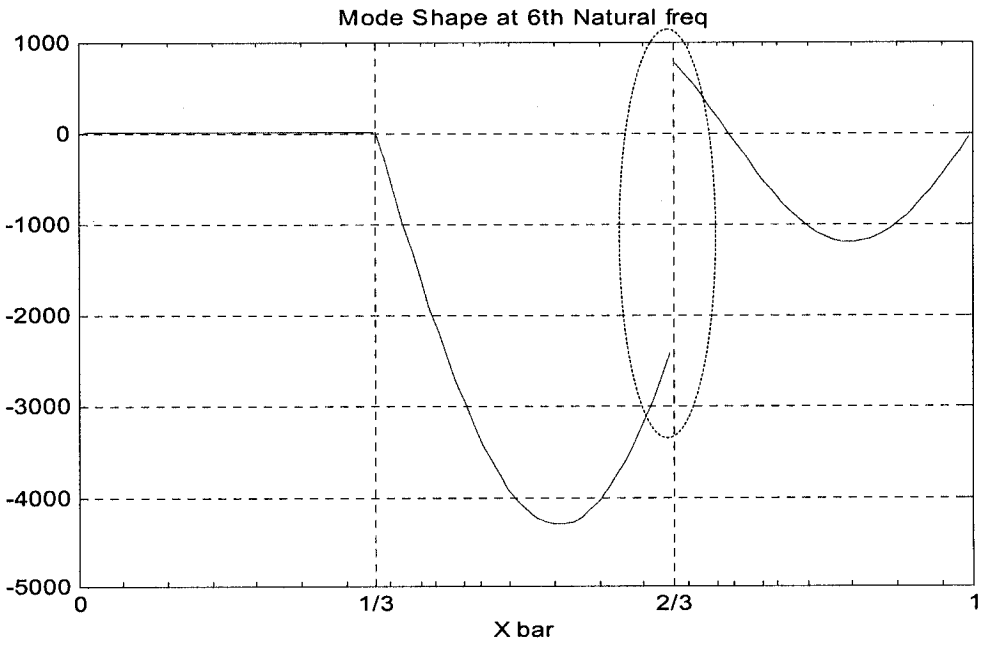

Figure 3.3.10 Mode shape at the 6th natural frequency

A negligible deviation is observed between the natural frequencies of the discrete model and the continuous model up to the 4^{th} mode. The continuous mode shapes of the gear drive accommodate the direction of rotation of the driving and driven shafts. The direction of the angular deflection of the driven gear at each mode is in opposite direction of the driving gear. Consequently discontinuity is observed at the gear pair location of each mode shape as indicated by dotted areas in figure 3.3.6 to 3.3.10. Mode shapes of 2^{nd} and 3^{rd} shafts become non-linear at natural frequencies above 4^{th} order. The linear mode shapes up to the 4^{th} order are discretized and normalized, the magnitudes of which match with the normal mode shapes of the discrete model.

Table 3.3.2 provides the normalized mode at the four rigid mass locations. The normalized modes incorporate the opposite direction of angular deflection of the driven gear with respect to the driving gear.

TABLE 3.3.2 NORMALIZED MODES AT FOUR RIGID MASS POSITIONS OF THE CONTINUOUS MODEL:

Location	1st	2nd	3rd	4th
Disk-1	1	1	1	1
Disk-2	1	0.7188	0.0491	4.8452
Gear Pair	1	1.7115	0.0636	308.11
Disk-3	-0.33333	-11.4856	-0.0059	-4.5061

Normalized mode shapes at four rigid mass locations are shown in figures 3.3.11 to 3.3.14. In comparing these modes with those of the discrete model it must be noted that the sign changes at the gear location.

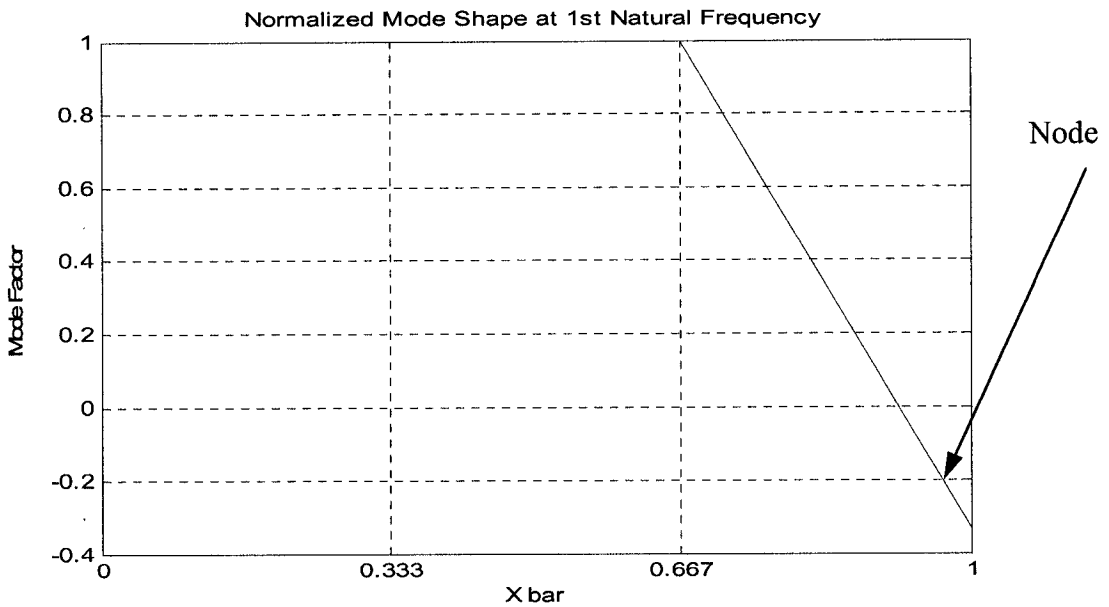

Figure 3.3.11 Rigid body mode shape (normalized) at discrete mass locations

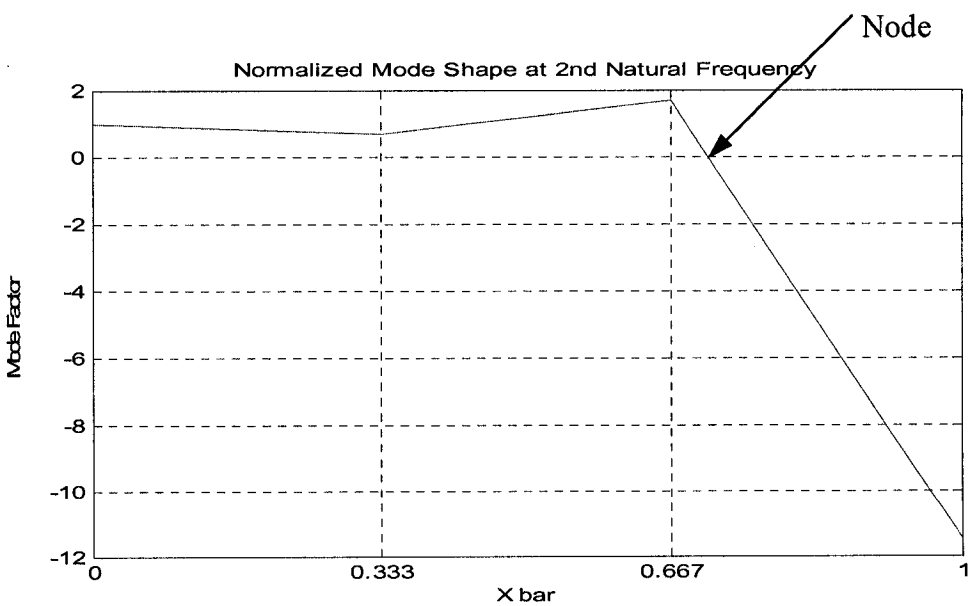

Figure 3.3.12 2nd mode (normalized) at discrete mass locations

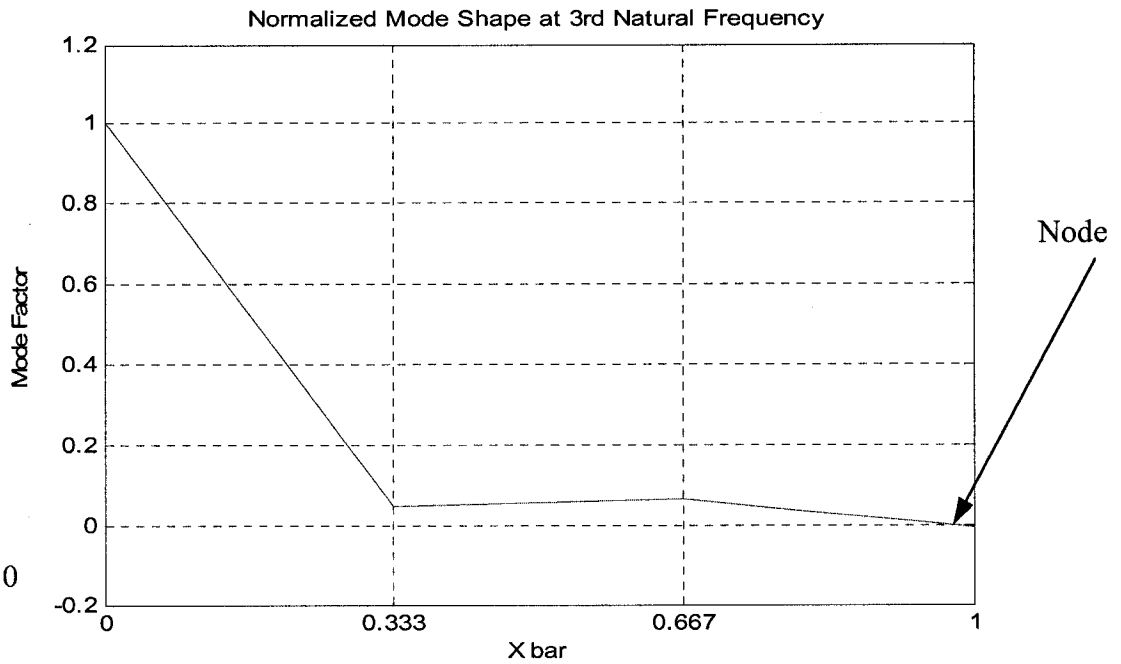

Figure 3.3.13 3rd mode (normalized) at discrete mass locations

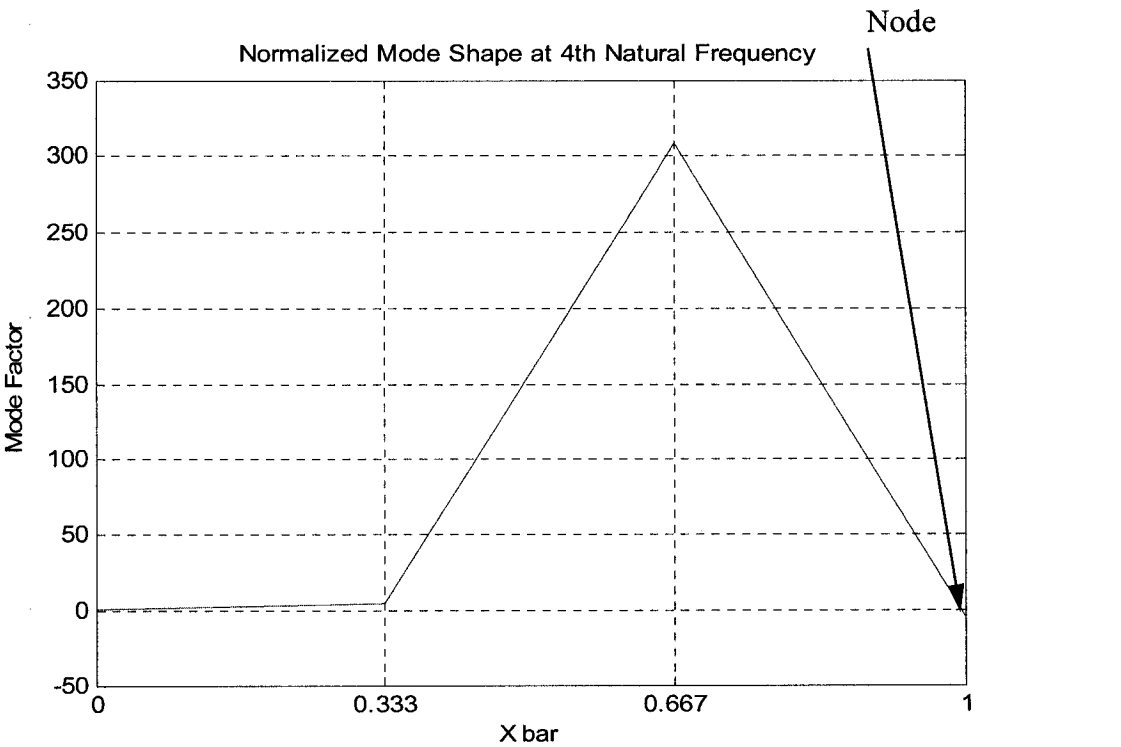

Figure 3.3.14 4th mode (normalized) at discrete mass locations

Steady-state responses due to harmonic transmission error at driving shaft speed: 3000 rpm are shown in figures 3.3.15 to 3.3.19.

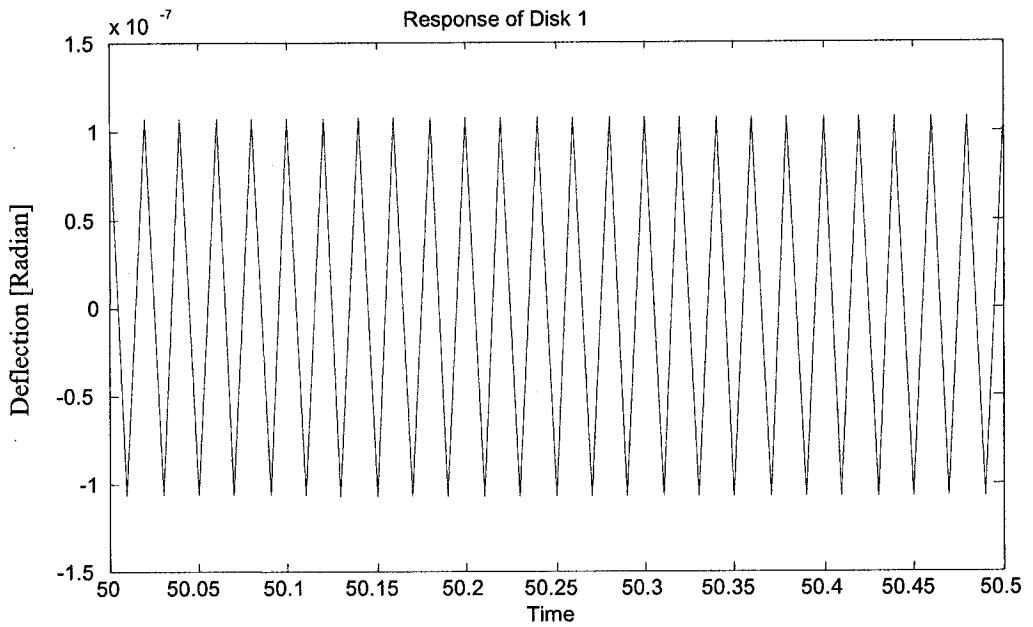

Figure 3.3.15 Steady-state response of Disk-1 with harmonic transmission error in radian, $\gamma(t) = .0001 \sin \omega t$; $\omega = 314.16$ rad/s (f = 50 Hz)

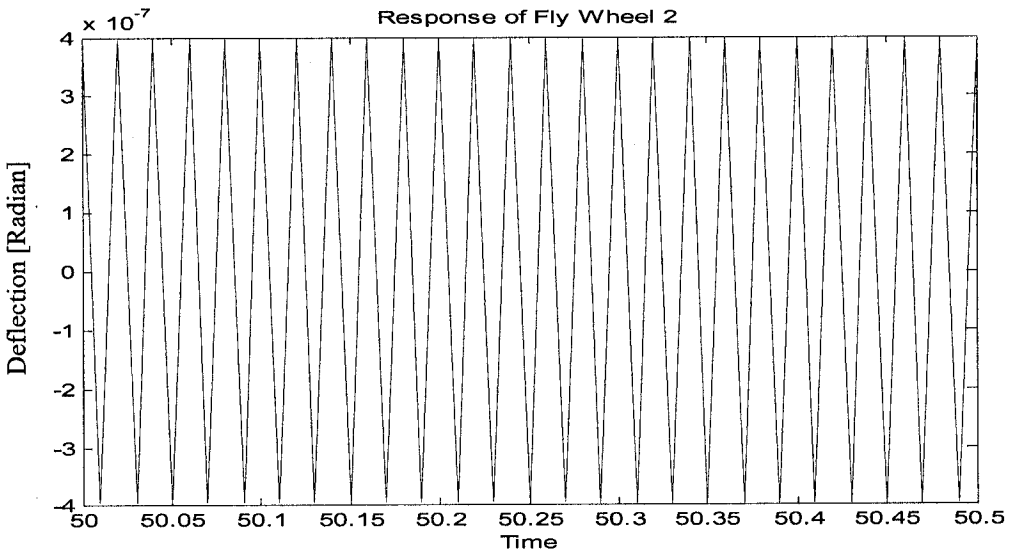

Figure 3.3.16 Steady-state response of Disk-2 with harmonic transmission error in radian, $\gamma(t) = .0001 \sin \omega t$; $\omega = 314.16$ rad/s (f = 50 Hz)

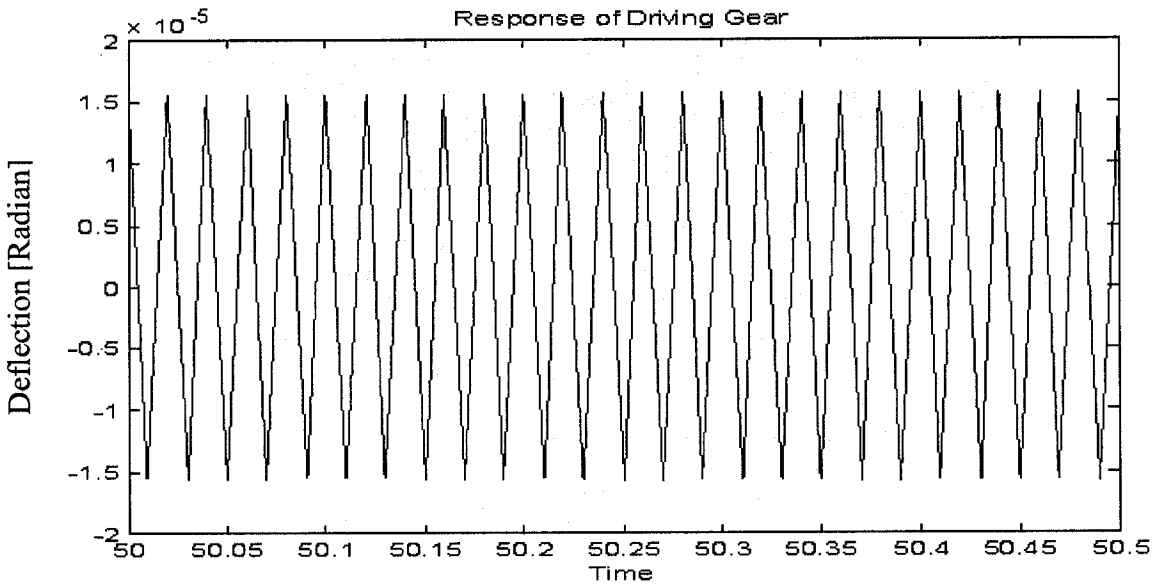

Figure 3.3.17 Steady-state response of Driving gear with harmonic transmission error in radian, $\gamma(t) = .0001 \sin \omega t$; $\omega = 314.16$ rad/s (f = 50 Hz)

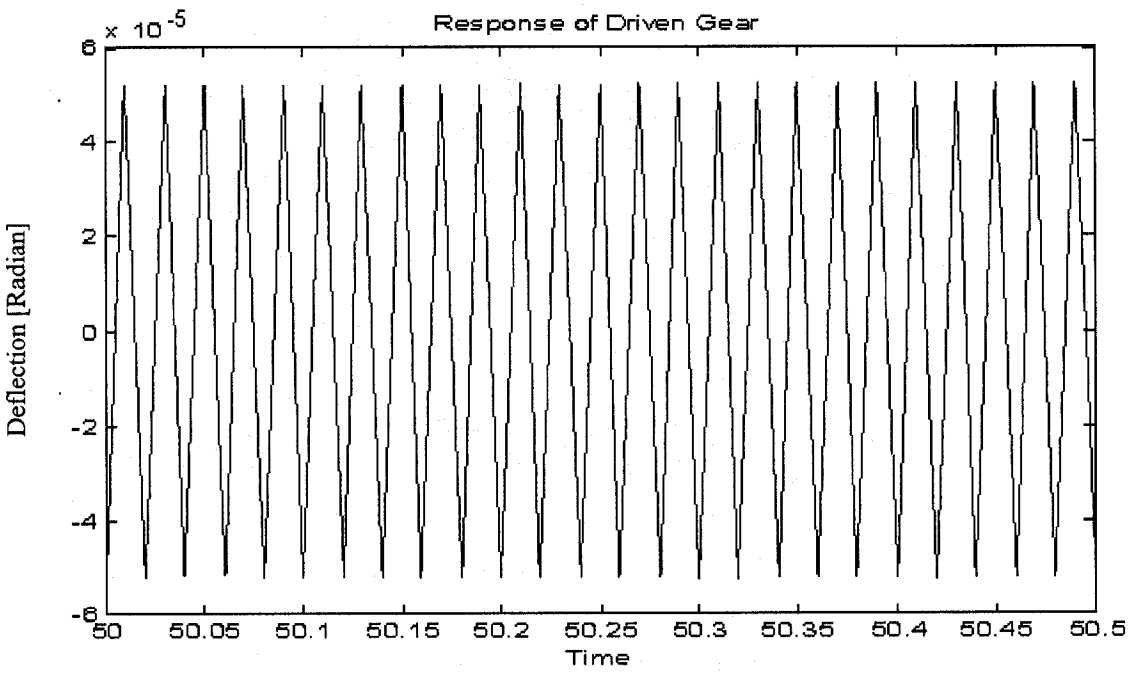

Figure 3.3.18 Steady-state response of Driven gear with harmonic transmission error in radian, $\gamma(t) = \gamma(t) = .0001 \sin \omega t$; $\omega = 314.16$ rad/s (f = 50 Hz)

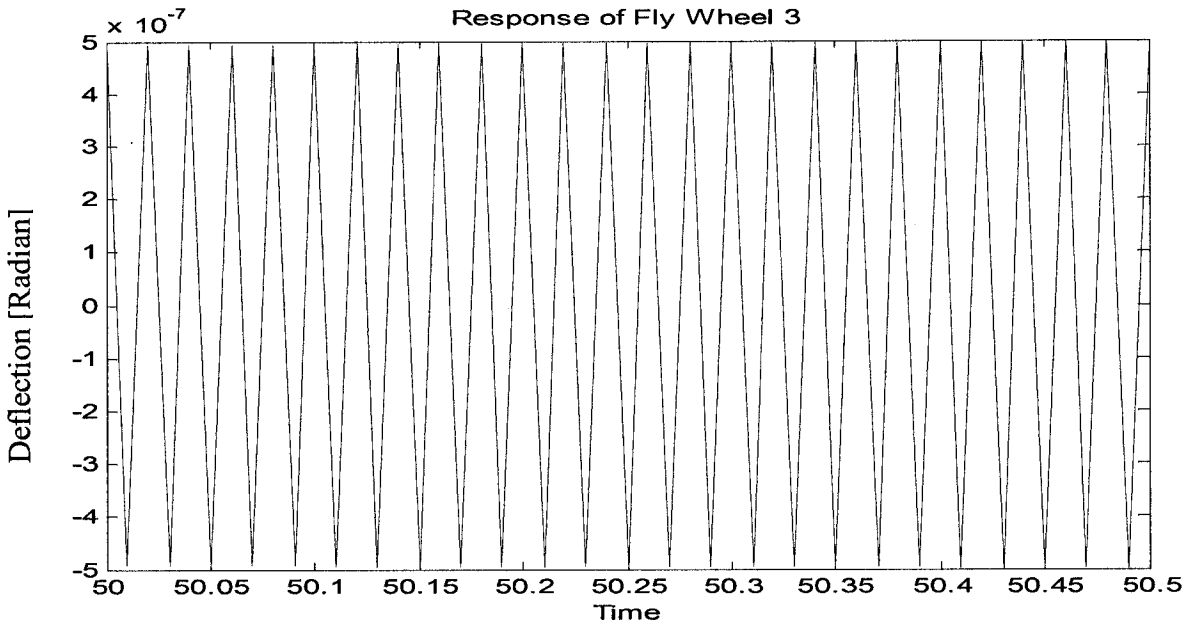

Figure 3.3.19 Steady-state response of Disk-3 with harmonic transmission error in radian, $\gamma(t) = .0001 \sin \omega t$; $\omega = 314.16$ rad/s (f = 50 Hz)

The influence of harmonic transmission error is observed at driving and driven gears. However, the angular deflection of the driven gear is higher than that of the driving gear. Similar behavior is observed for the 3rd mass in the time domain of the 4DOF discrete model. In reality transmission error does not introduce harmonic excitation. Rather the factors involving into the static transmission error, such as shaft misalignment, mounting error, bearing misalignment, tooth error and variation of meshing stiffness introduces excitation of different frequencies. The linear combination of the sine components of those excitations as well as the natural frequency components are introduced within the gear pair as mixed harmonic transmission error. The responses at the time and frequency domains are determined as shown in figures 3.20 to 3.28.

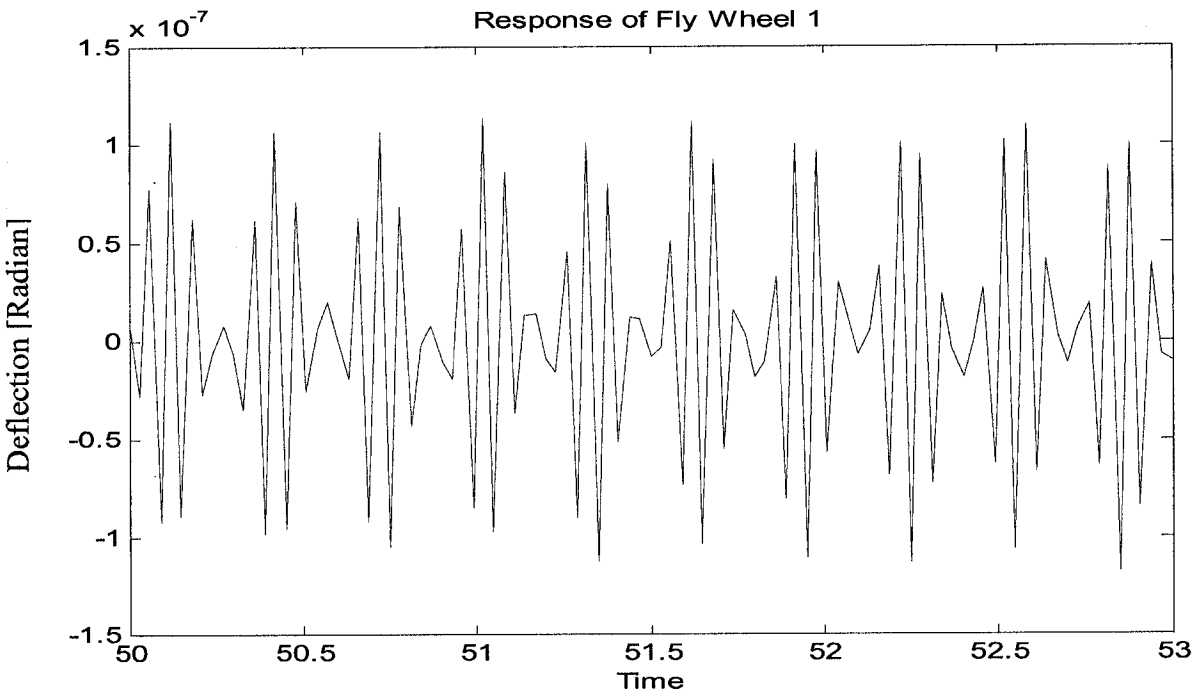

Figure 3.3.20 Response of disk-1 with mixed harmonic transmission error 0.0001 rad

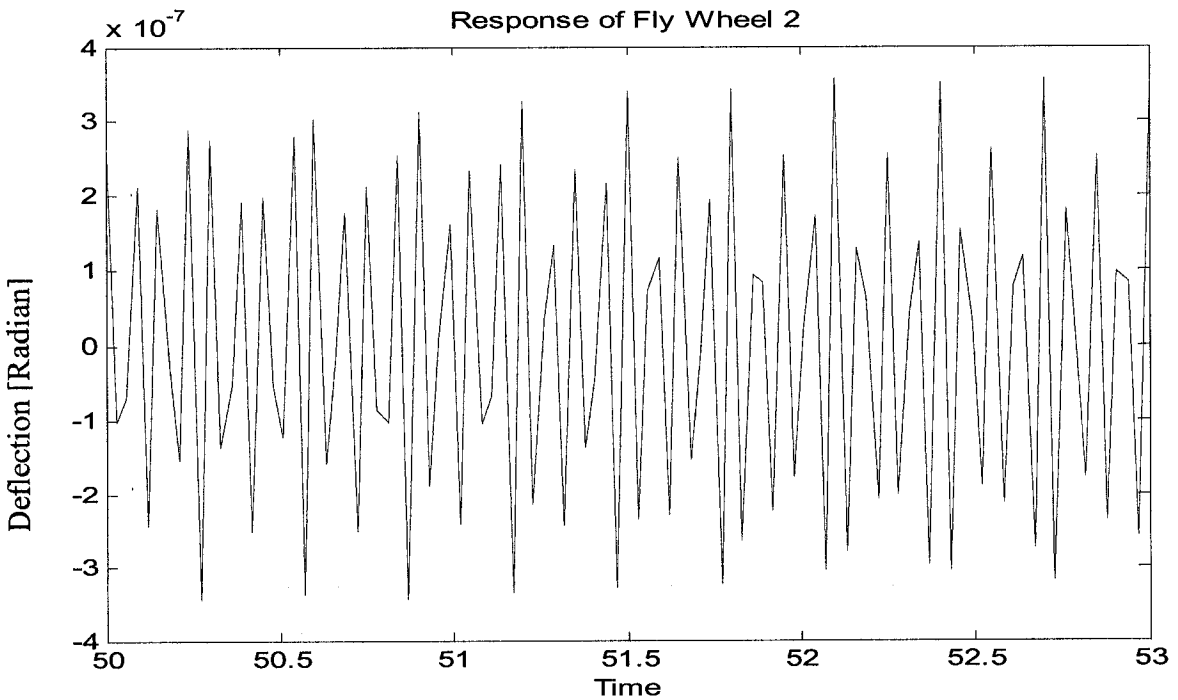

Figure 3.3.21 Response of disk-2 with mixed harmonic transmission error 0.0001 rad

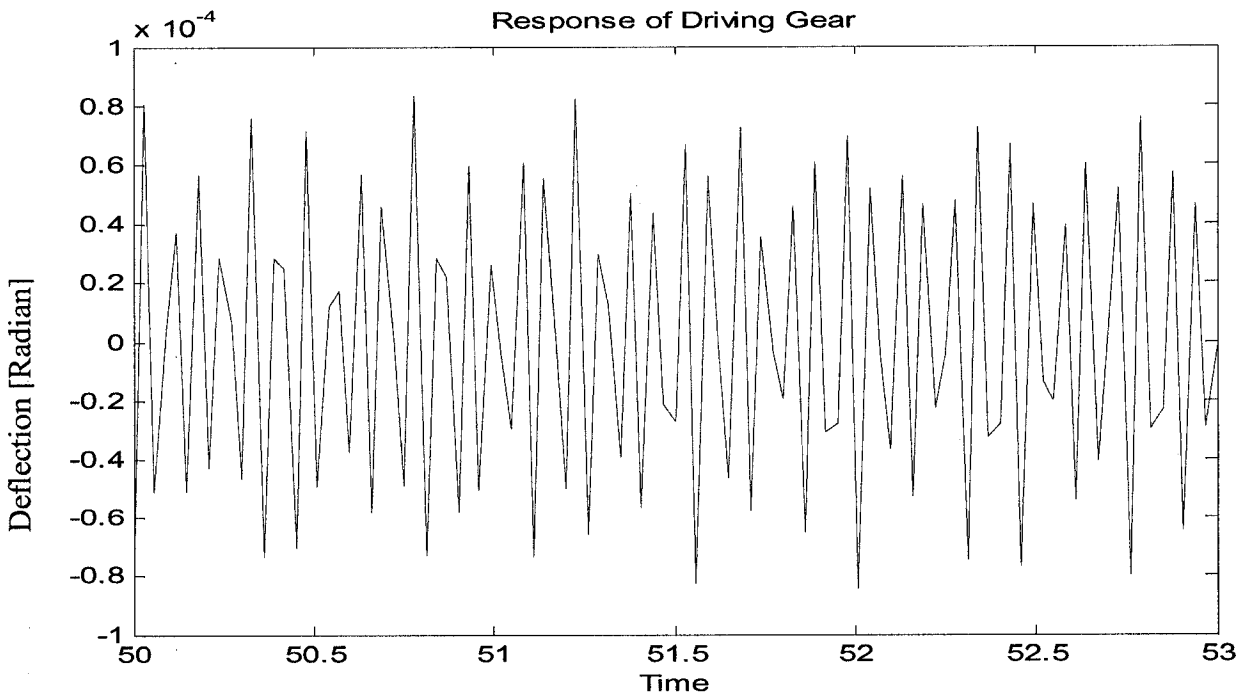

Figure 3.3.22 Response of driving gear with mixed harmonic transmission error 0.0001 rad

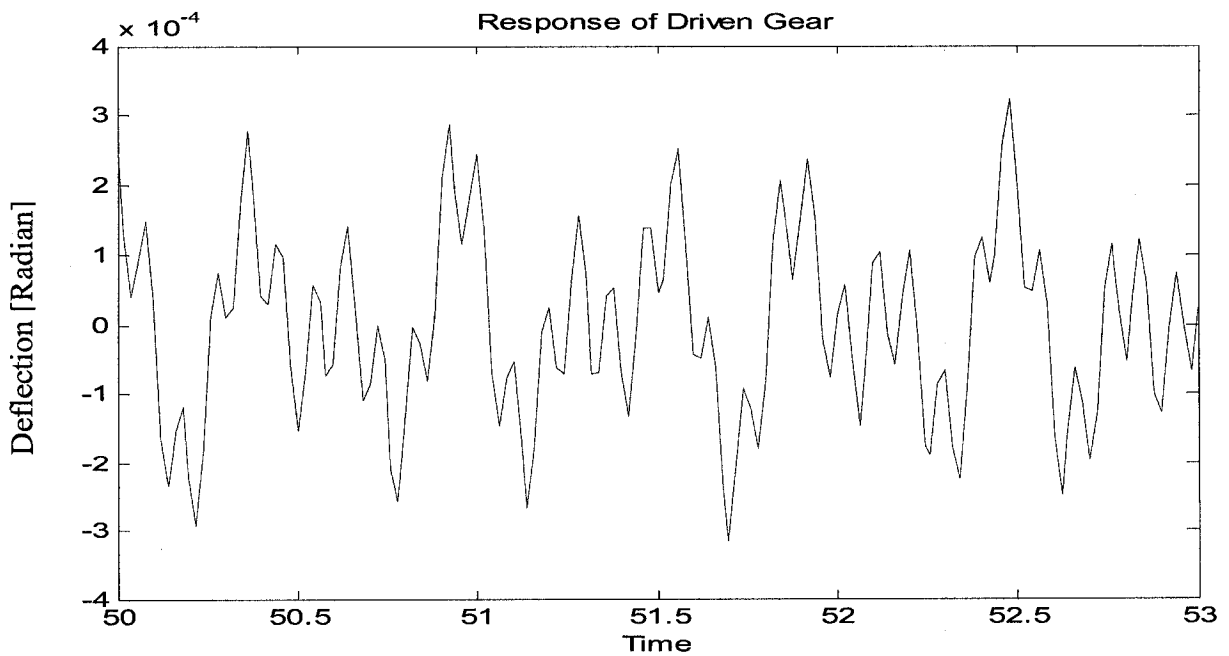

Figure 3.3.23 Response of driven gear with mixed harmonic transmission error 0.0001 rad

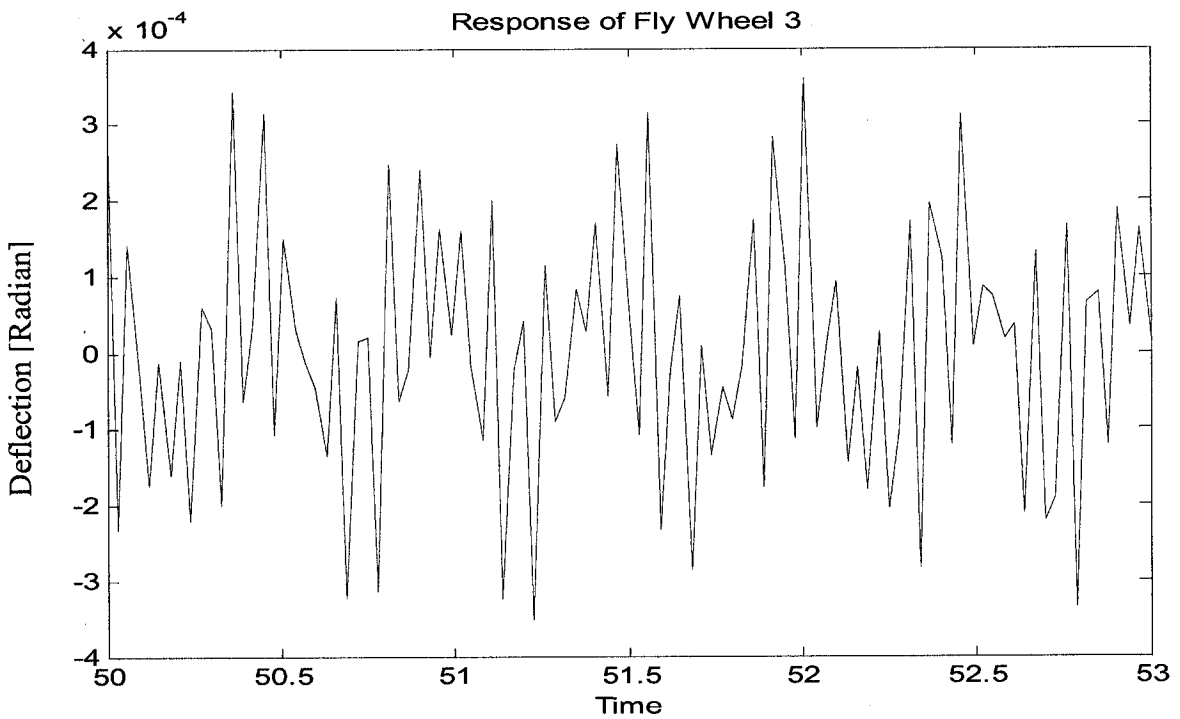

Figure 3.3.24 Response of Disk-3 gear with mixed harmonic transmission error 0.0001 rad

The modulated time waveforms of torsional vibration of the geared system as shown in figures 3.3.20 to 3.3.24 are the combined effect of vibrations at different frequencies induced by misalignment, tooth error and mounting error. Vibrations of different frequencies represent the influence of various factors contributing to the transmission error, which can be explained by the FFT responses in figures 3.3.25 to 3.3.28.

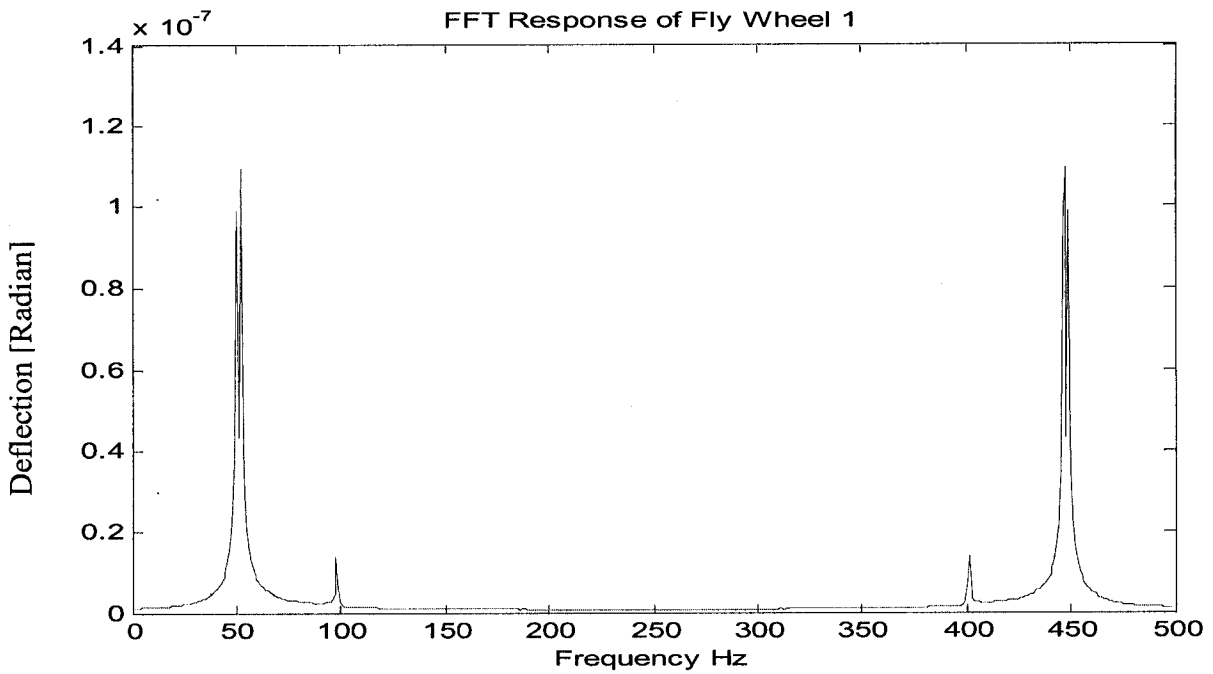

Figure 3.3.25 FFT response of Disk-1 with mixed harmonic transmission error 0.0001 rad

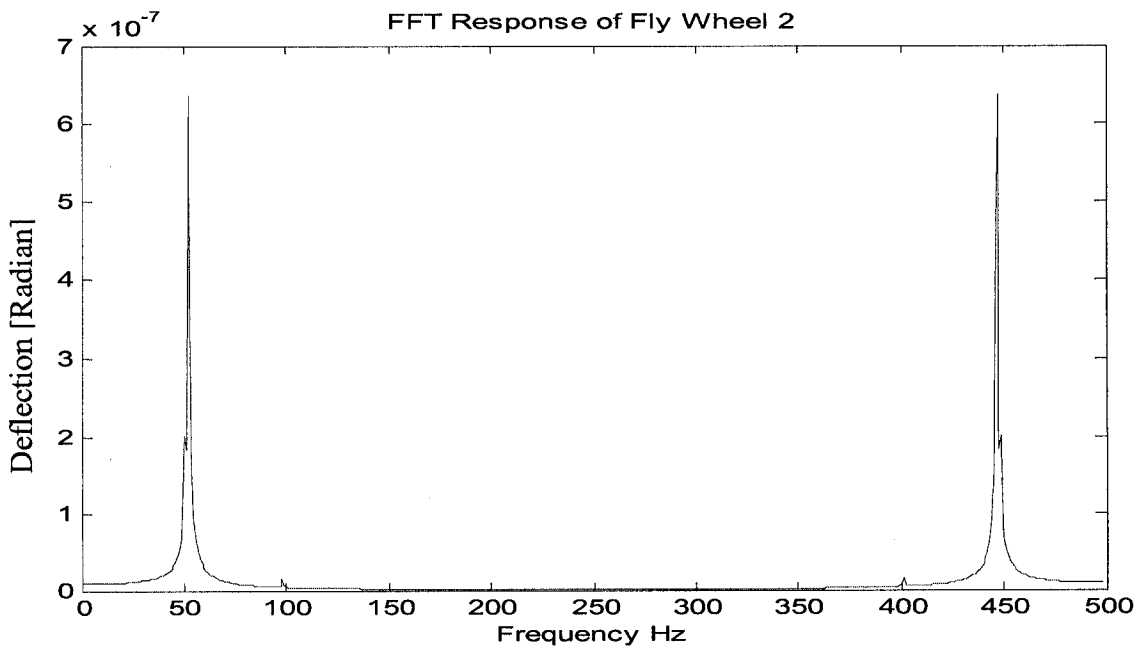

Figure 3.3.26 FFT response of Disk-2 with mixed harmonic transmission error 0.0001 rad

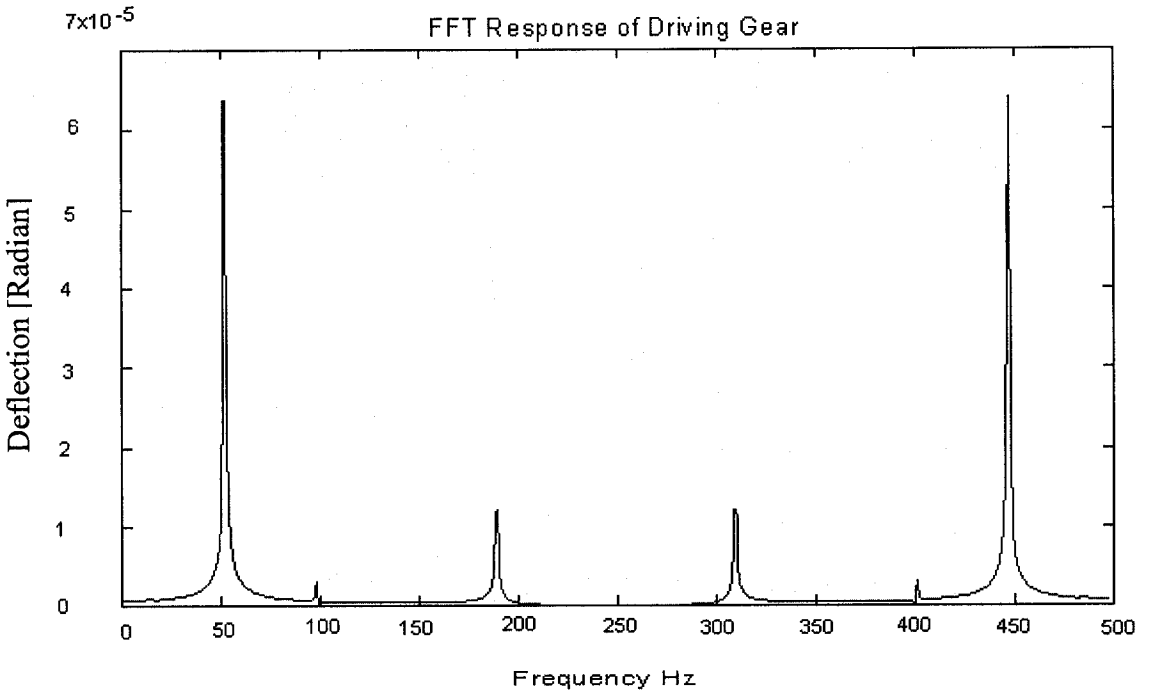

Fig. 3.3.27 FFT response of Driving gear with mixed harmonic transmission error 0.0001 rad

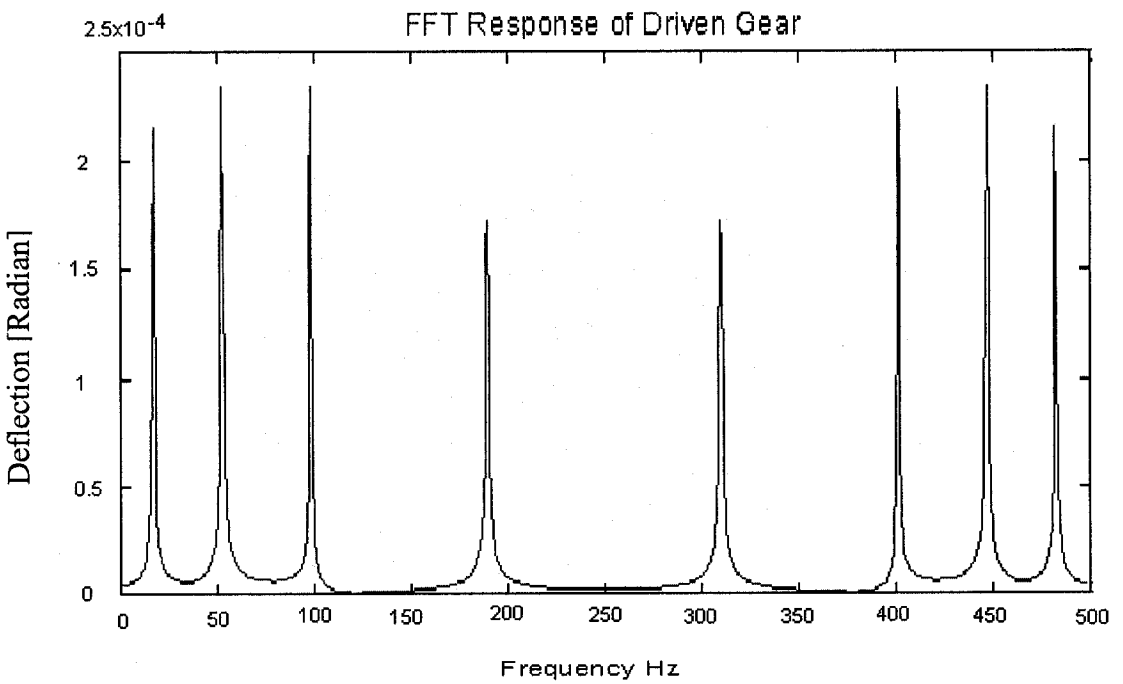

Fig. 3.3.28 FFT response of Driven gear with mixed harmonic transmission error 0.0001 rad

In the above FFT plots, vibration peaks at 50 Hz, 189.2 Hz and 450 Hz are the amplitudes of torsional vibrations corresponding to the driving shaft frequency, 3rd natural frequency and the 4th natural frequency. The 4th natural frequency plays the major role in the overall vibration responses at all discrete mass locations. This phenomenon satisfies the dominant role of the 4th mode in the modal analysis. 2X shaft frequency vibrations represent the shaft misalignment which is clearly identified within the spectrum of the driven gear at 100 Hz. The FFT response of the driven gear also shows the side bands of vibration close to the 4th natural frequency. Such vibrations are observed when the gear pair experience significant tooth wear. Manufacturing error or defective tooth can be identified by the high vibration at frequency lower than the shaft frequency which is observed at 22 Hz in the FFT plot of the driven gear.

Gear mesh frequency of a 20-tooth gear pair is out of the frequency range of the above FFT plots. The influence of eccentric mounting of gears could be observed by the high-amplitude side bands and harmonics closer to the tooth-mesh frequency. The simulation also excludes the effect of cracked tooth that produces wide bands across the spectrum.

From the above spectrum analysis it must be noted that the FFT plot of the driven gear provides the best information to identify manufacturing error, misalignment, mounting error, tooth wear, back lash etc within the geared system.

3.4 Summary

In this chapter torsional vibration of a geared system has been analyzed with two rigid masses and two rigid gears coupled by three shafts with continuously distributed mass and torsional rigidity. The continuous model is dedicated for the investigation of the influence of internal displacement excitation on gear dynamics. External excitation therefore is not considered in this analysis. A mathematical model has been proposed for solving the torsional vibration problem of a set of homogeneous differential equations with non-homogeneous boundary conditions arising from the presence of harmonic transmission error generated within the gear pair.

Natural frequencies up to the 4^{th} mode of the continuous system have a minimum deviation over the discrete results. Mode shapes and normalized mode shapes at rigid mass locations accommodate the direction of rotation of the driven sub-system with respect to the driving sub-system. The continuous model is able to analyze the individual response of driving and driven gears within the geared system. FFT plot of the driven gear is found as the best indicator to identify the root cause/s of transmission error within the gear pair. On the contrary, the time response of the equivalent mass of the 4DOF discrete model merely identifies the presence of transmission error within the geared system but can not characterize the vibrations arising from individual causes. Moreover, the continuous analysis is found to be computationally efficient and informative that can be effectively used for identification of the source/s behind the internal excitation within the geared system.

The higher mode natural frequencies can be compared with the free vibration results of a classical model that incorporates shaft mass and elasticity. In the following chapter Rayleigh-Ritz method is used to devise a torsional vibration model with approximation of a set of shape functions closer to the actual mode shapes.

CHAPTER 4
RAYLEIGH-RITZ METHOD USING BHAT'S ORTHOGONAL POLYNOMIAL FUNCTIONS

4.1 Introduction to Rayleigh-Ritz Torsional Model

In the previous chapter a mathematical model has been developed for analyzing torsional vibrations of the geared system with shafts having distributed mass and torsional rigidity. The natural frequencies and normal modes of first four modes of the model agreed with the results of the 4-DOF discrete model analyzed in the chapter 2. In order to consider the distributed elasticity of the shaft and retain the simplicity of a discrete system model, the Rayleigh-Ritz model is developed in this chapter for the four mass geared system. Finite element method or any other numerical method also would be a potential tool for such analysis. However, "..... such discretization methods provide a general framework for general structures, they invariably result in problems with a large number of degrees of freedom" [36]. The Rayleigh-Ritz method is simple and becomes computationally efficient if orthogonal polynomial shape functions are chosen.

The Rayleigh-Ritz method involves equating the maximum potential and kinetic energies of vibration. The outcomes of the classical method greatly depend on the appropriate assumption of the shape functions. For better accuracy of results and computational efficiency, the boundary characteristic orthogonal polynomial functions proposed by Bhat [39] are used.

4.2 Equations of Motion

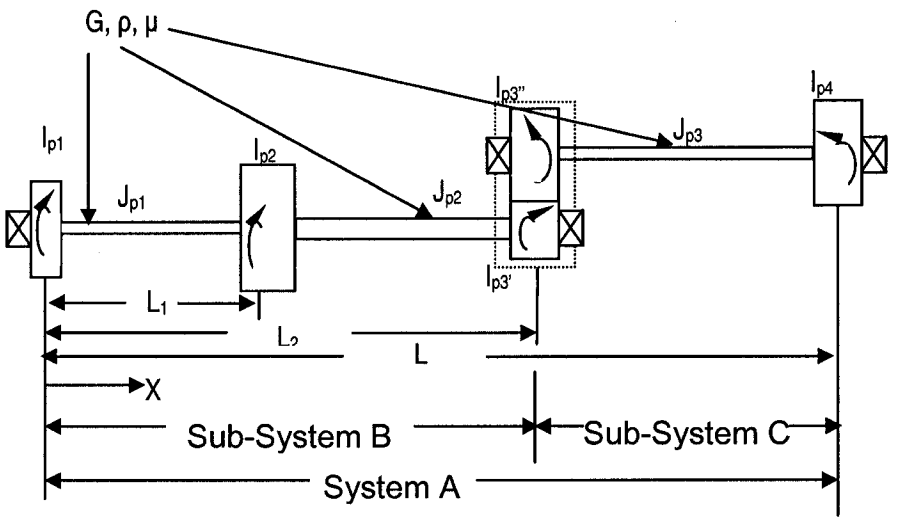

Figure 4.2.1: Schematic diagram of the Rayleigh-Ritz model for the analytical geared shaft

Let the angular deflection of the continuous system A be $\theta(x)$. It should be noted that the sub- system B is capable of rotating the sub system C and hence the maximum kinetic energy of the vibrating system A is given by

$$T_{\max} = \frac{\rho\omega^2}{2}[J_{P1}\int_0^{L_1}\theta^2(x)dx + J_{P2}\int_{L_1}^{L_2}\theta^2(x)dx + J_{P3}\int_{L_2}^{L}\theta^2(x)dx] + \frac{\omega^2}{2}[I_{P1}\theta^2(0) +$$

$$I_{P2}\theta^2(L_1) + I_{P3'}\theta^2(L_2) + I_{P3''}\theta^2(L_2) + I_{P4}\theta^2(L)] \qquad (4.1)$$

Here ω is the frequency of the free vibration of the system and $\omega^2 = T_{\max}/T^*_{\max}$

Thus $T^*_{\max} = \frac{\rho}{2}[J_{P1}\int_0^{L_1}\theta^2(x)dx + J_{P2}\int_{L_1}^{L_2}\theta^2(x)dx + J_{P3}\int_{L_2}^{L}\theta^2(x)dx] + \frac{1}{2}[I_{P1}\theta^2(0) +$

$$I_{P2}\theta^2(L_1) + I_{P3'}\theta^2(L_2) + I_{P3''}\theta^2(L_2) + I_{P4}\theta^2(L)] \qquad (4.2)$$

Maximum potential energy of the system "A" is given by

$$U_{\max} = \frac{G}{2}[J_{P1}\int_0^{L_1}\theta'^2(x)dx + J_{P2}\int_{L_1}^{L_2}\theta'^2(x)dx + J_{P3}\int_{L_2}^{L}\theta'^2(x)dx] \qquad (4.3)$$

The modulus of rigidity $G = E/2(1+\mu)$; where E is the modulus of elasticity, μ is the Poisson ratio and ρ is the density of the shaft material, distributed along the length.

Let us consider a non-dimensional variable, $\xi = \frac{x}{L}$

Then $\frac{d\xi}{dx} = \frac{1}{L}$ Then $dx = Ld\xi$

Again $\frac{d\theta}{dx} = \frac{d\theta}{d\xi} \times \frac{d\xi}{dx}$ or $\theta'(x) = \frac{1}{L}\theta'(\xi)$

Then equations (4.2) and (4.3) take the non-dimensionalized form as:

$$T^*_{\max} = \frac{\rho L}{2}[J_{P1}\int_0^{\xi_1}\theta^2(\xi)d\xi + J_{P2}\int_{\xi_1}^{\xi_2}\theta^2(\xi)d\xi + J_{P3}\int_{\xi_2}^{1}\theta^2(\xi)d\xi] +$$

$$\frac{1}{2}[I_{P1}\theta^2(0) + I_{P2}\theta^2(\xi_1) + I_{P3'}\theta^2(\xi_2) + I_{P3''}\theta^2(\xi_2) + I_{P4}\theta^2(1)] \quad (4.4)$$

$$U_{\max} = \frac{G}{2L}[J_{P1}\int_0^{\xi_1}\theta'^2(\xi)d\xi + J_{P2}\int_{\xi_1}^{\xi_2}\theta'^2(\xi)d\xi + J_{P3}\int_{\xi_2}^{1}\theta'^2(\xi)d\xi] \quad (4.5)$$

Here $\xi_1 = \frac{L_1}{L}$, $\xi_2 = \frac{L_2}{L}$ and $\xi_3 = \frac{L}{L} = 1$

According to the Rayleigh-Ritz method, the deflection of a vibrating structure (here angular deflection of the complete gear drive or system A) can be expressed as the linear combination of the deflection shape functions $\phi_i(\xi)$ and deflection coefficients A_i. [i = 1, 2, 3,.....n, and n is the number of modes or degree of freedom, associated in the Rayleigh-Ritz analysis].

Accordingly, $\theta(\xi) = \sum_{i=1}^{n} \phi_i(\xi) A_i$ (4.6)

Values of natural frequencies obtained by the Rayleigh-Ritz method depends on the selection of the deflection shape functions for all individual modes and number of degree of freedom considered for the analysis.

Procedure of Rayleigh-Ritz method starts with Rayleigh's equation [37]

$$\omega^2 = \frac{U_{max}}{T^*_{max}} \tag{4.7}$$

where U_{max} is the maximum potential energy and $\omega^2 T^*_{max}$ is the maximum kinetic energy of the vibrating system.

The deflection coefficients can be adjusted so that the natural frequencies remain stationary with respect to the shape functions. The natural frequencies are not to be always minimum with respect to the shape functions; rather they are minimum with respect to the natural modes [38]. The condition of stationarity of the natural frequencies with respect to the deflection coefficients is $\frac{\partial \omega^2}{\partial A_i} = 0$.

The partial differentiation of equation (4.7) with respect to each deflection function yields that

$$\frac{\partial \omega^2}{\partial A_i} = \frac{\partial}{\partial A_i}\left(\frac{U_{max}}{T^*_{max}}\right) = \frac{T^*_{max}\frac{\partial U_{max}}{\partial A_i} - U_{max}\frac{\partial T^*_{max}}{\partial A_i}}{T^{*2}_{max}} = 0$$

$$\frac{\partial U_{\max}}{\partial A_i} - \frac{U_{\max}}{T^*_{\max}} \frac{\partial T^*_{\max}}{\partial A_i} = 0$$

This results in the eigenvalue problem,

$$\frac{\partial U_{\max}}{\partial A_i} - \omega^2 \frac{\partial T^*_{\max}}{\partial A_i} = 0 \tag{4.8}$$

The maximum kinetic and potential energies can also be expressed in terms of "mass" and "stiffness" matrices M_{ij} and K_{ij} as:

$$T^*_{\max} = \frac{1}{2} \sum_i^n \sum_j^n M_{ij} A_i A_j \tag{4.9}$$

$$U_{\max} = \frac{1}{2} \sum_i^n \sum_j^n K_{ij} A_i A_j \tag{4.10}$$

$$\frac{\partial T^*_{\max}}{\partial A_i} = \sum_{i=1}^n \sum_{j=1}^n M_{ij} A_j \tag{4.11}$$

$$\frac{\partial U_{\max}}{\partial A_i} = \sum_{i=1}^n \sum_{j=1}^n K_{ij} A_j \tag{4.12}$$

Substituting equations (4.11) and (4.12) into equation (4.8) one will get

$$\sum_{i=1}^n \sum_{j=1}^n [K_{ij} - \omega^2 K_{ij}] A_j \tag{4.13}$$

Correlating equations (4.4), (4.5) (4.11) and (4.12) the mass and stiffness matrices for the existing system become:

$$[M_{ij}] = \sum_{i=1}^n \sum_{j=1}^n [\rho L \{ J_{P1} \int_0^{\xi_1} \phi_i(\xi) \phi_j(\xi) d\xi + J_{P2} \int_{\xi_1}^{\xi_2} \phi_i(\xi) \phi_j(\xi) d\xi \} + J_{P3} \int_{\xi_2}^{1} \phi_i(\xi) \phi_j(\xi) d\xi \} +$$

$$\{I_{P1}\phi_i(0)\phi_j(0)+I_{P2}\phi_i(\xi_1)\phi_j(\xi_1)+I_{P3'}\phi_i(\xi_2)\phi_j(\xi_2)+I_{P3'}\phi_i(\xi_2)\phi_j(\xi_2)+I_{P4}\phi_i(1)\phi_j(1)\}] \quad (4.14)$$

$$[K_{ij}]=\sum_{i=1}^{n}\sum_{j=1}^{n}\frac{G}{L}[J_{P1}\int_0^{\xi_1}\phi_i(\xi)\phi_i(\xi)d\xi+J_{P2}\int_{\xi_1}^{1}\phi_i(\xi)\phi_i(\xi)d\xi] \quad (4.15)$$

Expanding equation (4.13) one will get

$$\sum_{i=1}^{n}[A_1(K_{i1}-\omega^2M_{i1})+A_2(K_{i2}-\omega^2M_{i2})+.....+A_n(K_{in}-\omega^2M_{in})]=0 \quad (4.16)$$

For $i=1,2,3,.....n$, such equations in a matrix form is as follows:

$$\begin{bmatrix} K_{11}-\omega^2M_{11} & K_{12}-\omega^2M_{12} & \cdots & K_{1n}-\omega^2M_{1n} \\ K_{21}-\omega^2M_{21} & & & \vdots \\ \vdots & & & \\ K_{n1}-\omega^2M_{n1} & \cdots & & K_{nn}-\omega^2M_{nn} \end{bmatrix}\begin{Bmatrix} A_1 \\ A_2 \\ \\ A_n \end{Bmatrix}=0 \quad (4.17)$$

For the nontrivial solution of equation (4.17) its determinant must be equal to zero, which yields the characteristic equation for free vibration. It is an eigen value problem, the solution of which renders n numbers of eigen values $\lambda_i=\omega_i^2$ and eigen vectors $\{V_r^{(i)}\}$ for the ith mode.

The deflection coefficient modal matrix is given by

$[V]=[\{V_r^{(1)}\}\{V_r^{(2)}\}.....\{V_r^{(n)}\}]$.

Normalizing it one can get the normal deflection coefficient modal matrix $[\psi]$

The physical (angular) deflection mode is the product of the deflection coefficients modes and the deflection shape functions, as defined in equation (4.6).

4.3 Development of Deflection Shape Functions

Increasing the number of degrees of freedom one can refine the natural frequencies of the lower modes in the Rayleigh-Ritz analysis. However, the accurate values of natural frequencies depend on the selection of deflection shape functions that should satisfy at least the geometrical boundary conditions of the system. Bhat's boundary characteristic orthogonal polynomials [39] with the Rayleigh-Ritz method provide excellent approximation for the natural frequencies of beams, plates and various structures of arbitrary shapes and have been conveniently used in huge number of research papers. The same method is used here for developing angular deflection shape functions of the geared system with a goal of obtaining excellent natural frequencies. In this method the orthogonal polynomials have been generated that satisfy the geometric boundary conditions of the system. Orthogonality of adjacent shape functions on the other hand reduces the computational work in the Rayleigh-Ritz method involving a large number of degrees of freedom.

The polynomial functions have been assumed for the shape functions that satisfy the following geometric boundary conditions for each mode.

I. $\theta(0) \neq 0$ (4.18.1)

II. $\theta(\xi_1)$ = a finite value (4.18.2)

III. $\theta(\xi)\Big|_{DE} = -N\theta(\xi)\Big|_{NDE}$ (4.18.3)

It must be noted here that the direction of rotation is taken into account between driving and driven shaft, as considered in the proposed continuous model.

IV. $\theta(1)$ = a finite value (4.18.4)

The deflection shape function of the first mode is assumed so that it satisfies the rigid body mode shape of the geared shafts at 1st natural frequency. Accordingly,

$$\phi_1(\xi) = 1 \qquad 0 \le \xi \le \xi_1$$

$$= 1 \qquad \xi_1 \le \xi \le \xi_2$$

$$= -N \qquad \xi_2 \le \xi \le 1$$

Let the 2nd mode deflection shape function, $\phi_2(\xi) = (\xi - B_1)\phi_1(\xi)$

For computation efficiency, the 2nd mode deflection shape function must be orthogonal to the 1st mode function.

i.e. $\int_0^1 \phi_1(\xi)\phi_2(\xi)d\xi = 0$ (4.19)

or $\int_0^{\xi_1} \phi_1(\xi)\phi_2(\xi)d\xi + \int_{\xi_1}^{\xi_2} \phi_1(\xi)\phi_2(\xi)d\xi + \int_{\xi_2}^{1} \phi_1(\xi)\phi_2(\xi)d\xi = 0$ (4.20)

Simplifying equation (8) and (9)

$$B_1 = \frac{\int_0^{\xi_1} \xi\phi_1^2(\xi)d\xi + \int_{\xi_1}^{\xi_2} \xi\phi_1^2(\xi)d\xi + \int_{\xi_2}^{1} \xi\phi_1^2(\xi)d\xi}{\int_0^{\xi_1} \phi_1^2(\xi)d\xi + \int_{\xi_1}^{\xi_2} \phi_1^2(\xi)d\xi + \int_{\xi_2}^{1} \phi_1^2(\xi)d\xi} \tag{4.21}$$

Let the higher order deflection shape functions be:

$$\phi_i(\xi) = (\xi - B_{i-1})\phi_{i-1}(\xi) - C_{i-1}\phi_{i-1}(\xi) \tag{4.22}$$

where $i = 3,4,.....n$

The higher order polynomials are chosen so that those are orthogonal to two of their adjacent lower functions, which will make them orthogonal to all the previously constructed polynomials. Accordingly,

$$\int_0^1 \phi_i(\xi)\phi_{i-1}(\xi)d\xi = 0 \text{ and } \int_0^1 \phi_i(\xi)\phi_{i-2}(\xi)d\xi = 0$$

Then

$$\int_0^{\xi_1} \phi_i(\xi)\phi_{i-1}(\xi)d\xi + \int_{\xi_1}^{\xi_2} \phi_i(\xi)\phi_{i-1}(\xi)d\xi + \int_{\xi_2}^1 \phi_i(\xi)\phi_{i-1}(\xi)d\xi = 0 \tag{4.23.1}$$

and

$$\int_0^{\xi_1} \phi_i(\xi)\phi_{i-2}(\xi)d\xi + \int_{\xi_1}^{\xi_2} \phi_i(\xi)\phi_{i-2}(\xi)d\xi + \int_{\xi_2}^1 \phi_i(\xi)\phi_{i-2}(\xi)d\xi = 0 \tag{4.23.2}$$

Simplifying equations (4.22), (4.23.1) and (4.23.2) the constants can be derived as

$$B_{i-1} = \frac{\int_0^{\xi_1} \xi\phi_{i-1}^2(\xi)d\xi + \int_{\xi_1}^{\xi_2} \xi\phi_{i-1}^2(\xi)d\xi + \int_{\xi_2}^1 \xi\phi_{i-1}^2(\xi)d\xi}{\int_0^{\xi_1} \phi_{i-1}^2(\xi)d\xi + \int_{\xi_1}^{\xi_2} \phi_{i-1}^2(\xi)d\xi + \int_{\xi_2}^1 \phi_{i-1}^2(\xi)d\xi} \tag{4.24}$$

$$C_{i-1} = \frac{\int_0^{\xi_1} \xi\phi_{i-1}(\xi)\phi_{i-2}(\xi)d\xi + \int_{\xi_1}^{\xi_2} \xi\phi_{i-1}(\xi)\phi_{i-2}(\xi)d\xi + \int_{\xi_2}^1 \xi\phi_{i-1}(\xi)\phi_{i-2}(\xi)d\xi}{\int_0^{\xi_1} \phi_{i-2}^2(\xi)d\xi + \int_{\xi_1}^{\xi_2} \phi_{i-2}^2(\xi)d\xi + \int_{\xi_2}^1 \phi_{i-2}^2(\xi)d\xi} \tag{4.25}$$

Above polynomial functions, also satisfy the slope continuity relationship

$$\theta'(\xi_1)\Big|_{DE} = -N\theta'(\xi_1)\Big|_{NDE}$$

4.4 Modal Analysis:

Solution of equation (4.17) will provide the natural frequencies ω_i and corresponding mode shapes $\{\psi^{(i)}\}$. Using this information, response evaluation of the structure can be carried out using modal analysis.

Orthogonality of the modes is checked with the normal deflection coefficient modal matrix $[\psi]$. Following operation makes the mass and stiffness matrices diagonal.

$$\{\psi^{(i)}\}^T [M] \{\psi^{(j)}\} = M_{ii} \quad \text{for i = j}$$

$$\{\psi^{(i)}\}^T [M] \{\psi^{(j)}\} = 0 \text{ for } i \neq j \qquad \text{and}$$

$$\{\psi^{(i)}\}^T [K] \{\psi^{(j)}\} = [K_{ii}] \text{ for } i = j$$

$$\{\psi^{(i)}\}^T [K] \{\psi^{(j)}\} = 0 \text{ for } i \neq j$$

M_{ii} and K_{ii} are the generalized mass and generalized stiffness for the ith mode. Then the physical coordinate, (angular distortion) $\{q(t)\} = [\psi] \{p(t)\}$ (4.26)

where $\{p(t)\}$ is time variable modal coordinate.

Since there is close agreement between the natural frequencies and mode shapes obtained by the Rayleigh-Ritz method and the previous methods, the response analysis is not repeated for this approach.

4.5 Analytical Results of Rayleigh-Ritz Model

The natural frequencies are given in table 4.5.1 and normalized modes are shown in table 4.5.2. It must be noted that the proposed continuous model results and those from Rayleigh-Ritz analysis are compared with the results from the discrete model.

TABLE 4.5.1 NATURAL FREQUENCIES OF CONTINUOUS MODEL AND RAYLEIGH-RITZ MODEL IN COMPARISON TO DISCRETE MODEL

Mode	**Discrete Model**	**Proposed Continuous Model**		**Rayleigh-Ritz Model**	
	f_n (cpm)	**f_n (cpm)**	**Difference %**	**f_n (cpm)**	**Difference %**
1st	0	0	0	0	0
2nd	5,881	5,892	0.19	6,156	4.48
3rd	11,350	11,332	-0.16	11,605	2.35
4th	26,797	26,833	0.13	27,454	2.31
5th	-	191,580	-	190,857	-
6th	-	354,838	-	346,910.	-

TABLE 4.5.2 NORMALIZED MODES AT FOUR RIGID MASS POSITIONS:

Location	1st	2nd	3rd	4th
Disk-1	1	1	1	1
Disk-2	1	0.4805	0.0598	0.9252
Gear Pair	1	1.7104	0.1143	54.9701
Disk-3	-0.33333	-7.6686	-0.0228	-1.3043

Normalized mode shapes are shown in figures 4.5.1 to 4.5.4

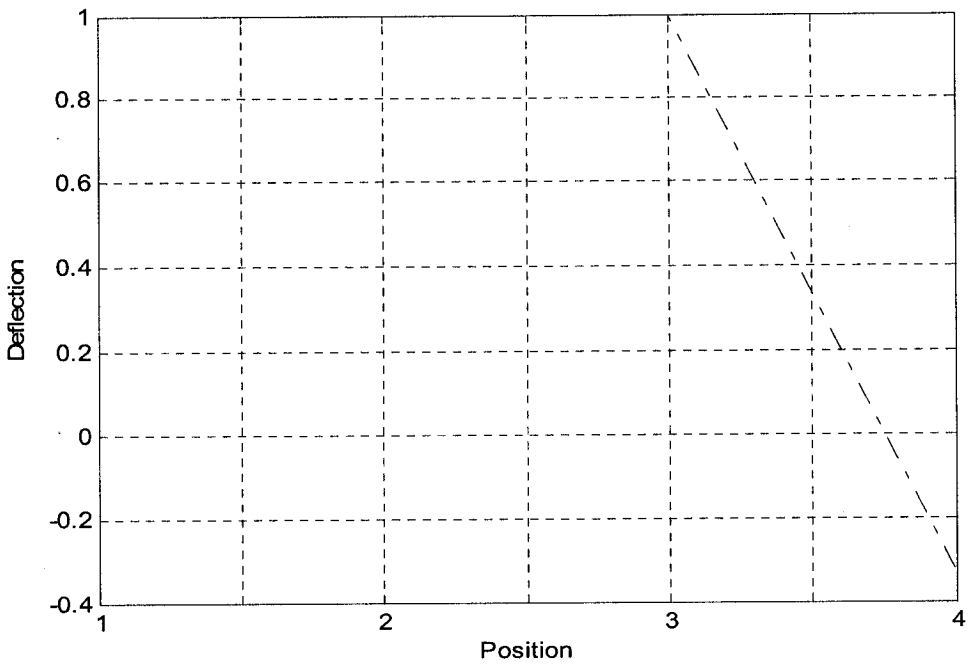

Figure 4.5.1 Rigid body mode at discrete mass locations

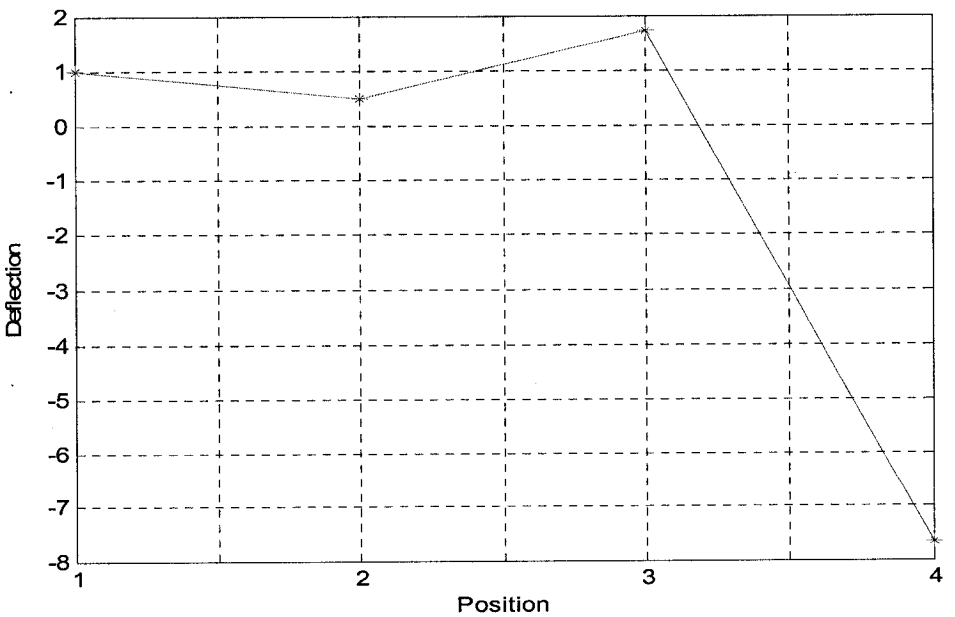

Figure 4.5.2 2nd mode (normalized) at discrete mass locations

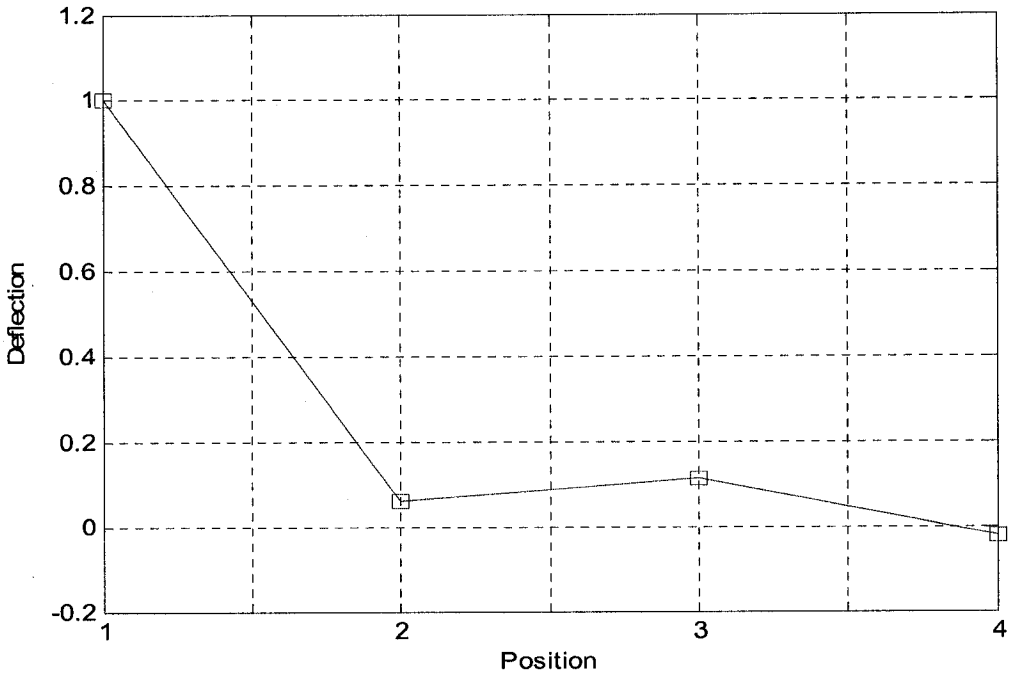

Figure 4.5.3 3rd mode (normalized) at discrete mass locations

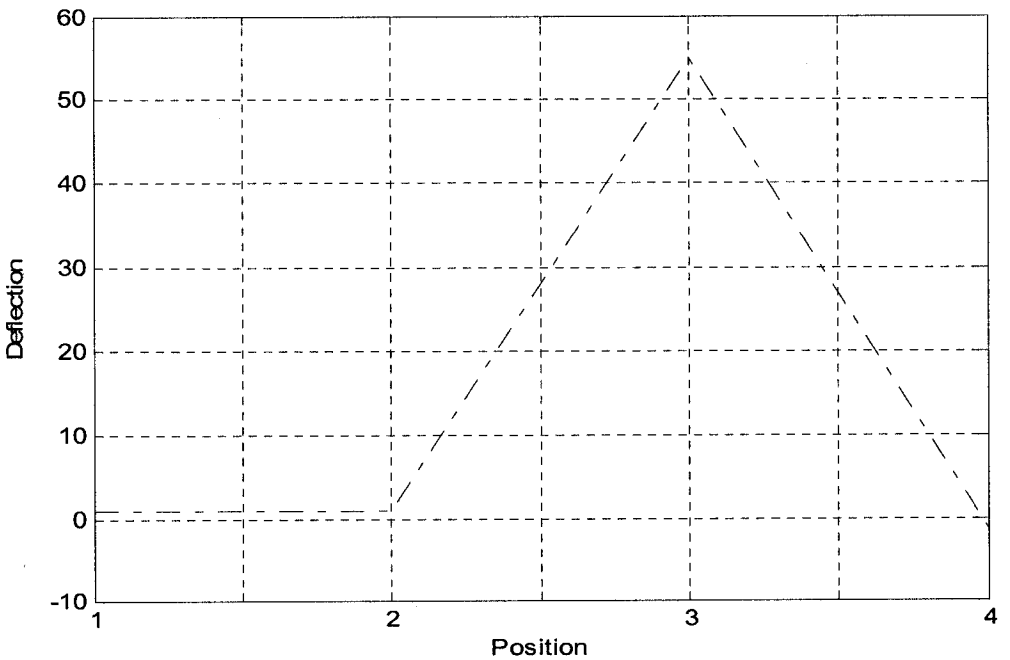

Figure 4.5.4 4th mode (normalized) at discrete mass locations

It has been observed that 2^{nd}, 3^{rd} and 4^{th} order natural frequencies obtained by Rayleigh-Ritz method are larger than the corresponding mode results of the continuous model. On the other hand natural frequencies at 5^{th} and 6^{th} modes are smaller than those of the continuous model. Normal mode shapes at lumped mass locations indicates that the 4^{th} mode is dominating. However, the deflection of the Mass-3 (equivalent mass of gear pair) at 4^{th} mode of Rayleigh-Ritz model is less than those observed in the discrete analysis in chapter 2 and in the normalized 4^{th} mode (of lumped mass locations) of the continuous model in chapter 3.

1^{st} mode of the gear system is a rigid mode, while the 4^{th} mode is stronger than the adjacent modes. Thus the shape functions of the 2^{nd} and 3^{rd} modes share major contribution of the shape function of the 4^{th} mode. As the shape functions of the 2^{nd} and 3^{rd} modes hold some portion of the higher mode shape components within them, the natural frequencies of 2^{nd} and 3^{rd} modes are higher than the actual values. Such analysis is also satisfied by a comprehensive study of Bhat [40] that investigates the influence of relative strengths of normal mode contents in the shape functions affecting the Rayleigh Ritz results.

4.6 Summary

In this chapter torsional vibration of geared system is analyzed by the Rayleigh-Ritz method. Natural frequencies of the continuous model are compared with results of the Rayleigh-Ritz method. Maximum deviation is 4.5% at the 2nd mode. Orthogonality of modes have been checked. The analytical results show that the use of Bhat's boundary characteristic orthogonal polynomials [39] in the Rayleigh-Ritz method for torsional vibration analysis of gear drives give results which are quite close to those by the continuous system model.

The proposed continuous model of chapter 3 will be further validated by an experimental investigation. The experimental aspects are described in the following chapter.

CHAPTER 5

EXPERIMENTAL ASPECTS

5.1 Introduction to Experimental Aspects

Free vibration results up to the 4^{th} mode of the proposed continuous system model closely match with those of the 4DOF discrete model [30]. Minor deviations are observed while comparing the results of the continuous model with the corresponding mode results of the classical Rayleigh-Ritz method. An experimental investigation of free vibration is done to validate the continuous model and the Rayleigh-Ritz model. This chapter describes the experimental aspects and measurement of torsional free vibration of a simplified geared system. The experimental model comprises of two shafts coupled by a pair of spur gears. Bonded resistance strain gauges are used to measure the free torsional vibration. The results obtained by the application of the proposed mathematical model and the discrete model [30] are compared with the experimental results.

5.2 Experimental Model

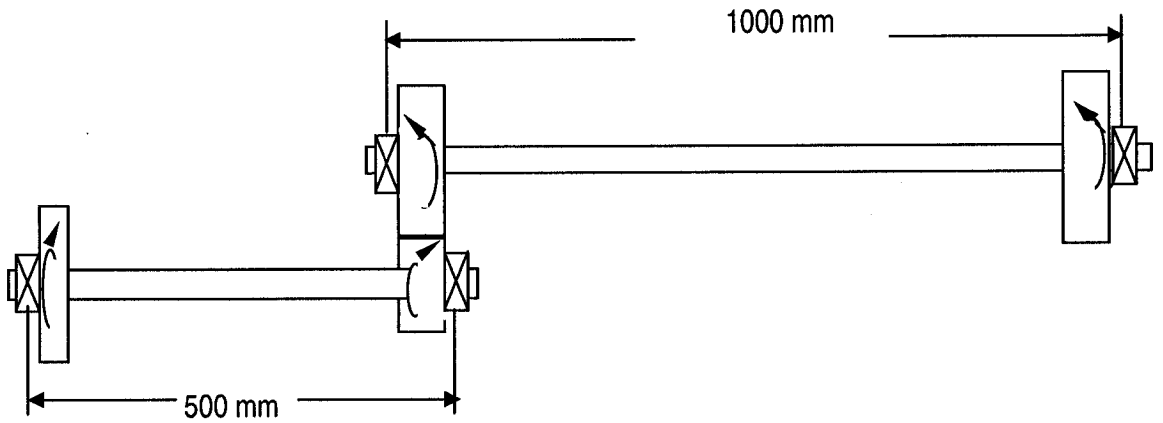

Figure 5.2.1 Schematic diagram of the experimental model

The experimental model consists of two shafts with 1 inch diameter and mounted by a spur gear pair. Two rigid disks are installed at the driving and driven sides as shown in the schematic diagram in Figure- 5.1. Length of the driving shaft is 500 mm and that of the driven shaft is 1000 mm. CATIA V-5 Release 12 is used for designing the model. Bearing pillows, precision shafts and high-precision spur gears have been purchased from the local market. Other accessories are fabricated and the complete model is assembled in the Machine Shop of Concordia University. Material and sizing details are mentioned in the table 5.2.1.

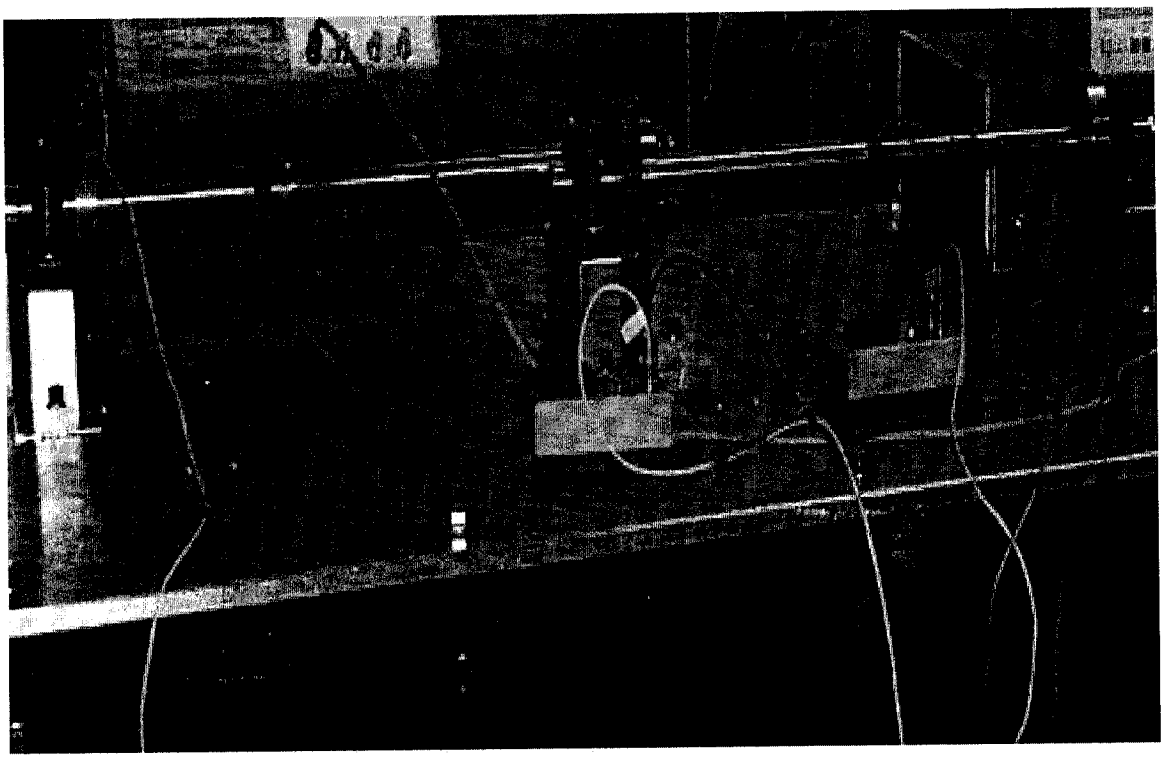

Figure 5.2.2 Experimental model- a simplified geared system

Heavy supporting pedestals and thick plate top of experimental tables are made of aluminum, in order to suppress the resonant response of the supporting structure. Very low clearance deep groove ball bearings are mounted on pedestals, which are rigidly fastened to the experimental table. Free end of the driven shaft is machined to hexagonal shape in order to tightly hold the torsion bar, which is used for torsional excitation by impact.

The Bill of Material used in the experimental setup is given in Tableb5.2.1.

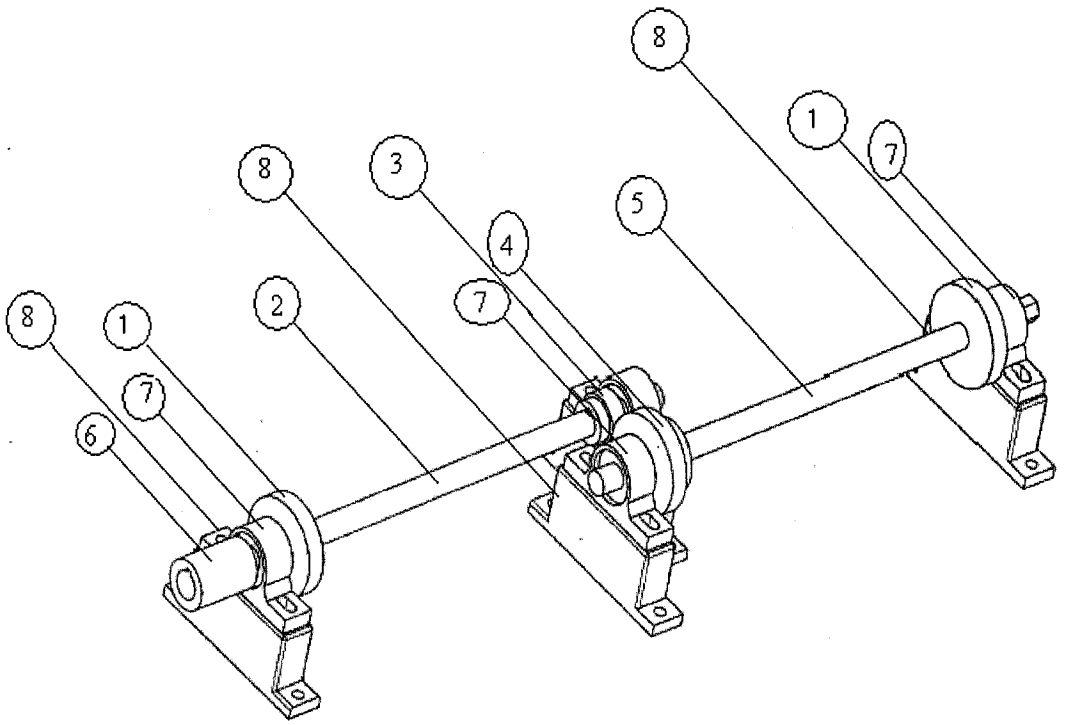

Figure 5.2.3: Experimental model, designed and fabricated by CATIA V-5 Release 14

TABLE 5.2.1: BILL OF MATERIAL OF THE EXPERIMENTAL MODEL

Part #	Description	Qty	Size	Material
1	Disk	2	4 inch dia, 0.75 inch thick	Steel
2	Driven Shaft	1	1 inch dia, 1000 mm length	Steel
3	Driven Gear	1	4 inch dia, 0.75 inch thick	Steel
4	Driving Gear	1	2 inch dia, 0.75 inch thick	Steel
5	Driving Shaft	1	1 inch dia, 500 mm length	Steel
6	Rigid Coupling	1		Steel
7	Pillow Block	4	HRP bearings	SKF
8	Supporting Pad	4		Aluminum
9	Variable speed Motor	1	5 hp, 3600 rpm, 575 V, 60 Hz	Steel Shaft

5.3 Experimental Setup

The experimental set up is shown in figure 5.3.1 and a schematic diagram of the set up is shown in figure 5.3.2.

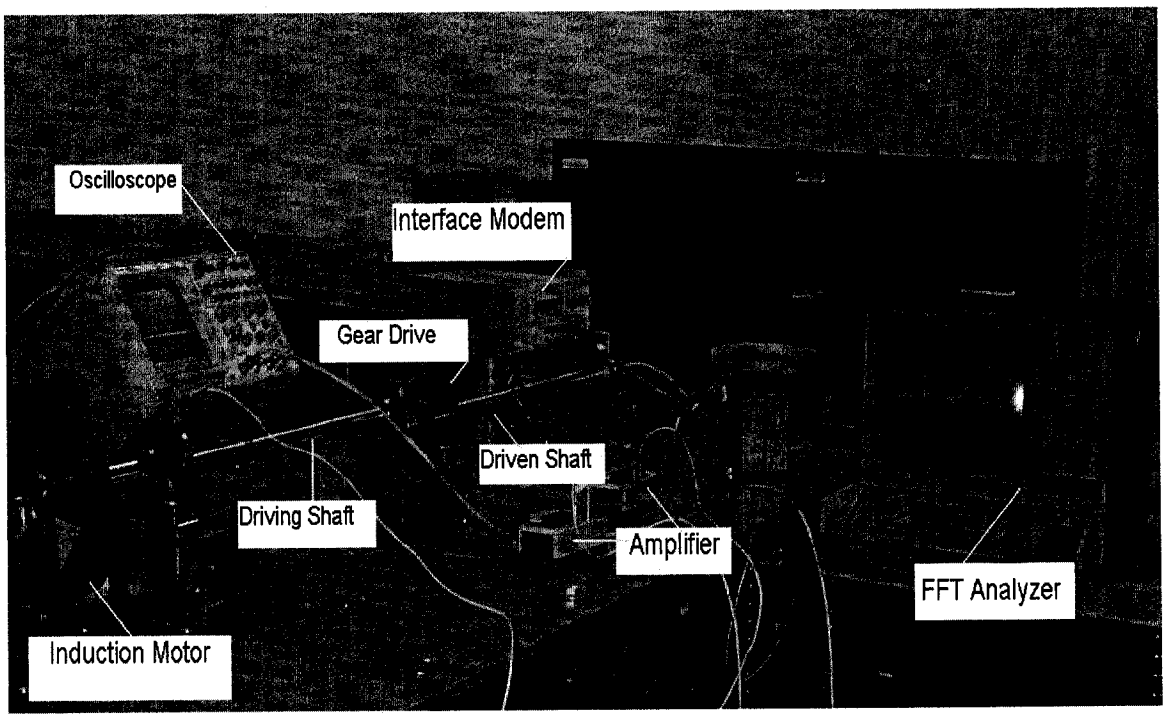

Figure 5.3.1 Experimental setup for free torsional vibration measurement

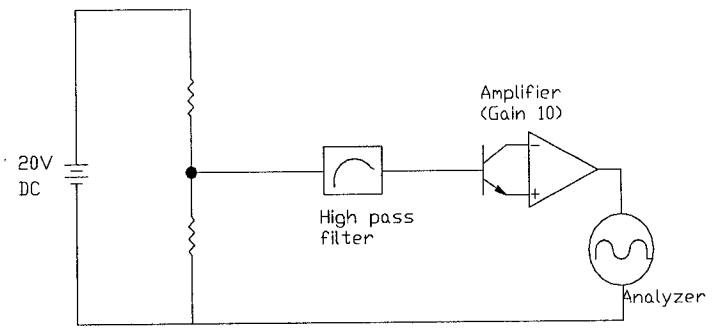

Figure 5.3.2: Schematic diagram of experimental setup

A simplified ½ Wheatstone Bridge is used for the measurement accuracy, which is illustrated in the figure 5.4.2.

5. 4 Strain Gauge

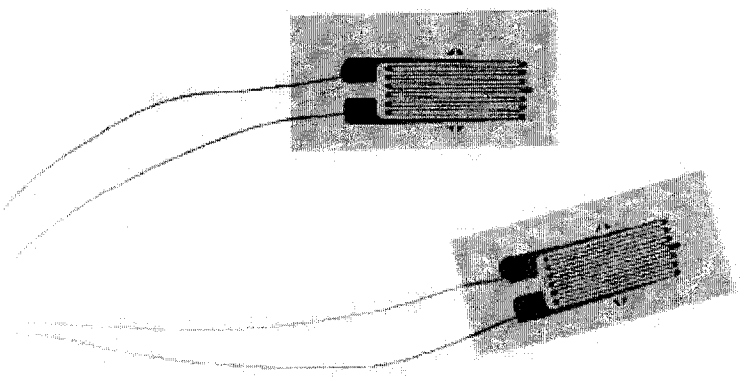

Figure 5.4.1 Bonded metallic foil grid resistance strain gauge

Bonded Resistance Strain gauge is most widely used to measure the torsional deflection. The BRS gage consists of a grid of very fine metallic wire, foil, or semiconductor material bonded to the strained surface or carrier matrix by a thin insulated layer of epoxy (Figure 2-5). When the carrier matrix is strained, the strain is transmitted to the grid material through the adhesive. The variations in the electrical resistance of the grid are measured as an indication of strain.

5.4.1 PRINCIPLE OF STRAIN GAUGE

Wheatstone bridge principle is used in the commercially available bonded resistance strain gauges. A general Wheatstone Bridge consists of four resistive arms arranged in a diamond orientation with an excitation DC voltage, V_{EX}, supplied across the bridge.

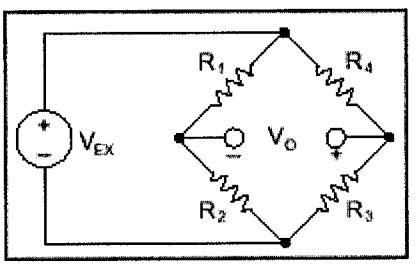

Figure 5.4.2 Wheatstone bridge circuit

The output voltage of the bridge, V_O, will be equal to:

$$V_0 = \left[\frac{R_3}{R_3 + R_4} - \frac{R_2}{R_1 + R_2}\right] * V_{EX}$$

When $R_1/R_2 = R_4/R_3$, the voltage output V_O will be zero and then the bridge is completely balanced. Any change in resistance in any arm of the bridge will result in a

nonzero output voltage appear across the middle of the bridge. In case of torsional vibration measurement the resistance of the strain gauge changes only in response to torsional deflection. However, strain gauge material, as well as the specimen material to which the gauge is applied, will also respond to changes in temperature. Compensated gauges are used to reduce the thermal sensitivity.

In a quarter bridge arrangement one resistance arm is an active resistor and other resistors have fixed values known as completion resistors. On the other hand in case of half-bridge configuration, two resistors are used for measuring strain and two for completing the circuit. The half-bridge circuit yields an output voltage that is linear and approximately doubles the output of the quarter-bridge circuit. For better sensitivity and compensating the effect of temperature, half-bridge configuration is preferable.

5.4.2 INSTRUMENTATION

The experimental set up comprises of the following instrumentation:

- Strain Gauge
- Power Supply Unit with Input voltage 20 volt DC
- High Pass Filters
- Amplifier with gain 10
- An Oscilloscope for torsional free vibration measurement in time domain
- FFT analyzer for torsional free vibration measurement in frequency domain

Some of the advantages of the strain gauge are:

- Better accuracy, +/-0.10%
- Highly sensitive to strain.
- Compact size with negligible mass
- Available in a short gage length
- Negligible temperature effect
- Comparatively less expensive
- Suitable for a wide variety of environmental conditions

The following are some limitations of the strain gauge:

- Electrical noise and interference may alter the micro-level strain readings.
- Shielded leads and adequately insulating coatings prevent these problems.

5.5 Experimental Procedure

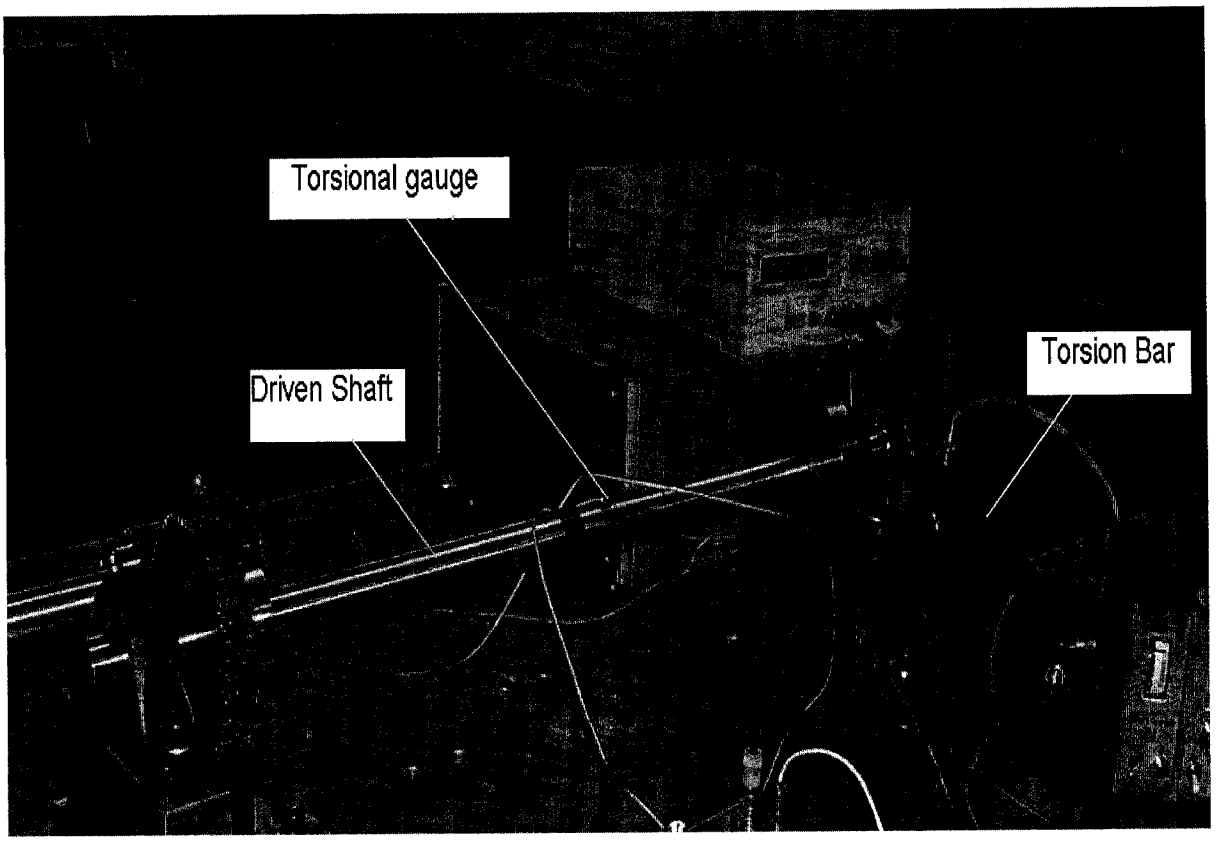

Figure 5.5.1 Free torsional vibration measurement on the driven shaft

An instrumented impact hammer is applied on a torsion bar, rigidly attached to the free end of the driven shaft. The impact of the hammer generates free torsional vibrations within the system. Torsional vibrations of the experimental model are measured by bonded resistance torsional strain gauges, installed on the driving shaft. The signal is amplified by an amplifier and then displayed in time domain on an oscilloscope. Torsional free vibration in the frequency domain is measured and recorded by a spectrum analyzer.

The spectrum of free vibration of the geared system is mixed with external noise disturbance. Kistler 4382, uni-axial piezoelectric type accelerometers were mounted on the table and supporting pedestal to investigate the nature of disturbance from these components. The tip probe of the impact hammer captures the disturbance vibration of the impact hammer-torsion bar system. Nature of disturbance signals from the supporting structures and torsion bar-impact hammer are characterized by the FFT analyzer. The peak frequencies of the accelerometer signals match with some of the side band frequencies in the free torsional vibration measurement. Free vibration peaks are identified neglecting the peaks at disturbance frequencies. The same procedure is followed to measure the natural frequencies of the geared drive with installation of the strain gauges on the driven shaft.

5.6 Experimental Results

Free torsional vibration analysis of experimental model with torsional strain gauge installed on driving shaft are represented in figures 5.6.1 to 5.6.5.

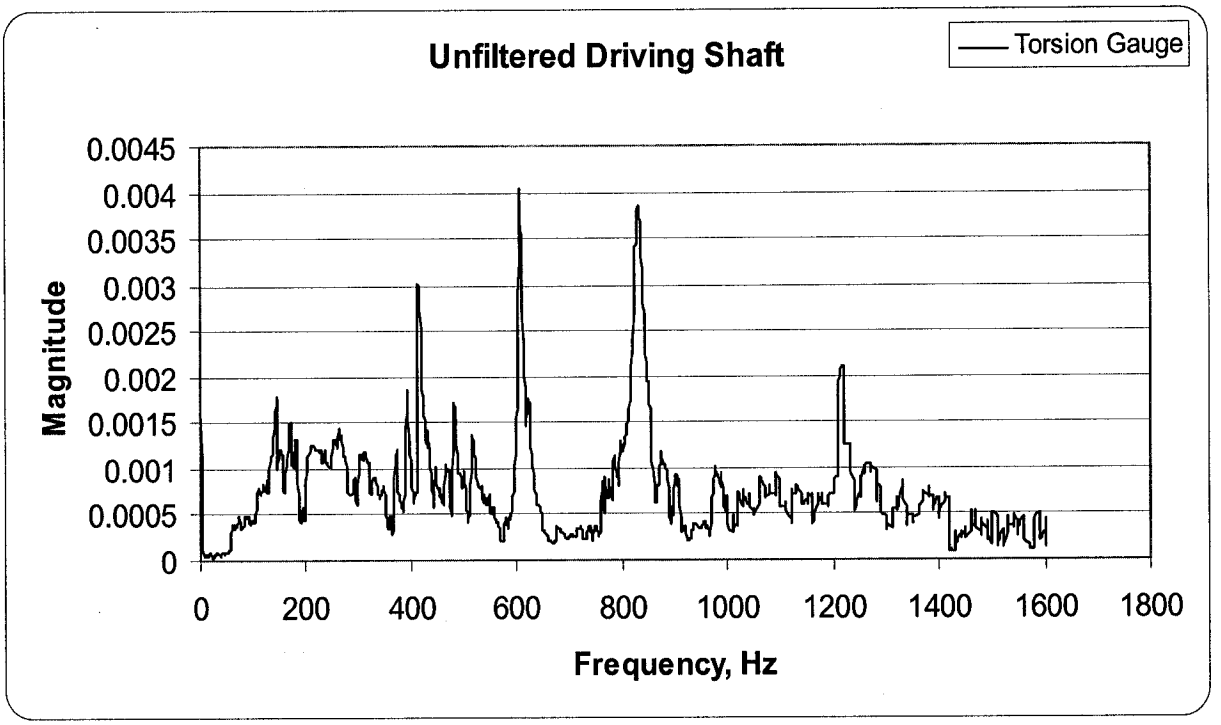

Figure 5.6.1 Spectrum of free torsional vibration measured by torsional strain gauge installed on driving shaft with disturbing signals of structural support and torsion bar.

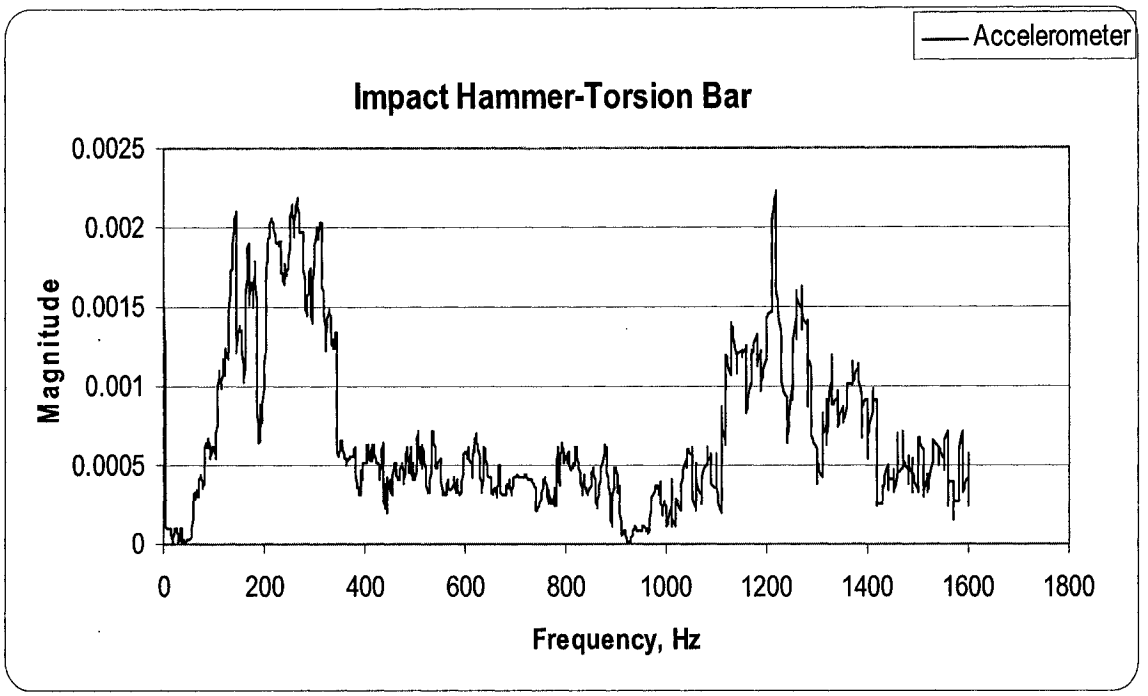

Figure 5.6.2 Spectrum of the disturbing signal of impact hammer-torsion bar

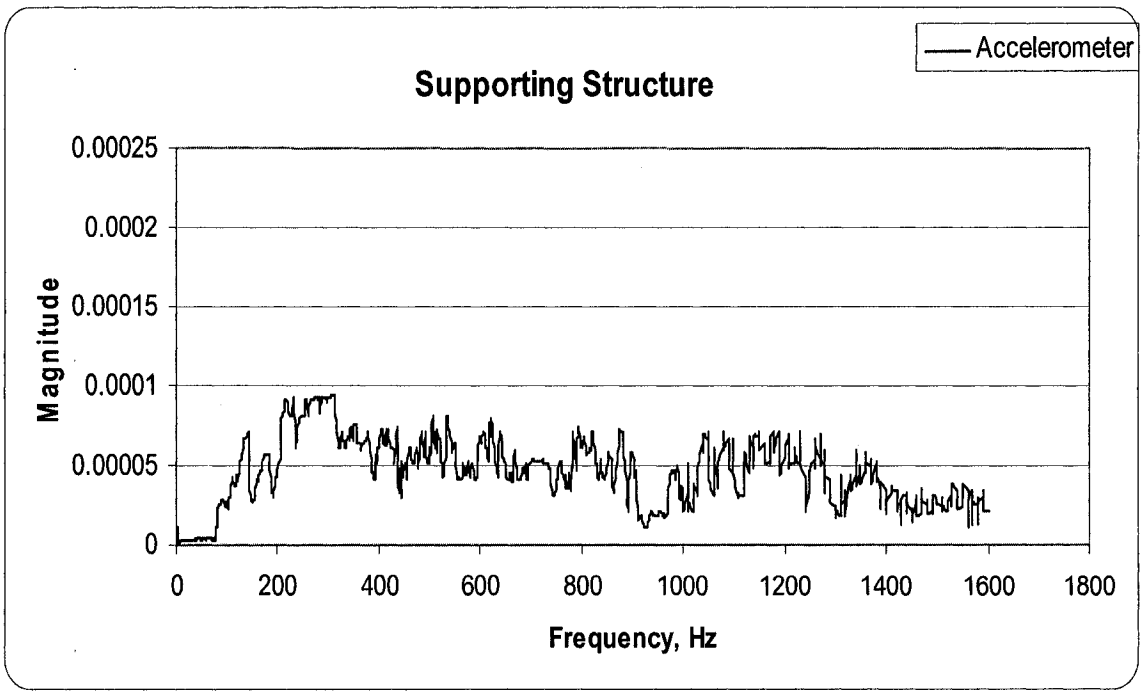

Figure 5.6.3 Spectrum of the disturbing signal of supporting structure

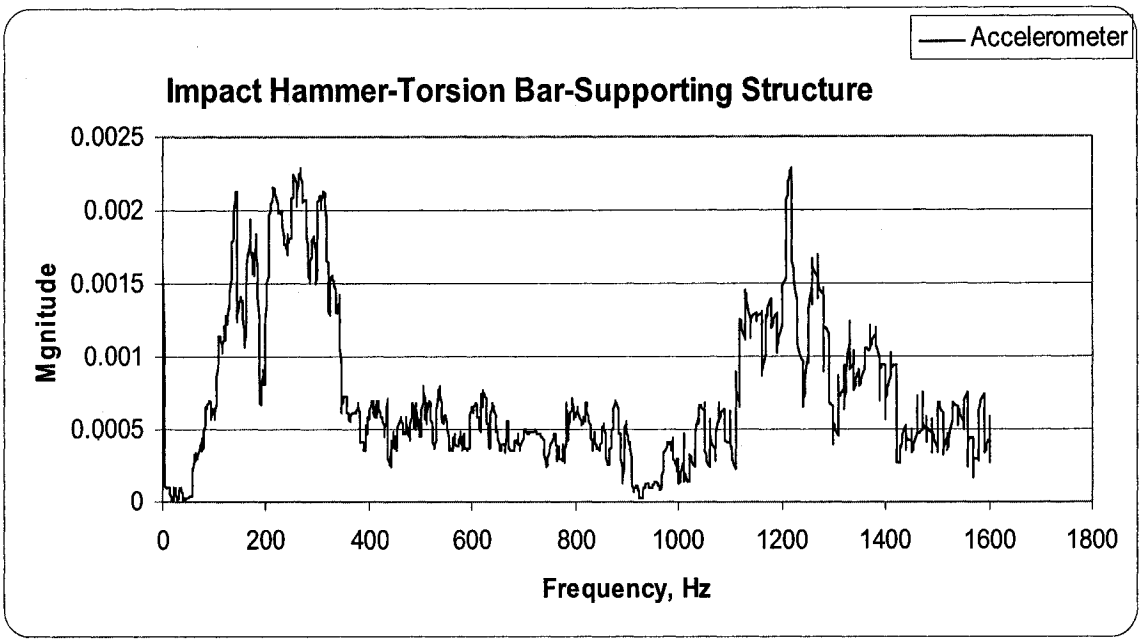

Figure 5.6.4 Spectrum of the disturbing signal of impact hammer-torsion bar and supporting structure

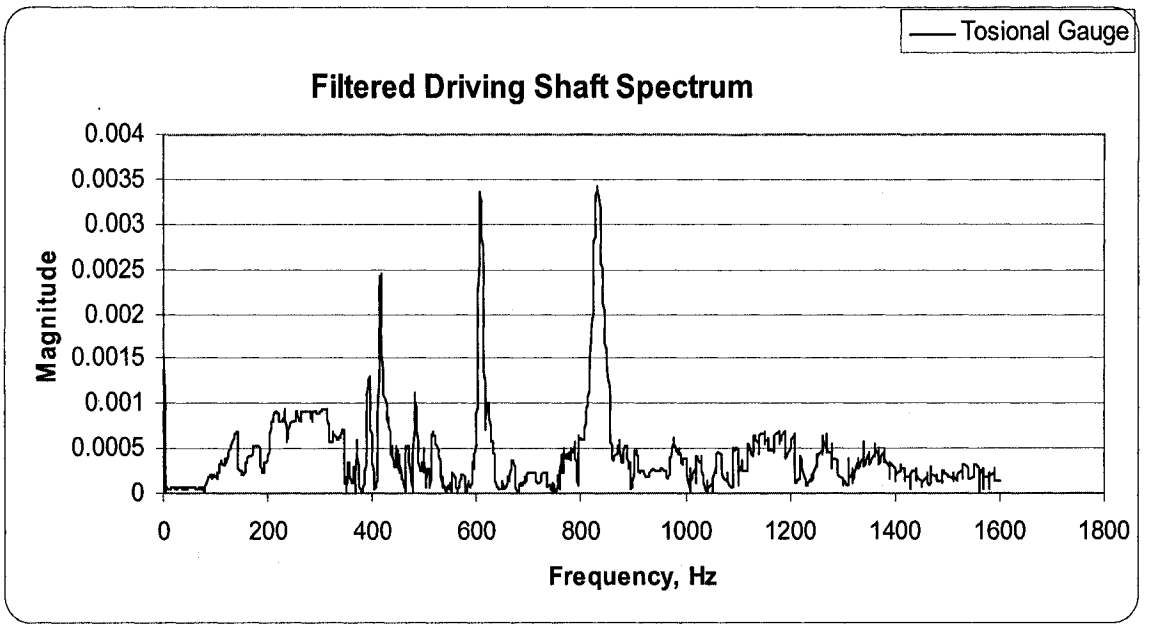

5.6.5 Spectrum of free torsional vibration measured by torsional strain gauge installed on driving shaft after subtracting disturbing signals of structural support and torsion bar.

Free torsional vibration analysis of experimental model with torsional strain gauge installed on driven shaft are represented in figures 5.6.6.and 5.6.7.

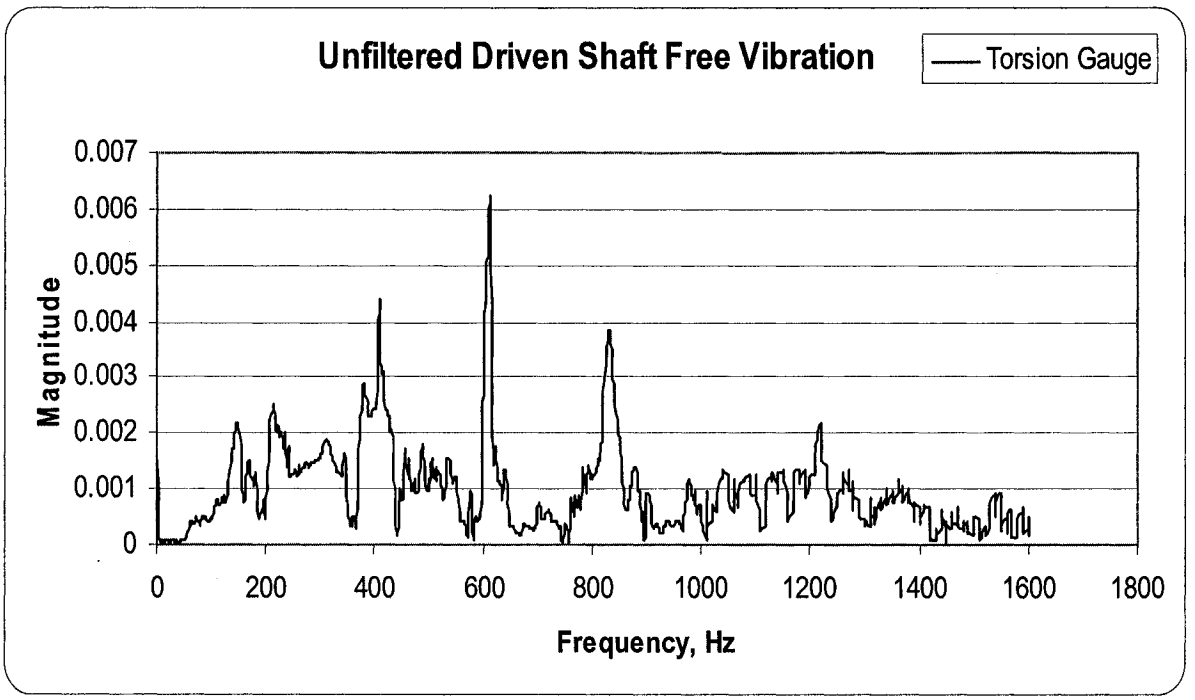

5.6.6 Spectrum of free torsional vibration measured by torsional strain gauge installed on driven shaft with disturbing signals of structural support and torsion bar.

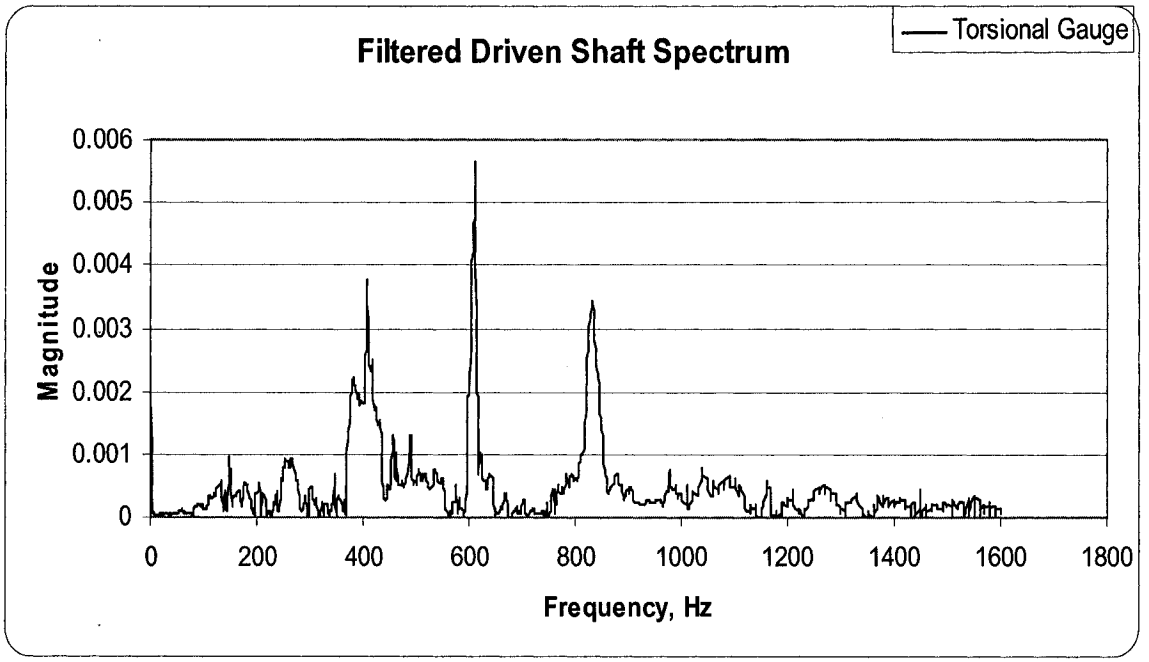

Figure 5.6.7 Spectrum of free torsional vibration measured by torsional strain gauge installed on driven shaft after subtracting the signals of structural support and torsion bar.

Eliminating the external noise, three peaks are observed in the measured response spectra at the driving and driven shafts, which are shown in Figures 5.6.5.and 5.6.7. The third peak frequency matches with the third natural frequency of the experimental geared system as determined by using the continuous model and by the discrete analysis. Similarly, the frequency of the second peak is close to the 2nd natural frequency of the experimental geared system applying the proposed model and the discrete model. The first peak frequency of the measured response spectra at both of the driving and driven shafts is however just half of the 3rd natural frequency. It can be mentioned that the 1st mode of the geared system is a rigid body mode with zero natural frequency. Table 5.6.1 summarizes the experimental values of the natural frequencies measured by torsional gauges installed on the driving and driven shafts. Table 5.6.2 on the other hand compares

the experimental results with the analytical results applying the proposed continuous model and discrete analysis for the simplified experimental geared system.

TABLE 5.6.1 SUMMARY OF NATURAL FREQUENCIES OF THE EXPERIMENTAL GEARED SYSTEM

Mode	**Experimentally Measured Natural Frequency, cpm**		
	with Torsional Gauge at Driving Shaft	with Torsional Gauge At Driven Shaft	Average
1	0	0	0
2	38,040	37,920	37,980
3	51,240	51,300	51,270
4	Limited by the Frequency Range of the FFT Analyzer: 1000 Hz		

TABLE 5.6.2 NATURAL FREQUENCIES OF ANALYTICAL MODEL IN COMPARISON TO THE EXPERIMENTAL RESULTS:

Mode	**Natural Frequency of the Simplified Geared System**				
	Experimental Result	Cont Model Results		3 DOF Discrete Model Results	
	fn, cpm	fn, cpm	Difference %	fn, cpm	Difference %
1	0	0	0	0	0
2	37,980	38,520	+1.42	37,320	-1.74
3	51,270	50,880	-0.76	50,520	-1.46
4	Limited by range of FFT analyzer	144,480	-	Limited by 3DOF	-

5.7 Summary

While comparing the analytical results with the experimental natural frequencies, it is observed that the results of proposed continuous model for the experimental geared system are slightly closer than those of the discrete model. The third mode dominates over the second mode. The peak at half of the 3rd natural frequency is anticipated to be caused by the misalignment of the driving shaft with respect to the driven shaft. A detailed investigation is required in future experiments for periodic torsional vibration analysis.

CHAPTER 6

CONCLUSIONS AND FUTURE WORK

6.1 Summary

A new continuous model is proposed for dynamic analysis of self excited geared system that involves time dependent boundary conditions. Natural frequencies of first four modes of the proposed model closely match with the results of a 4DOF discrete model of a previous paper [30]. SIMULINK models are added to the discrete analysis for investigating the influence of transient and steady state transmission error within the system.

Natural frequencies of the continuous model are also compared with the corresponding modes of Rayleigh-Ritz model and a minor deviation is observed. Boundary characteristic orthogonal polynomials are used with the Rayleigh-Ritz method for the determination of natural frequencies. Influence of a stronger mode is observed in adjacent modes.

A simplified geared system is designed and fabricated for the experiment of free torsional vibration. Bonded metallic foil grid resistance strain gauges are installed on the driving and driven shafts for comparing the natural frequencies of both of the shafts. Thus the experimental aspects validate the proposed continuous model.

6.2 Conclusions:

The following important conclusions can be drawn from the analytical and experimental studies undertaken in this research:

1. The proposed continuous model provides better results and can be used for the dynamic analysis of gear drives.

2. Rigid body mode is observed at 1st natural frequency in both of the discrete and continuous models. However non linear mode shapes are found for two shafts coupled by a gear pair in the continuous model at higher modes.

3. The SIMULINK model determined the magnification factor of resonant dynamic torque for accurate measurement of responses by the discrete modal analysis.

4. The discrete model merely indicates the development of transmission error. However, the continuous model identifies the sources of transmission error.

5. The continuous model determines the mode shapes and responses of the driving and driven gears individually.

6. The Rayleigh-Ritz method with boundary characteristic orthogonal polynomials provides better approximation of natural frequencies and can be conveniently used for forced vibration analysis of geared shaft.

7. In the Rayleigh-Ritz model the 4th mode is stronger than the adjacent modes and causes upper bound natural frequencies in lower modes and lower bound natural frequencies at higher modes.

8. Rayleigh-Ritz method with Bhat's boundary characteristic orthogonal polynomials is easier for computer implementation, but the proposed continuous model is computationally more efficient.

6.3 Future Work

This thesis has built a concrete foundation of a new continuous approach for analyzing the self excited dynamic load in gear drives that encompasses effects of manufacturing error, mounting error, elastic deformation and linear meshing stiffness variation. Although the comparative model analysis proves the effectiveness of this model, incorporation of following aspects further improve the dynamic load analysis, which ultimately improves gear design.

- Free and Forced vibration analysis with non-homogeneous anisotropic shaft material with variable cross section.
- Integrating damping, backlash, friction and other nonlinearities within the continuous model of the geared systems.
- Extending the continuous model incorporating the coupled effect of lateral, torsional and axial vibrations considering rotor-bearing system of geared systems.
- Extending the experimental investigation for studying the individual influence of tooth profile error, misalignment, eccentric bearing and gear installation as well as the bent shafts on the natural frequencies and responses of geared systems.
- A comprehensive study of analyzing the influence of modes on the natural frequencies of the Rayleigh-Ritz model for geared systems.
- Developing the Rayleigh-Ritz model for forced vibration analysis of geared systems.

REFERENCES

[1] BUCKINGHAM, E., Analytical Mechanics of Gears New-York: McGraw-Hill, pp. 453-473, 1949.

[2] TUPLIN,W. A., "Dynamic Loads on Gear Teeth", Machine Design **25**, pp. 203-211, 1953.

[3] TUPLIN, W. A., "Dynamic Loads on Gear Teeth", Proceedings of the Institution of Mechanical Engineers **16**, pp. 24-30, 1958.

[4] HARRIS, S. L., "Dynamic Loads on the Teeth of Spur Gears", Proceedings of the Institution of Mechanical Engineers **172**, pp. 87-112, 1958.

[5] JOHNSON, D. C., "Excitation of Resonant Vibrations by Gear Tooth Meshing Effects", Proceedings of the International Conference on Gearing, Institution of Mechanical Engineers, pp. 18-23, 1958.

[6] GREGORY, R. W., HARRIS, S. L. and MUNRO, R. G., "Dynamic Behavior of Spur Gears", Proceedings of the Institution of Mechanical Engineers **178**, pp. 207-226, 1963-1964.

[7] AIDA, T., "Fundamental Research on Gear Noise and Vibration", Transactions of the Japanese Society of Mechanical Engineers, **34**, pp. 2226-2264, 1968.

[8] Ozguvent, H. N. and Houser, D.R., "Mathematical Models Used in Gear Dynamics- A Review", Journal of Sound and Vibration, **121(2)**, pp. 383-411, 1988.

[9] VELEX, P. and MAATAR, M., "A Mathematical Model for Analyzing the Influence of Shape Deviations and Mounting Errors on Gear Dynamic Behaviour", Journal of Sound and Vibration, **191(5)**, pp. 629-660, 1996.

[10] HUANG, K. J. and LIU, T. S., "Dynamic Analysis of a Spur Gear by the Dynamic Stiffness Method", Journal of Sound and Vibration, **234(2)**, pp. 311-329, 2000.

[11] NADOLSKI, W. and PIELORZ, A., "The Influence of Variable Stiffness of Teeth on Dynamic Loads in Single-Gear Transmission", Archive of Applied Mechanics, **68**, pp. 185-194, 1998.

[12] THEDOSSAIADES, S. and NATSIAVAS, S., "Non-Linear Dynamics of Gear-Pair Systems with Periodic Stiffness and Backlash", Journal of Sound and Vibration, **229(2)**, pp. 287-310, 2000.

[13] PARKER, R. G., VIJAYAKAR, S. M. and IMAJO, T., "Non-Linear Dynamic Response of a Spur Gear Pair: Modeling and Experimental Comparisons" Journal of Sound and Vibration, **237(3)**, pp. 435-455, 2000.

[14] VAISHYA, M. and SINGH, R., "Sliding Friction-Induced Non-Linearity and Parametric Effects in Gear Dynamics", Journal of Sound and Vibration, **248 (4)**, pp. 671-694, 2001.

[15] VELEX, P. and SAINSOT, P., "An Analytical Study of Tooth Friction Excitations in Errorless Spur and Helical Gears", Mechanism and Machine Theory, **37**, pp. 641-658, 2002.

[16] WOJNAROWSKI, J. and ONISHCHENKO, V., "Tooth Wear Effects on Spur gear Dynamics", Mechanism and Machine Theory, **38**, pp. 161-178, 2003.

[17] VEDMAR, L. and ANDERSSON, A., "A Method to Determine Dynamic Loads on Spur Gear Teeth and on Bearings", Journal of Sound and Vibration, **267**, pp. 1065-1084, 2003.

[18] LI, M. and YU, L., "Analysis of the Coupled Lateral Torsional Vibration of A Rotor-Bearing System with a Misaligned Gear Coupling", Journal of Sound and Vibration, **243(2)**, pp. 283-300, 2001.

[19] LI, M., HU, H. Y., JIANG P. L. and YU, L., "Coupled Axial-Lateral-Torsional Dynamics of A Rotor-Bearing System Geared by Spur Bevel Gears", Journal of Sound and Vibration, **254(3)**, pp. 427-446, 2002.

[20] LUO, Z., SUN, X. and FAWCETT, J.N., "Coupled Torsional-Lateral-Axial Vibration Analysis of A Geared Shaft System Using Substructure Synthesis", Mechanical Machine Theory, **31 (3)**, pp. 345-352, 1996.

[21] RAO, M. A., SRINIVAS, J., RAMA RAJU, V. B. V. and KUMAR, K. V. S. S., "Coupled Torsional-Lateral Vibration Analysis of Geared Shaft Systems Using Mode Synthesis", Journal of Sound and Vibration, **261(2)**, pp. 359-364, 2003.

[22] LEE, A. S., HAB, J. W. AND CHOIC, D. H., "Coupled Lateral and Torsional Vibration Characteristics of a Speed Increasing Geared Rotor-Bearing System", Journal of Sound and Vibration, **263**, pp. 725-742, 2003.

[23] VINAYAK, H., SINGH, R. AND PADMANABHAN, C., "Linear Dynamic Analysis of Multi-Mesh Transmissions Containing External, Rigid Gears", Journal of Sound and Vibration **185(1)**, pp.1-32, 1995.

[24] ROOK, T. E. AND SINGH, R., "Dynamic Analysis of A Reverse-Idler Gear Pair with Concurrent Clearances", Journal of Sound and Vibration **182(2)**, pp. 303-322, 1995.

[25] YUKSEL, C. AND KAHRAMAN, A., "Dynamic Tooth Loads of Planetary Gear Sets Having Tooth Profile Wear", Mechanism and Machine Theory, **39**, pp. 695–715, 2004.

[26] LEE, A. S. AND HA, J. W., "Prediction Of Maximum Unbalance Responses Of A Gear-Coupled Two-Shaft Rotor-Bearing System", Journal of Sound and Vibration **283**, pp. 507–523, 2005.

[27] LITAK, G. AND FRISWELL, M., "Dynamics of a Gear System with Faults in Meshing Stiffness", Nonlinear Dynamics, **41**, pp. 415–421, 2005.

[28] VELEX, P. AND AJMI, M., "On the modelling of excitations in geared systems by transmission errors", Journal of Sound and Vibration **290**, pp. 882–909, 2006.

[29] BONORI, G. AND PELLICANO, F., "Non-smooth dynamics of spur gears with manufacturing errors" Journal of Sound and Vibration **306**, pp. 271–283, 2007.

[30] MAHALINGAM, S. AND R. D. BISHOP, "Dynamic Loading of Gear Teeth", Journal of Sound and Vibration **36(2)**, pp. 179-189, 1974.

[31] BISHOP, R. E. D., GLADWELL, G. M. L. AND MICHAELSONSON, S., "The Matrix Analysis of Vibration", Cambridge at the University Press, pp. 36-53, 1965.

[32] MEIROVITCH, LEONARD, The Macmillan Company, New York, Collier Macmillan Limited, London, "Analytical Methods in Vibrations" pp. 300-308, 1967.

[33] GRANT D. A., "Beam Vibration with Time-Dependent Boundary Conditions", Journal of Sound and Vibration **89(4)**, pp. 519-522, 1983.

[34] WEDYAN, H. A, "Control of Whirling Vibrations in BTA Deep Hole Boring Process using Fuzzy Logic Modeling and Active Suppression Technique", a PhD thesis, Department of Mechanical, Concordia University, Montreal, Quebec, Canada, pp. 38-77, 2004.

[35] GIRDHAR, P., "Practical Machinery Vibration Analysis and Predictive Maintenance", Elsevier, pp. 116-120, 2004.

[36] CHAKRAVARTY, S., BHAT, R.B., STIHARU, I., "Recent Research on Vibration of Structures Using Boundary Characteristic Orthogonal Polynomials in the Raleigh-Ritz method", Shock and Vibration Digest, **31 (3)**, pp.187-194, 1999.

[37] THOMPSON, W. T. AND DAHLEH, M. D., "Theory of Vibration with Applications" Prentice Hall, Inc. 5th edition, pp. 363 -365 and pp. 263-265, 1998.

[38] BHAT, R.B., "Nature of Stationarity of the Natural Frequencies at the Natural Modes in the Rayleigh-Ritz Method", Journal of Sound and Vibration **203(2)**, pp.251-263, 1997.

[39] BHAT, R.B., "Natural Frequencies of Rectangular Plate Using Characteristic Orthogonal Polynomials in Rayleigh-Ritz Method", Journal of Sound and Vibration **102**, pp.493-499, 1985.

[40] BHAT, R.B., "Letter to the Editor on Effect of Normal Mode Contents in Assumed Deflection Shapes in Raleigh-Ritz Method", Journal of Sound and Vibration **189(3)**, pp.407-419, 1996.

[41] SMITH, J. D., "Gear Noise and Vibration", Marcel Derek, Inc., 1999.

[42] TOWSEND, D. P. (Editor in Chief), "Dudley's Gear Handbook", McGraw-Hill Inc., Second Edition, 1992.

[43] BISHOP, R. E. D. and JOHNSON, D. C., "The Mechanics of Vibration", Cambridge University Press, Reissued with minor revisions, 1979.